LBL-28042

Lawrence Berkeley Laboratory
UNIVERSITY OF CALIFORNIA

Accelerator & Fusion Research Division

Center for X-Ray Optics

Biological Soft X-Ray Contact Microscopy: Imaging Living CHO-SCI Cells and Other Biological Materials

G.D. Guttmann
(Ph.D. Thesis)

August 1989

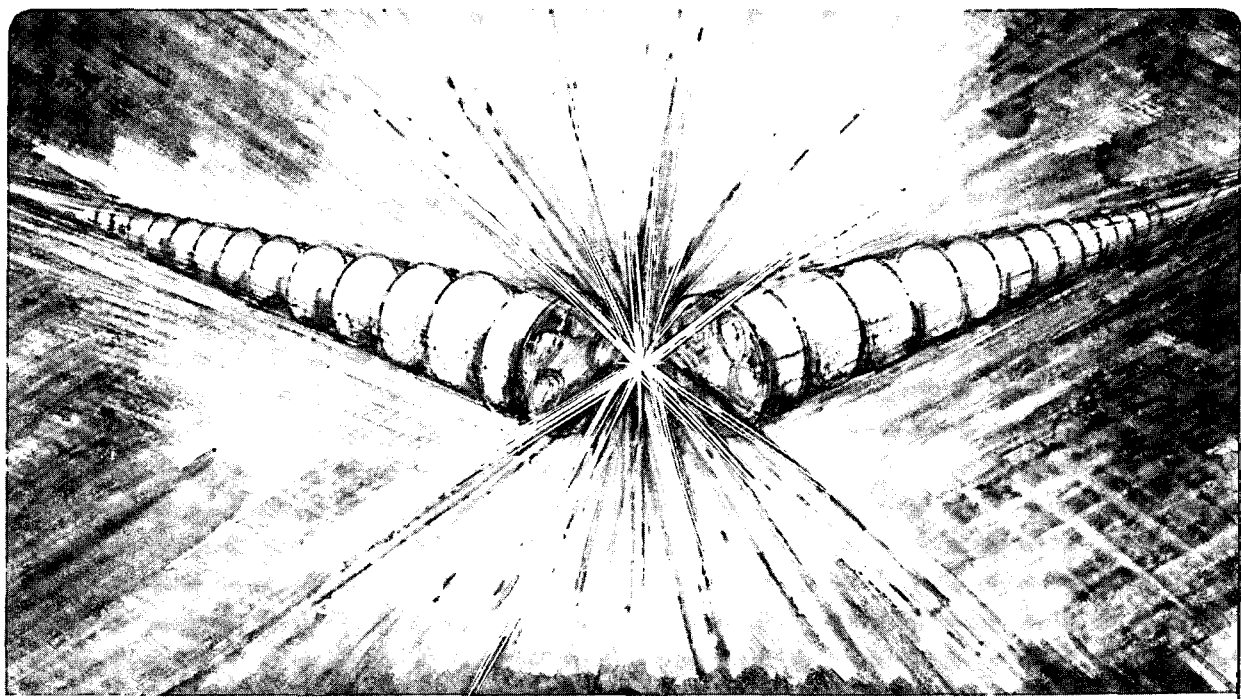

Prepared for the U.S. Department of Energy under Contract Number DE-AC03-76SF00098.

DISCLAIMER

LBL-28042

Biological Soft X-Ray Contact Microscopy: Imaging Living CHO-SCI Cells and Other Biological Materials

Geoffrey D. Guttmann

Center for X-Ray Optics
Accelerator and Fusion Research Division
Lawrence Berkeley Laboratory
1 Cyclotron Road
Berkeley, California 94720

DISSERTATION

Submitted in partial satisfaction for the requirements for the degree of

DOCTOR OF PHILOSOPHY

in

MEDICAL PHYSICS

in the

GRADUATE DIVISION

of the

UNIVERSITY OF CALIFORNIA at Berkeley

August 1989

Biological Soft X-ray Contact Microscopy:
Imaging Living CHO-SC1 Cells and Biological Materials

Biological Soft X-ray Contact Microscopy: Imaging Living CHO-SC1 Cells and other Biological Material

by

Geoffrey David Guttmann

Abstract

Soft x-ray contact microscopy (SXCM) is a form of x-ray lithography however the biological cell is imaged instead of an electron-cut microcircuit mask. Imaging of the biological sample is by soft x-rays within the "water window", which has an energy range, 277-525 eV, or λ, 4.5-2.4 nm. The contrast mechanism is based upon the x-ray absorption lengths of carbon and nitrogen, which are ~10 times shorter than that of oxygen in the "water window". The soft x-ray were generated by a conventional laboratory source or a laser-induced plasma x-ray source. The conventional laboratory soft x-ray source, a modified Henke tube, was a converted electron evaporator. The target materials were vanadium, which can generate $V_{L\alpha}$ (511 eV or 2.4 nm), and carbon, $C_{K\alpha}$ (277 eV or 4.5 nm). The laser-induced plasma x-ray source, which generates a nanosecond pulse, was the Lawrence Livermore National Laboratory JANUS laser facility. The target material was tantalum. A radiachromic nylon film was used to calibrate the exposure dose. The imaging detector was an x-ray sensitive resist, such as polymethylmethacrylate (PMMA) or a copolymer (90% PMMA and 10% methacrylic acid). A wet cell chamber (WCC) was designed to keep a biological sample alive at atmospheric pressure yet permit imaging by soft x-rays. Si_3N_4 thin windows, ~120 nm thick, made the WCC a feasible holder within a high vacuum. The limits of resolution required an understanding of the interaction of soft x-rays with matter (the biological cell and the resist), Fresnel diffraction (a wavelength-dependent phenomenon), penumbral blurring (a geometric effect) and secondary electron travel within a resist. The imaging of the biological samples included sample preparation, resist development and electron microscope readout of the resist. The biological samples were fixed erythrocytes and zymogen granules, and critical point dried 9L glialsarcoma cells. The major result of this work was the first pictures of living mammalian cells, CHO-SC1, by SXCM. The LLNL JANUS laser facility was the x-ray source for the living cell x-ray micrographs, which had a resolution of ~30 nm.

Professor Edward L. Alpen

DEDICATION

TO
Ralph Feder
who taught me the technique
and was always a "gentleman scientist"

AND
Burton Henke
who always appreciated my smile
and said, "you are the happy-go-luckiest graduate student I have ever known."

These scientists were in the twilight of their career when I met them, however they are gentlemen who reflect the positives and goodness of science.

May I do just as well!

ACKNOWLEDGEMENTS

I would like to thank the many friends and collaborators, who have helped make graduate life bearable and this research project successful. This dissertation would not have reached completion without the support of my thesis advisor, Prof. Ed Alpen. I appreciate his efforts in helping me wend my way through the academic rules and regulations at the University of California, Berkeley, and the politics of Lawrence Berkeley Laboratory. I also thank Professors Sumner Davis (Department of Physics) and Ray Keller (Department of Zoology) for their helpful suggestions, encouragement and advice.

I am deeply indebted to Ralph Feder for teaching me the technique of soft x-ray contact microscopy and the relevent and important associated technologies. Ralph is also a good friend, a helper, a resource and a "true gentleman scientist". I will never forget the winter of 1987, when I spent two weeks at the IBM T. J. Watson Research Center in Yorktown Heights learning the technique and its secrets from a master.

The project involved the building and operation of large pieces of equipment. The project goals would not have been met without the help, friendship (aargh!!!!) and moral (or is it demoralizing?) support of Phil Batson, supervisory mechanical technician at the Center for X-ray Optics. A portion of this research was done at Lawrence Livermore National Laboratory. I thank Dr. Jim Trebes, staff physicist in Y Division, who got approval for me to use the JANUS laser system and Dr. Jim Swain, the operator, caretaker, and parent of JANUS, who allowed me to "shoot some bugs". The late night and saturday shots (that included the broken door!!) were made courtesy of Jim-for this I am very grateful.

Two fellow graduate students provided a tremendous amount of help, collegial support and friendship. Marc Mendonca and I found a solution to "keeping cells happy on some difficult and nasty substrates". Our friendship continued through the food poisoning/flu "epidemic" at the Yorktown Motel Lodge during the winter of 1987. Marc and I even managed to tear Ralph Feder away from his family on a Sunday just to do some experiments and make up for lost time. Marc also got me to try 9L glialsarcoma cells for some of my soft x-ray contact microscopy experiments. My friendship with Ed Goodwin started when we collaborated on the preparation of the CHO-SC1 cells for x-ray imaging at JANUS. We have achieved success in x-ray imaging living CHO-SC1 cells to a high resolution. Ed has been a co-worker and silent critic-I thank him for this role and for providing the CHO-SC1 cells. I sincerely hope that I may have a long and healthy collaboration with both Ed and Marc.

I am thankful for having met and known Burton Henke before he retired from a very active scientific career. Burton provided insight and encouragement. He enjoyed my smile and relaxed attitude and made me feel that being a scientist was fun. My collaboration with Jon Kerner, a postdoctoral fellow in Burton Henke's lab, in calibrating radiachromic nylon films for soft x-ray dosimetry, was very fruitful and enjoyable.

Dulcynea Wilson, graduate assistant for the Graduate Group in Biophysics and Medical Physics, has helped me over the bumps and potholes of Graduate Division, for which I am thankful. When I was in need of a friendly face or a piece of advice, I could always count on Professor Alex Nichols; for this, I say thank-you. I appreciate the assistance of Jacob Bastacky with scanning electron microscopy and Carolyn Schooley at the LSB EM Lab with transmission electron microscopy. I thank the following people at LBL who have made graduate life bearable, given fair and incisive scientific criticism and provided friendship: Eric Gullikson, Yan Wu, Amy Kronenberg, Adrian Rodriguez, Randy deGuzman, Patti Powers-Risius, Polly Chang and Kathy Bjornstad.

I would like to acknowledge Dr. M. Raju and Bob Sebring of Los Alamos National Laboratory for providing the SEMs of the CHO-10B cells and allowing me to use them in this dissertation.

This dissertation signifies a couple of milestones at Lawrence Berkeley Laboratory. First, this is the first dissertation to be done and completed at the Center X-ray Optics. Second, I am the first graduate student to have completed his research for the degree of Ph.D. within the Center for X-ray Optics. I thank Dr. Malcolm Howells for initiating the project and Dr. Dave Attwood, the Director of the Center for X-ray Optics, for providing a GSRA. The research for this dissertation was supported by the Director, Office of Energy Research, Office of Basic Energy Sciences, Materials Sciences Division, of the U.S. Department of Energy under Contract No. DE-AC03-76-SF00098 and by the U.S. Department of Defense, Air Force Office of Scientific Research through University Research Initiative Contract F49620-87-K-0001.

Finally, I would to thank my wife, Alice Wershing, for being a constant companion, enduring the rigors of graduate student life and making my life a little more bearable and comfortable.

TABLE OF CONTENTS

TABLE OF FIGURES

The alphanumeric numbers in parentheses refer to the Lawrence Berkeley Laboratory Photographic Services record number.

I INTRODUCTION

This dissertation is a description of soft x-ray contact microscopy (SXCM) and the successful efforts to expand this technique to image at high resolution, living mammalian cells. The goal of this work is the imaging of living CHO-SC1 cells to a resolution of < 50 nm by soft x-ray contact microscopy. The first section, **Introduction**, is a brief history of the x-ray contact microscopy technique. A continuation of the introductory material is found in Section II, **Techniques of Soft X-ray Contact Microscopy**, which describes the image contrast within the "water window", properties of resist materials, types of x-ray sources and a comparison of SXCM with charged-particle microscopy. The physical aspects and technology of the project are explained in Sections III-VI. The conventional laboratory x-ray source and station are reported in Section III (**Technology Development-Soft X-ray Contact Microscopy Station**), while the calibration of this source is detailed in Section IV (**Dosimetry**). Section V is a physical review of the **Limits of Resolution**. The **Wet Cell Chamber** is described in Section VI. The applications and results, which include the soft x-ray contact micrographs of living CHO-SC1 cells, are considered in Section VII, **Biological Applications**. The last section is the **Conclusions**.

The history of SXCM starts with Rontgen's first x-ray in 1895. This led to the first x-ray contact micrograph by Goby in 1913. The progress of the technique was halted by World War II, however, a rebirth was triggered by Engstrom in 1946. During the 1950's, soft x-ray contact micrographs were made on silver halide photographic film, but in 1957, Ladd and Ladd made efforts to find a better x-ray detector. Due to an inadequacy of a high resolution x-ray detector and the surge of greatly improved electron microscopes, soft x-ray microscopy became a dormant technique during the 1960's and the early 1970's. In 1977, resists used for x-ray lithography were proposed as detectors for soft x-ray contact microscopy by Feder. At the same time, Sayre demonstrated the feasibility of transmission soft x-ray microscopy. The revival of soft x-ray microscopy has begun and appears to be

"alive and well". Technology of the 1980's has provided new and higher intensity x-ray sources, a better understanding of resists, new resists, x-ray optics and new readout devices. The history, description and physical principles of light (LM) and electron microscopy (EM) will not be discussed since it may be found in numerous texts, (**LM-Jenkins 1976, Born 1980, Spencer 1982, Hecht 1987; EM-Agar 1974, Goldstein 1981, Chescoe 1984, Reimer 1984, Reimer 1985**).

A. EARLY MICROGRAPHS (BEFORE WORLD WAR II)

The history of soft x-ray contact microscopy begins with Roentgen's discovery of x-rays on November 8, 1895. The first contact x-ray image was a picture of his wife's hand and ring (**Rontgen 1896**). However the first x-ray contact micrographs were done by **Goby** (1913a,b, c). The imaged samples were plant tissues, insects and foraminfera. In 1925, **Goby** did stereomicroradiography, which is the generation of stereo-pairs from thick specimens. This technique is similar to the stereo-pairs one may obtain from electron microscopy. A few years later, **Dauvillier** (1927, 1930) used a high resolution emulsion to make contact micrographs of histological sections with a magnification of 600X. The emulsion was the Lippmann type with silver grains of $< 1\mu m$ in size. Dauvillier made an important observation, which was the x-ray image contrast improved as the wavelength increased. **Lamarque** (1936) used the x-ray contact microscopy technique to image other biological specimens. World War II interrupted the development of this technique.

B. REBIRTH (AFTER WORLD WAR II)

In 1946, **Engstrom** initiated a rebirth of x-ray contact microscopy. The thesis, "Quantitative micro- and histochemical elementary analysis (by roentgen absorption spectrography)", was published in *Acta Radiologica.* The detector was silver halide photographic film. Engstrom, who became Chief of Department of Medical Physics (formerly Department for Physical Cell Research), Karolinska Institutet, Stockholm, was an advisor for numerous theses (**Bellman 1953, Wallgren 1957 and Nilsonne 1959**) related to x-ray contact microscopy.

X-ray sources were being constructed to generate polychromatic (**Engstrom 1957**) and monochromatic (**Henke 1957a**) soft x-rays in 1957. Attempts to improve the contrast of the x-ray contact micrographs (**Henke 1957b**) were reported at the first X-ray Microscopy and Microradiography Symposium held at the Cavendish Laboratory, Cambridge, England in 1956 (**Cosslett 1957**).

To improve contrast, efforts to find another x-ray sensitive detector were made in 1956 by **Ladd**. The film was replaced by ammonium dichromate crystals, which were developed in methanol after x-ray exposure. A replica was made from the etched relief pattern and viewed in the electron microscope (**Ladd 1957**). Other proposed x-ray sensitive detectors were single crystals of rock salt and cesium bromide, photoreactive dyes and Saran (**Pattee 1960b**). The single crystals changed color upon x-ray exposure however they lacked photon efficiency therefore long exposures are required. A photoreactive dye, such as pararosanaline leuconitrile dissolved in a gelatin film or nylon, became highly colored upon exposure to x-rays but was insensitive to visible light. Vinylidene chloride, which is Saran Wrap, acts a x-ray detector because plastics undergo a change in solubility produced by chain scission or crosslinking from the absorption of x-rays. Development of this plastic required several hours of washing in a 20% solution of NH_4OH (**Pattee 1960b**).

Enlargement of x-ray contact images by electron microscopy was reported theoretically (**Pattee 1960a**) and practically (**Asunmaa 1960**) at the Second International Symposium of X-ray Microscopy and X-ray Microanalysis at Stockholm, Sweden (**Engstrom 1960**). The current history and principles of x-ray microscopy were described by **Cosslett and Nixon** (1960). In 1961, **Engstrom** wrote a tome on the biological and medical applications of x-ray microanalysis with an emphasis on microscopy. X-ray microscopy of cell division was done on a film emulsion containing layers of nitrocellulose at the University of Strasbourg (**Dietrich 1963**).

X-ray microscopy (**Cosslett 1963, Henke 1963**) became a small session within the Third International Symposium on X-ray Optics and X-ray Microanalysis at Stanford University, Stanford (**Pattee 1963**). A proposal for x-ray holography and some initial images were reported at the Fourth International Congress on X-ray Optics and Microanalysis at Orsay, France (**Stroke 1965**). X-ray microscopy became dormant due to a lack of a x-ray sensitive, photon efficient, high resolution detector, however, tissue radiography research continued (**Saunders 1969a,b, Hobdell 1969, Saunders 1972**).

C. REVIVAL (1970'S AND 80'S)

The seed for the revival of x-ray contact microscopy was the first efforts to do x-ray lithography to imprint electric circuits. Resists, which were used in electron beam lithography, were found to be x-ray sensitive and have high resolution (**Feder 1970, Spears 1972, Spiller 1976a**). The first high resolution contact micrographs using resists were made of *Drosophila* giant chromosomes with a C_{K_α} x-ray source and with synchrotron radiation (**Spiller 1976b, Feder 1977**). Other resists were developed to be more sensitive and photon efficient yet maintain a high resolution (**Haller 1979**). In the meantime the feasibility of x-ray microscopy was considered in terms of dose requirements to image a sample (**Sayre 1977a,b, 1978**). By 1979, a conference was organized in New York City to discuss the various x-ray microscopy techniques (**Parsons 1980**). One of the topics was x-ray contact microscopy (**Feder 1980**), especially the study of *Drosophila* interphase chromosomes (**Manuelides 1980**).

Further developments came rapidly, especially in the type of x-ray sources. The feasibility of using a gas puff z-pinch plasma x-ray source for x-ray lithography was proposed by **Pearlman** (1981). High resolution x-ray contact micrographs of hydrated muscle filaments and proteoglycans were made using a spark pulse plasma x-ray source (**Panessa 1981a,b**). The introduction of Si_3N_4 thin windows to make TEM resists was a major improvement in the readout technique (**Feder 1981, Cheng 1982**). This effort

also included an intense study of blood platelets by soft x-ray contact microscopy (**Baldini 1983, 1985, Feder 1985b**). This led to the first soft x-ray contact image of a living biological sample, the blood platelet (**Feder 1985a**). Structures undetected by the electron microscope were seen in the x-ray image (**Baldini 1985**). Attempts were made to use x-ray microscopy to do elemental analysis on materials by contact techniques (**Bigler 1983**) and biological samples by transmission scanning methods (**Kenney 1985**).

The x-ray microscopy meetings of the past started to become a regular event in 1983, with an International Symposium on X-ray Microscopy at Gottingen, West Germany (**Schmahl 1984**). At this meeting, discussion centered upon the sources and design of the various types of x-ray microscopes. The following year, x-ray microscopy gathered much publicity with a special issue of the *Journal of Microscopy* and a couple of review articles (**Howells 1985, Kirz 1985**). Flash or pulse x-ray sources, such the gas puff z-pinch (**Feder 1985a**) or laser-induced plasma sources (**Rosser 1985a,b, Rumsby 1985, Eason 1986, Michette 1986**), became widespread and now numerous experiments have been done using this type of source. The latest work has either involved technology development such as the x-ray laser (**Matthews 1985, 1988, Suckewer 1985, 1986**) or x-ray holography (**Howells 1987, Trebes 1987**) and comparative studies using different imaging methods, such as transmission or scanning electron microscopy, light microscopy and SXCM using synchrotron radiation or plasma x-ray sources (**Hill 1987, Richards 1988, Stead 1988**). Since the 1983 Gottingen International Symposium, two x-ray microscopy meetings and a NATO ASI Summer Course (**Feder 1986a**) have been held, 1986 Meeting on Instrumentation and Biological Applications at Taipei, Taiwan (**Cheng 1987**) and 1987 International Symposium on X-ray Microscopy at Brookhaven, New York (**Sayre 1988**). This work has taken SXCM to the stage of imaging living mammalian cells to a high resolution.

II TECHNIQUES OF SOFT X-RAY CONTACT MICROSCOPY

A. WHY ARE SOFT X-RAYS USEFUL FOR BIOLOGICAL IMAGING?

The region of interest for soft x-ray contact microscopy is defined by x-rays with wavelengths 1 to 10 nm. There are five major benefits from using soft x-rays to do biological imaging. The first is good contrast for all elements but more importantly there is excellent contrast for low Z materials (**Sayre 1977a, 1977b and 1978**). Low Z materials are the predominant biological materials. A typical mammalian cell is 70% water, 18% proteins, 1.35% nucleic acids, 2% sugars, 5% lipids and phospholipids, 1% inorganic ions (Na^+, K^+,Mg^{2+}, Ca^{2+}, Cl^-, etc.), and 3% miscellaneous small metabolites (**Alberts 1983**). It can be deduced that the general percentages for each element within a mammalian cell approximate 48% H, 24% C, 24% O, 1.5% N, 0.5% Ca and Mg, 0.4% Na and K, 0.3% P, 0.3% Si and 1% other elements (**Alberts 1983**). The second benefit is the ability to use monochromatic x-rays, which may be produced from a conventional line source or chosen by use of a monochromator on synchrotron radiation. Furthermore, it is known that the absorption of x-rays by each element is dependent upon the incident x-ray energy. Electron microscopy requires electron-dense stains to enhance the structures of interest. Without staining contrast is very poor with electrons as seen in Figure 1. Further discussion will appear below when the "water window" is mentioned. Third, x-rays are much more penetrating than electrons. **Kirz and Sayre (1980)** discuss the quantitative relationship of penetration of biological samples by electrons or x-rays, or stated in another manner, the absorption lengths of x-rays and electrons in biological materials as illustrated in Figure 1. X-rays travel almost 100 times further than electrons in water. This difference suggests that soft x-ray microscopy can image a living biological cell. Transmission

Figure 1.. Linear absorption coefficients of x-rays and electrons in water and proteins

The top half of the graph describes the absorption length of x-rays within proteins and water. The "water window" is indicated by the region bounded from .284-.532 keV. A difference between the absorption length of x-rays within protein (solid line) and water (dashed line) is noticeable in this region. The bottom half of the graph illustrates the electron elastic or inelastic mean free path (denoted as absorption length) in water (dashed lines) and protein (solid lines). There is very little contrast indicated between the mean free path in water and that in protein.

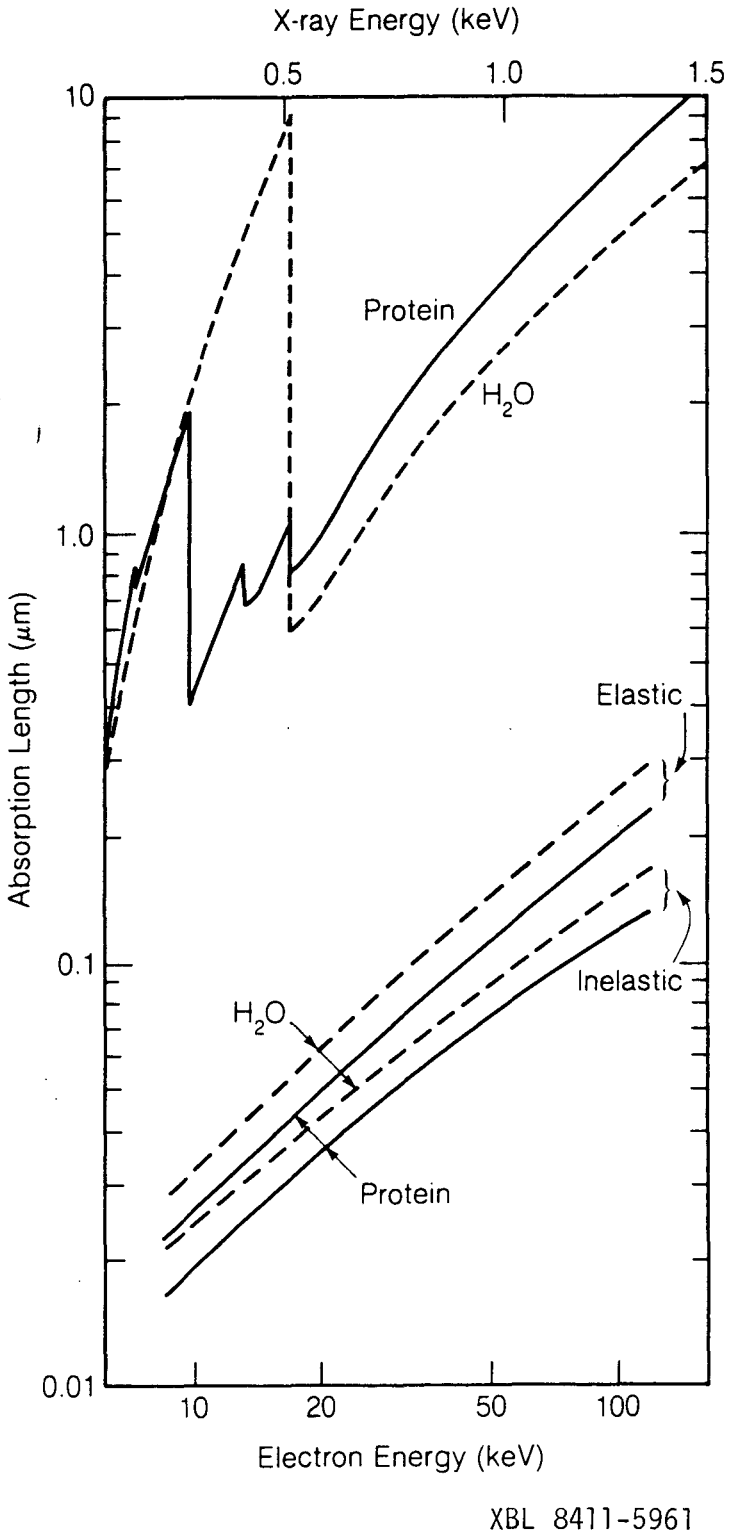
X-ray Energy (keV)
0.5
1.0
1.5
10
1.0
0.1
0.01
Absorption Length (μm)
Protein
H2O
Elastic
Inelastic
H2O
Protein
10
20
50
100
Electron Energy (keV)
XBL 8411-5961

Fig. 1

electron microscopy, a high resolution imaging method, requires sample preparation such that the specimen is sliced to a thickness of 0.1 μm. Fourth, a three-dimensional picture can be generated. There are numerous x-ray imaging techniques available. A couple of suggested approaches are microtomography or a "micro-CAT" scanner (**Feder 1986**), stereographic projections or "stereo pairs" as used in electron microscopy, and holographic methods (**Aoki 1974, Howells 1987, and Trebes 1987**). Finally, the fifth benefit arises from our combined knowledge of the x-ray absorption characteristics of protein and water with the selection of suitable x-rays from appropriate x-ray sources, (i.e. plasma sources), to provide maximum contrast and fast exposure, especially in imaging intact living cells.

1. "WATER WINDOW"

The concept of the "water window" is illustrated by Figure 1. The region of interest for x-rays is 283-532 eV or λ = 4.37-2.33 nm. The C_K absorption edge is at 283.8 eV or λ = 4.37 nm, while the O_K absorption edge is 531.7 eV or λ = 2.33 nm. It is in this "window", or region, that water is transparent to x-rays. In actuality, x-rays at the V_{L_α} emission line of 511 eV or λ = 2.43 nm have an absorption length nearing 10 μm in water and approximately 0.9 μm in proteins. The ratio of previously mentioned absorption lengths gives an indication of a good signal-to-noise ratio for detecting proteins and other carbon-rich macromolecules within the living, wet cell. From the previous discussion, one can deduce the factors affecting the contrast mechanism. As an aside, Figure 1 shows a N_K absorption edge at 400 eV or λ = 3.1 nm. Two elements that are useful to generate soft x-rays with a conventional tabletop laboratory source are titanium with the following emission lines: Ti_{L_l} at 395.13 eV or λ = 3.14 nm and Ti_{L_α} at 452.2 eV or λ = 2.74 nm and vanadium, V_{L_α} at 511 eV or λ = 2.43 nm. A commonly-used soft x-ray emission line is Al_{K_α}, which is at 1,486 eV or λ = 0.834 nm. This x-ray is not useful for imaging since it is extremely far from the "water window".

Figure 2. The procedure of soft x-ray contact microscopy or lithography

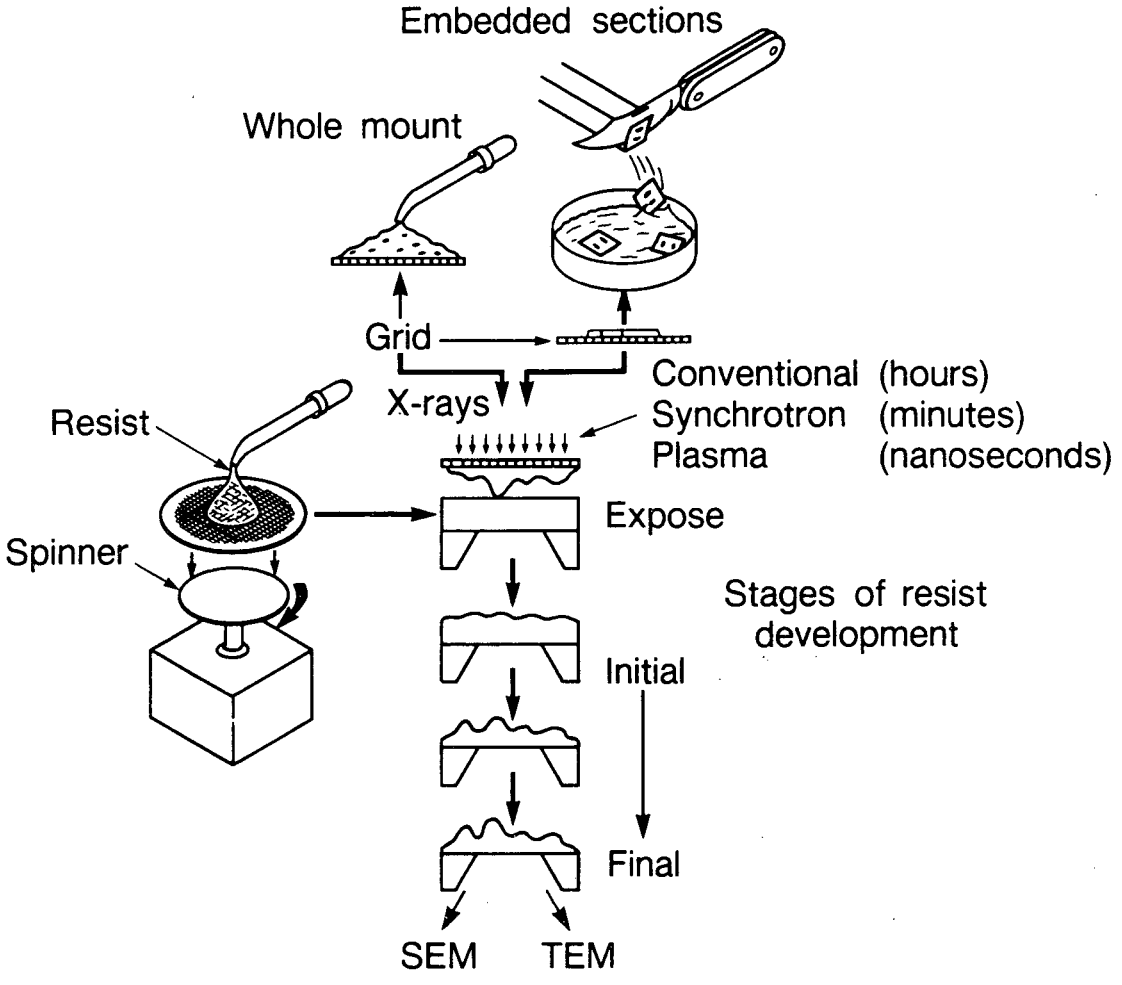
Embedded sections
Whole mount
Grid
X-rays
Conventional (hours)
Synchrotron (minutes)
Plasma (nanoseconds)
Resist
Spinner
Expose
Stages of resist development
Initial
Final
SEM
TEM
XBL 867-9849A

Fig. 2

Figure 3. An enhanced view of soft x-ray contact microscopy

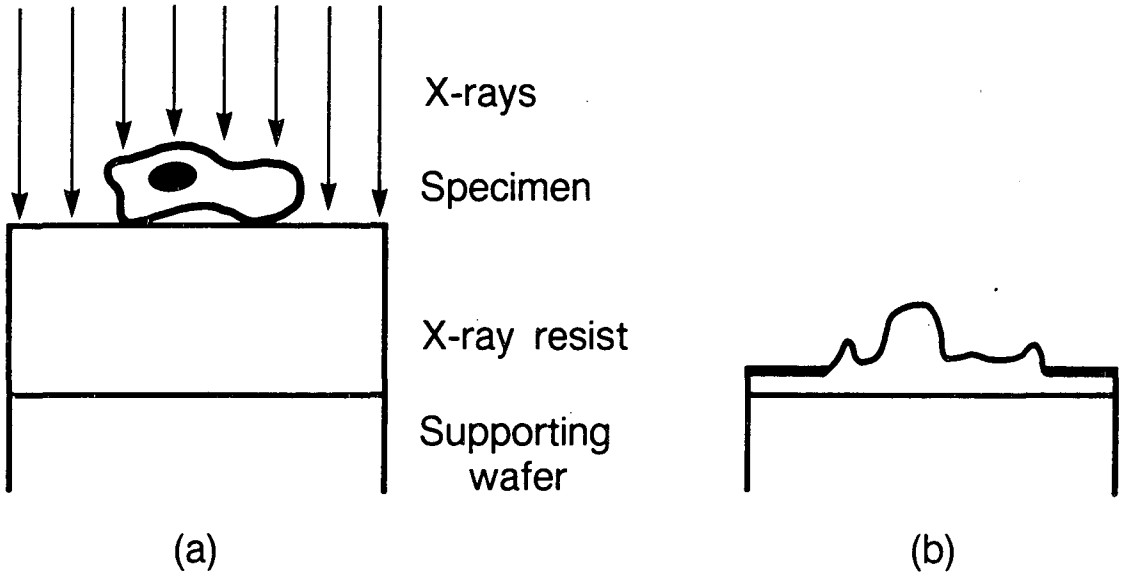

XBL 867-9851A

Schematic of contact imaging. (a) Contact imaging of specimen into resist where incident x-ray beam is modified by the absorption of the specimen. (b) The resist after development and metallization. The resist profile is then magnified and read out by electron microscopy.

Fig. 3

The electron elastic and inelastic mean free paths in water is only slightly greater than that in proteins. At 50 keV, the electron elastic mean free paths in water and protein are 0.15 μm and 0.12 μm respectively, while those of the inelastic component in water and protein are 0.09 μm and 0.078 μm. The implication of these measurements are twofold. First, electron-dense stains are necessary to image proteins, other biological macromolecules, or subcellular components and second, it is necessary to use thin sections with a maximum thickness approximating 0.1 μm.

2. THE SOFT X-RAY CONTACT MICROSCOPY TECHNIQUE

The procedure of soft x-ray contact microscopy is analogous to x-ray lithographic techniques. Figure 2 outlines the steps of the procedure. A biological sample may be prepared as either a whole-mount or an embedded tissue. Embedded tissue sections should have a thickness much less than 10 μm and preferably 5 μm or less. Whole mount samples may be placed on electron microscope grids prior to critical point drying. There are two other approaches to mounting biological cell samples. The first, developed by the author and Ed Goodwin, is to place a droplet of solution containing living cells onto a Si_3N_4 window, allow the cells to settle onto the window and then remove or wick away as much water as possible leaving enough of a water layer to keep them alive. The other approach, designed by the author and Marc Mendonca, is to grow or culture the cells onto the Si_3N_4 window. Once the cells have attached, spread out and formed a monolayer, the medium is removed or wicked away as much as possible. Enough medium is left to form a very thin water layer around the cell so that it can be kept alive prior to irradiation. Some moisture in the form of medium or buffered solution is added to sponges situated within the wet cell chamber. A resist is put onto the biological sample. At this time a sandwich is created. This sandwich is either an electron microscope grid or a Si_3N_4 window facing the x-ray source, the biological sample, and then the resist. The sandwich is then placed into a holder, which may be in the form of a wet cell chamber.

Figure 4. TEM and SEM resists

On the right is the SEM resist, PMMA supported by a solid silicon substrate. On the left is the TEM resist, PMMA supported by a 120 nm thick Si_3N_4 window.

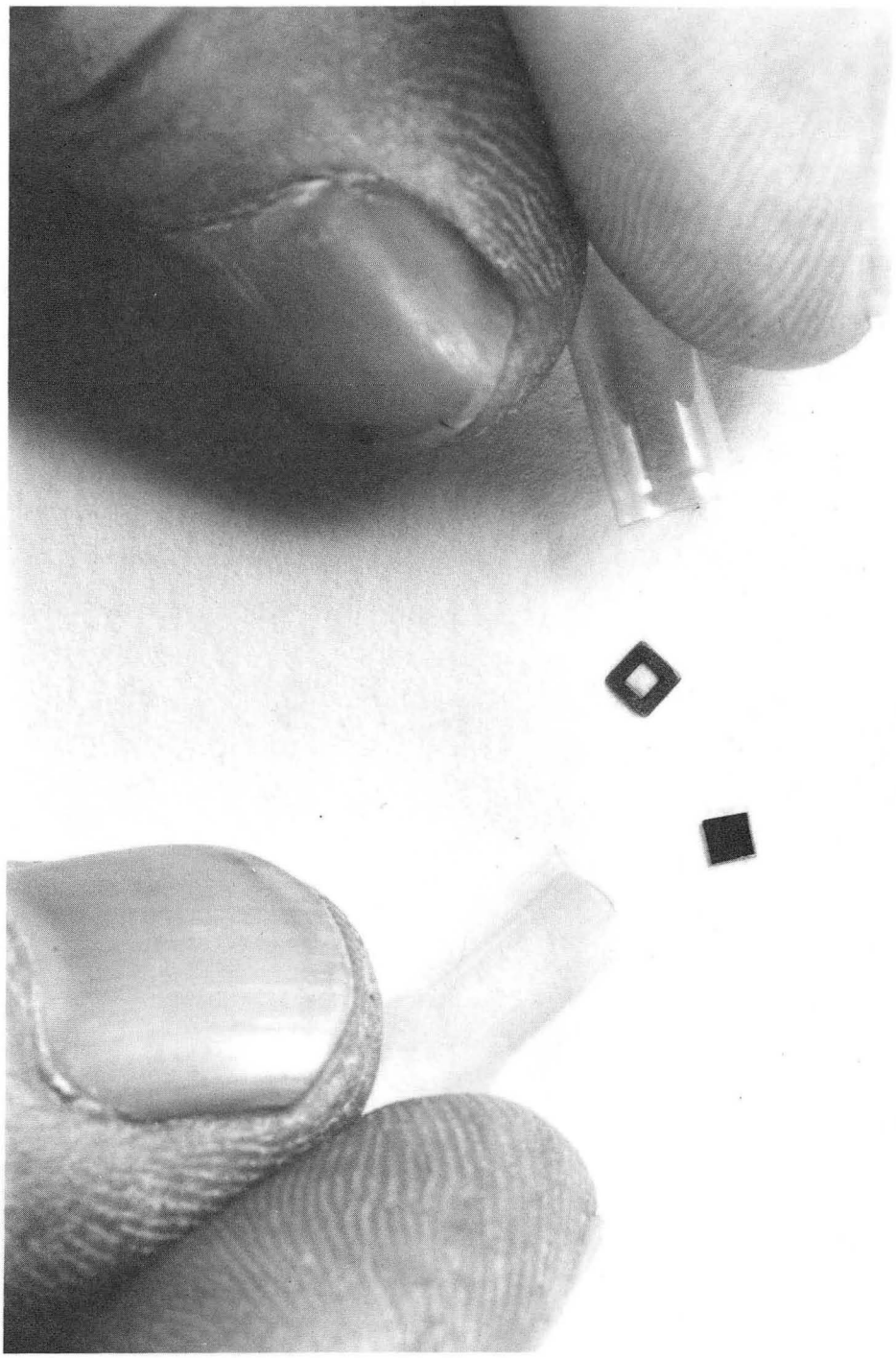

CBB 867-5029

Fig. 4

The resist is made by combining 5 g polymethylmethacrylate (Dupont Elvacite 2041 is the preferable type for soft x-ray microscopy) obtained in powder form with 95 ml chlorobenzene. This solution should be warmed to 30°C and stirred. It may be stored in dropper-type bottles until one is ready to use the solution. To prepare a resist for x-ray contact microscopy, a small amount of prepared solution is added to an equal amount of chlorobenzene. A substrate such as a solid silicon wafer (for SEM viewing) or an etched Si_3N_4 windowed wafer (for TEM viewing) is placed on a spinner and then spun at approximately 6000 rpm. The thickness of the resist can be determined by the spinner speed or by varying the amount of chlorobenzene in the diluted solution. Droplets of the diluted solution are applied to the spinning substrate and spun for 30-60 seconds. The resist is then baked in an oven at air at 160°C for 1 hour **(Kirz 1980)**. Other resist materials such as copolymer, 90% PMMA and 10% MMA, or terpolymer may be used. Preparation methods are similar to PMMA. Discussion of the properties of resists will be appear below.

Solid silicon wafers (commonly called SEM resists) are used for viewing the resulting replica in the SEM, while the etched Si_3N_4 windowed wafers (commonly called TEM resists) are used in the TEM. SEM resists are made at various thicknesses, the most common is 480 nm. TEM resists are approximately 120 nm thick and are thin enough for the electrons to pass through when placed inside the conventional TEM. Figure 4 illustrates the two types of resists.

Returning to the procedure for soft x-ray contact microscopy, the sandwich is exposed to an x-ray source. Various types of x-ray sources are available. There are conventional sources, which take hours to make a reasonably useful exposure, synchrotrons, which require only minutes, or plasma sources which deliver a useful exposure in a matter of nanoseconds. After the sandwich has been exposed to one of these x-ray sources, the resist is removed and developed in a solution of pure methyl isobutyl ketone (MIBK) or a dilution of MIBK in isopropyl alcohol (with ratios of 1:1, 1:5, 1:10,

depending on how quickly one wants to etch the resist). Once the resist has been etched to a point where the objects of interest are seen clearly under a high-powered differential-interference-contrast (DIC) microscope with Nomarski optics, the resist is coated and shadowed with Au-Pd. The resist is now ready for viewing in the SEM or TEM depending on its type.

Figure 3 illustrates a close-up view. The cell has been set on an x-ray sensitive resist. The x-rays pass through the Si_3N_4 window and interact with the biological material. The remaining x-rays will interact with the resist. In particular, positive resists are used and therefore one looks for chain-breaking within the polymer as an indicator of x-ray interaction. Once the broken chains are developed or etched away, a relief map is seen. This relief map may represent the densities within the cell but is indicative of the x-ray absorption that has taken place. The peaks and valleys indicate respectively the high and low x-ray absorption or attenuation within the cell.

B. PROPERTIES OF RESIST MATERIALS

Polymethylmethacrylate (PMMA) is one of the most commonly used resist materials for soft x-ray contact microscopy. Other possible resist materials are copolymer, which is 90% PMMA and 10% methylmethacrylic acid (MMA), terpolymer, poly (butene-1-sulfone) (PBS), poly (2,2,3,3-tetrafluoropropyl methacrylate), poly (glycidyl methacrylate), copolymer of glycidyl methacrylate and ethyl acrylate, and epoxidized polybutadiene. PMMA, the copolymer (PMMA-MMA, hereafter referred to as copolymer) and terpolymer are currently the most predominantly used resist materials for soft x-ray contact microscopy. Terpolymer is prepared by copolymerizing methyl methacrylate with methacrylic acid. This particular copolymer is then heated to produce intramolecular anhydride linkages such that the final product is a polymer of three distinct monomers: methyl methacrylate, methacrylic acid, and methacrylic anhydride **(Willson 1983)**.

The polymers of interest are acrylates, which are easily handled, commonly available, provide high resolution, have an intrinsic radiation sensitivity, and act as positive

resists. A positive resist is one whose material upon radiation exposure experiences polymer chain breaking or scissions. Once the resist has been exposed, the broken chains are developed or washed away with a solvent. The resulting image is comprised of peaks where the resist was not exposed to radiation, and valleys where it was exposed (**Willson 1983**). PMMA and copolymer, which are the particular polymers used in this work, are called one-component, positive resists.

A continuation of this discussion should include the definition of some terms as they pertain to microlithography and an understanding of the parameters affecting resist sensitivity and contrast. The first term is the G-value, G(s). G(s) is defined as the number of chain scissions or breaks produced per 100 eV of absorbed energy. G(s) can be thought of as the photochemical quantum efficiency of a resist and has a direct correlation to resist radiation sensitivity. A high G(s) number (i. e. one approaching 10) is indicative of very high radiation sensitivity. In this respect, various resists have been compared for their radiation sensitivity (**Willson 1983**). The next term is glass transition temperature, T_g. Polymeric resists are considered to be amorphous. Their physical properties are determined by the molecular motion allowed within the individual chain. At high temperatures, the polymer is fluid. Upon cooling, chain movement becomes restricted and is eventually stopped. It is at this temperature, T_g, that the polymer behaves like glass. If T_g is below room temperature, the polymer is considered to be rubber and if it is above room temperature, it is considered to be glass (**Thompson 1983**). The importance of this property is related to how much thermal stress the resist may withstand. The final term to be defined is resist contrast, γ. Resist contrast is directly related to the resist's resolution capability. The definition of γ is the slope of the log (dissolution rate) versus log (exposure) curve (**Haller 1979**). Further discussion and derivation of γ is found in **Spiller (1977)**.

The derivation of resist contrast, γ, begins by determining the resolution element of interest. In this case, the resolution element will be a lateral dimension, defined as δ. The number of photons absorbed in the volume of the resolution element is as follows:

$$\bar{n} = \frac{E_{inc}}{h\upsilon} A \delta^2 \qquad \text{Eqn. II-1}$$

where E_{inc} is the incident energy surface density (commonly measured as J/cm^2), $h\nu$ is the energy of each photon and A is the fraction of incident energy absorbed in the resolution element with a volume $\delta^2 d$. d is the thickness of the resolution element. Absorption, A, is given as

$$A = 1 - e^{-\alpha d}, \text{ but } A \approx \alpha d \text{ for } \alpha d << 1$$

with α being defined as the linear absorption coefficient.

It is now necessary to define the transmission effectiveness of the mask. The term, T_{abs}, is 1 when the transmission is through a clear area of the mask and may also be defined as

$$T_{abs} = \bar{n}_{abs} / \bar{n} . \qquad \text{Eqn. II-2}$$

The number of photons transmitted through a clear area of the mask is represented by $\bar{n}$ whereas $\bar{n}_{abs}$ represents the photons transmitted through the mask. Furthermore the contrast of the mask is defined as $C_{mask} = 1/ T_{abs}$.

Equation II-1 can be rewritten in the following manner:

$$E_{inc} = \bar{n} h\nu / A\delta^2 \qquad \text{Eqn. II-3}$$

At high resolution, where $\delta \rightarrow \lambda$, the resist must be very thin ($d \approx \delta$). The above may be rewritten as

$$E_{inc} = \bar{n} h\nu / \alpha\delta^3. \qquad \text{Eqn. II-4}$$

The minimum required exposure using the 3σ-criterion with overlapping Poisson distributions may be set up as follows:

$$\bar{n} - T_{abs}\bar{n} = 3\sigma_{clear} + 3\sigma_{opaque}, \qquad \text{Eqn. II-5}$$

this equation becomes

$$\bar{n} = 9/(1 - T_{abs})^2. \qquad \text{Eqn. II-6}$$

From this information, a resist must have these three properties:

1). High resolution resists must have low sensitivity. This property is seen by Equation II-3 where the incident energy required for exposure increases quadratically with the desired linear resolution.

2). Higher exposures are required for high energy photons (Eqn. II-4).

3). Higher exposures are required for low contrast masks as seen in Equation II-6. These properties are described in **Spiller (1977)**.

The dissolution rate S is proportional to the x-ray or electron-beam exposure. Also, the rate may be expressed as $S \propto M^{-a}$ where $M = NM_m$ and $a \approx 1.5$ for PMMA developed in concentrated MIBK at 21^0C. N is the average number of monomer units per chain and M_m is the molecular weight of the monomer unit. When considering low contrast masks, the development process can be characterized by the dissolution rate ratio $S(E_{inc})/S(T_{abs}E_{inc})$. Now, sidecutting, which is an effect of the developer on the resist, must be considered. The angle of the walls is defined by a tilt angle, ß, where ß = 90° for vertical walls. Thus

$$\tan ß = \{S(E_{inc})/S(T_{abs}E_{inc})\} - 1. \qquad \text{Eqn. II-7}$$

With light or very short development, sidecutting is minimal but the depth is also small. Further development will lead to a sloping of the walls and an increased depth. A harsh or long treatment will increase the sloping of walls and possibly reduce the resolution. The effects of sidecutting can be reduced by increasing the exposure dose. For very low contrast masks such as biological samples, the slope of the log(dissolution rate) versus log(exposure) curve generates a definition of sensitivity. Thus,

$$\log\{S(E_{inc})/S(T_{abs}E_{inc})\} = \gamma \log\{E_{inc}/T_{abs}E_{inc}\}. \qquad \text{Eqn. II-8}$$

Here, γ is a proportionality constant generated from the measurement of the slope. Lastly, the definition of d_{norm} is considered. The resist thickness, d, decreases linearly with dissolution time, t:

$$d = d_0 - St \qquad \text{Eqn. II-9}$$

The normalized remaining resist thickness:

$$d_{norm} = d_{remain} / d_0 = 1 - \{S(E_{inc})/S(T_{abs}E_{inc})\}. \qquad \text{Eqn. II-10}$$

Biological samples which act as very low contrast masks require a d_{norm} close to 1 **(Spiller 1977)**.

There are many parameters that determine the sensitivity and contrast of a resist. These parameters may be divided into three major categories: hardware, polymer (material), and processing. It is necessary to note that the units of sensitivity are mJ/cm^2 or $\mu J/cm^2$. Hardware aspects are the energy flux, wavelength, exposure ambience, mask absorption characteristics, source brightness, and exposure time. The mask for this work is biological material. The polymer parameters are chemical composition, molecular weight, molecular weight distribution, glass transition temperature (T_g), density, and average atomic number. Processing factors are the developing criteria, developing conditions, developer composition, and pre- and post-baking conditions **(Thompson 1983)**.

The discussion will now proceed to a description of the resists used in this work. The two resist materials were PMMA and copolymer. It is assumed that the characteristics of each resist are similar whether the resist is used for laboratory electron beam or x-ray experiments **(Spiller 1977)**. Figure 5 shows the mechanism of radiation- induced chain scission in PMMA **(Willson 1983)**. The initial radiochemical step is the homolysis of the main chain carbon to the carbonyl carbon bond or the homolysis of the carbonyl carbon to the oxygen sigma bond. The next step is rearrangement through beta scission to cleave the chain and generate an acyl-stabilized, tertiary radical. The fragments generated are carbon monoxide, carbon dioxide, and methyl and methoxy radicals. The G(s) values for PMMA and copolymer are 1.3 and 2.0 respectively. Sensitivity is the inverse of the G(s) value. The values for sensitivity using a 15 kV electron beam are 40 and 35 $\mu C/cm^2$ for PMMA and copolymer respectively. The characteristics of PMMA and copolymer upon exposure to Al K_α x-rays (λ = 0.83 nm) are as follows:

Figure 5. The mechanism of radiation-induced chain scission in PMMA

This is an illustration of the interaction of radiation, electron beam or x-rays, with PMMA. Once the chain is broken, the following fragments are left: carbon monoxide, carbon dioxide, methyl and methoxy radicals. Development or etching with a solvent such as MIBK washes away these fragments and some of the broken chains.

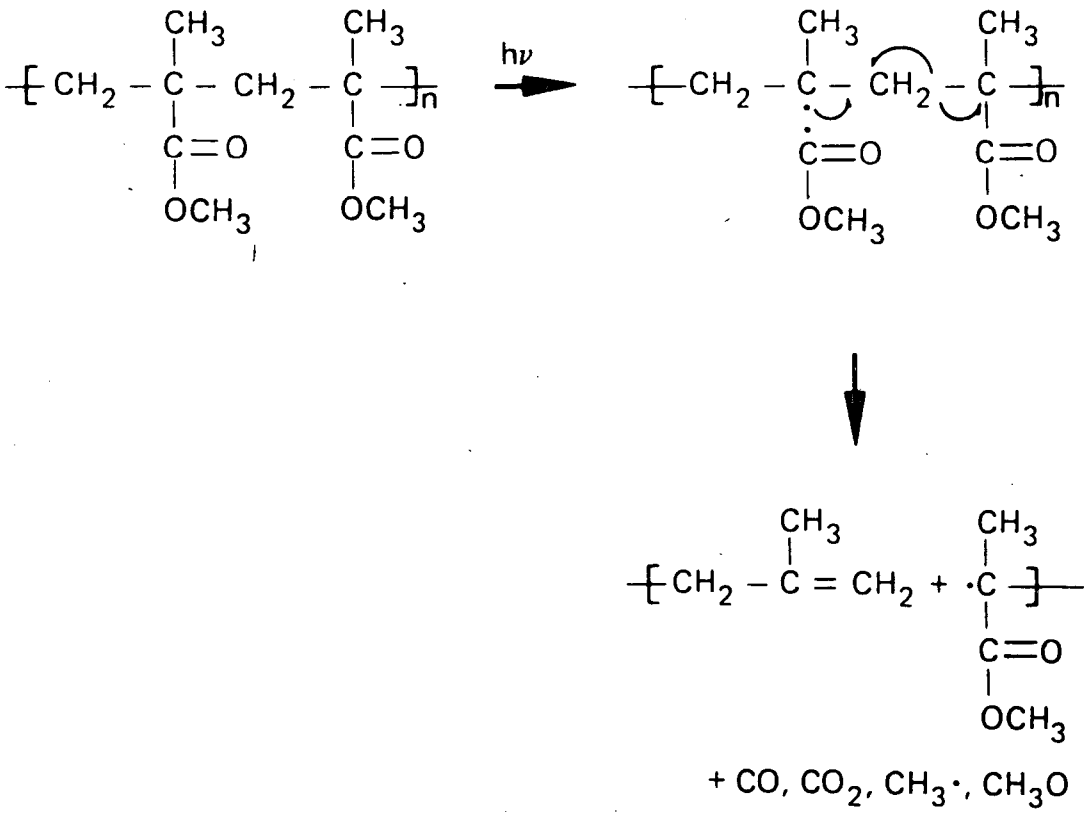

Fig. 5

Figure 6. The x-ray linear absorption coefficient of various materials

The linear absorption coefficient,α, is in μm^{-1}. Note the soft x-ray linear absorption coefficient of PMMA and Si_3N_4 in the "water window", which is in the region, λ=24-45 Å.

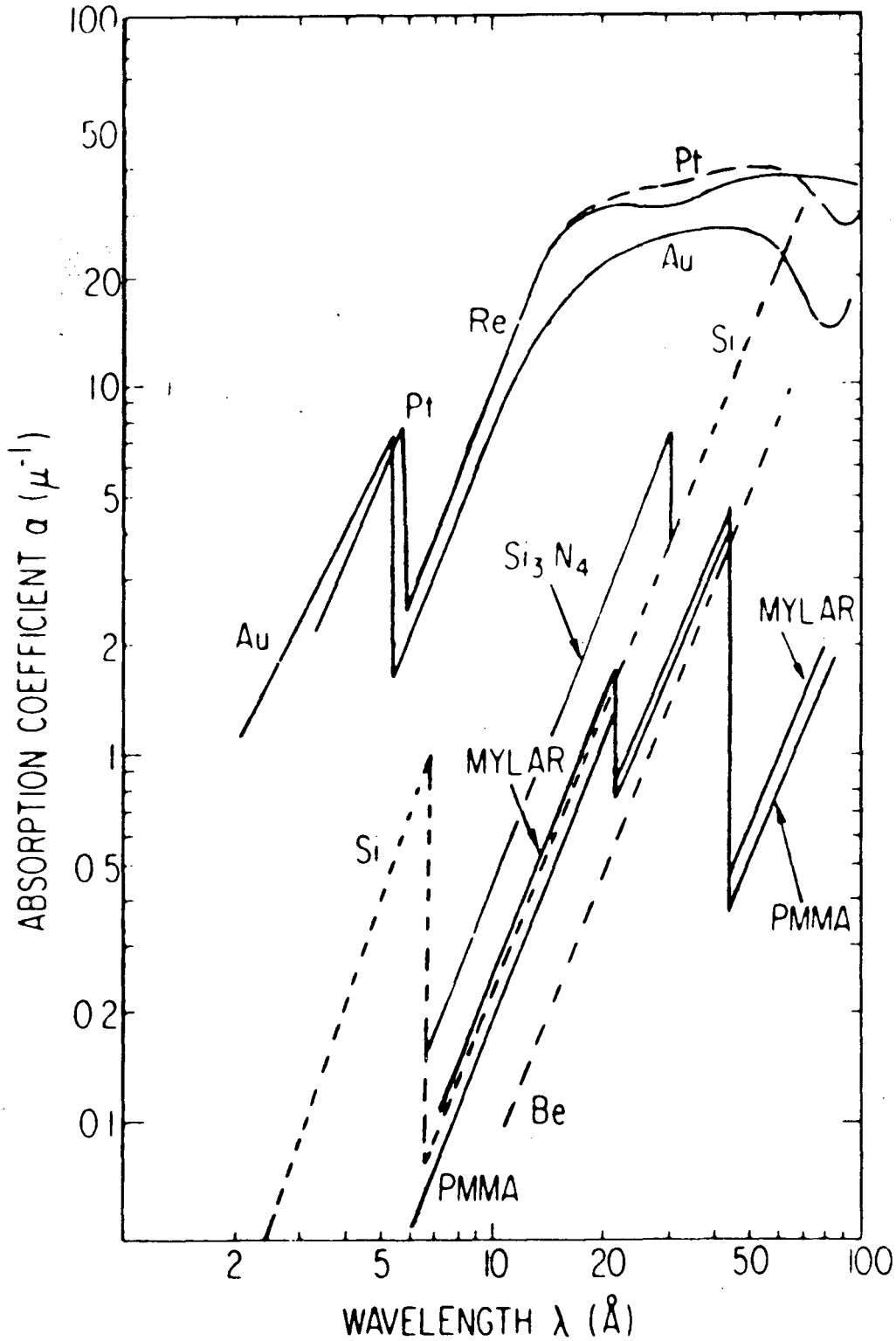
100
50
20
10
5
2
1
0 5
0 2
0 1
ABSORPTION COEFFICIENT α (μ⁻¹)
Pt
Au
Re
Si
Pt
Au
Si₃ N₄
MYLAR
MYLAR
Si
PMMA
Be
PMMA
2
5
10
20
50
100
WAVELENGTH λ (Å)

Fig. 6

Resist	Characterization	Req. inc. dose (J/cm^2)
PMMA	d_{norm}=0.5	0.07
	d_{norm}=0.9	0.2
Copolymer	d_{norm}=0.5	0.01
	d_{norm}=0.9	0.05

The required absorbed dose may be calculated by multiplying the required incident dose with the linear absorption coefficient, α, of the material (approximately 0.1 μm^{-1}). As an aside, terpolymer's G(s) value is 4.5 and its electron beam sensitivity is 10 $\mu C/cm^2$ at 20 kV. Terpolymer's characteristics as an x-ray resist are, at tan ß=5 and λ = 0.83 nm x-rays, 0.024 J/cm^2 for a required incident dose and 80 J/cm^3 for a required absorbed dose. It is obvious that terpolymer is more sensitive than PMMA, but its drawback is a poor resolution, 100 nm , in comparison to the aforementioned polymers.

Figure 6 illustrates the linear absorption coefficient, α, in units of μm^{-1}, of various materials. In particular, PMMA has an absorption coefficient between 1-4 μm^{-1} within the "water window" for soft x-rays. Therefore, most soft x-rays should be absorbed within the resist material.

C. TYPES OF X-RAY SOURCES

There are several types of x-ray sources available for use with soft x-ray contact microscopy and lithography. The three types that have been used to this time are conventional laboratory source, plasma sources, and synchrotrons. The fourth and fifth types, the x-ray laser and the free-electron laser (FEL), will be mentioned briefly. Conventional laboratory sources, which are electron-target arrangements, will be discussed first. These sources require hours to make an exposure for contact microscopy, however they produce a line spectrum. Next, there will be an overview of the two kinds of plasma sources, which are laser-induced and gas "puff" z-pinch. Plasma sources are pulse sources, in the nanosecond time region, and produce a semicontinuous spectrum with many x-ray emission lines. The third source type is synchrotrons, which require minutes

to make a contact microscopy exposure but provide high intensity radiation which can be tuned to the desired wavelength. The x-ray laser is a pulse source which has a nanosecond or less time span and emits radiation at a particular wavelength. The last source type, the FEL, is a high brightness device that operates with high efficiency compared to a conventional laser and is tunable to any wavelength.

1. CONVENTIONAL LABORATORY SOURCES

Conventional laboratory x-ray sources, also known as stationary target sources or x-ray tubes, are the most commonly used sources due to their low cost of construction and operation. Also, the x-ray tube was the first man-made source of x-rays **(Rontgen 1896)**. The laboratory source as used in contact microscopy requires a pumping station (typically a turbomolecular pump and a rotary pump), a vacuum chamber holding the x-ray gun, and a specimen chamber. In this arrangement, electrons are boiled off the filament and electrostatically focussed onto a target. The electron bombardment of the target yields x-rays characteristic to the target material, i.e. the target material's emission lines and bremsstrahlung. The energy of the electrons will determine the x-ray energies produced. This work used vanadium, titanium, and carbon. The x-ray emission lines have been given above. The flux for the apparatus used in this work was 4×10^8 photons/cm^2-sec at 18 cm from the target using V_{L_α} x-rays.

2. PLASMA SOURCES

The two types of plasma sources that have been used in soft x-ray contact microscopy are the laser-induced and gas puff z-pinch sources. A plasma is a highly ionized gas, consisting of positively charged nuclei (ions) and mobile negative electrons, and it is neutral (i.e. not charged). Plasmas are often considered to be the fourth state of matter. A more technical definition of a plasma is "an ionized gas in which the length that divides the small-scale individual-particle behavior from the large-scale collective behavior is small compared to the characteristic lengths of interest." **(Jackson 1975)** This length is the Debye length. **Kunkel (1971)** defines the Debye length, $\lambda_D \equiv \sqrt{kT_e/4\pi e^2 n_e}$, as

"the maximum displacement the bulk of the electrons can have with respect to the ions if their number density is n_e and if the resulting potential energy is not to exceed the electron random energy, kT_e." In retrospect, a plasma may be defined as a collection of charged particles whose dimensions are larger than λ_D. The collective effects dominate the charged-particle dynamics because $\lambda_D << \lambda_e$ where λ_e is the electron mean free path for momentum exchange.

Examples of plasmas are the sun, controlled fusion experiments, the earth's ionosphere or fusion reactors. The application of the Debye length to determine if an ionized gas is a plasma is demonstrated in the following example. An ionized gas with a $T_e = 2000°K$ and $n_e = 10^{18}$ electrons or ions/m^3, has $\lambda_D = 2.2 \times 10^{-6}$ m. This example has a sufficiently large number of charged particles to shield itself, electrostatically, in a distance that is small compared with other physical dimensions of interest (**Reitz 1979**).

a). Laser-induced plasma sources

Laser-induced plasma sources produce x-rays in the following manner. A powerful laser beam impinges onto a target material, such as Ta, and creates a plasma. X-rays are emitted due to the blackbody radiation occurring at high temperatures. Even though the spectrum is a continuum, plasmas emit strong emission lines indicative of the material or elements used in the target. The x-rays are emitted in a 4π direction.

An example of the typical experimental setup at LLNL's JANUS laser follows. The typical laser shot emits 48-60 joules of infrared light. The light passes through a 2ω crystal, where it undergoes frequency doubling, and is converted into 12-15 joules of green light if there is a proper 25% conversion efficiency. The green light enters a vacuum chamber and impinges upon a piece of Ta, 25 μm thick. The laser beam has been focussed to a 100 μm spot. A plasma is generated. Soft x-rays and vacuum ultraviolet radiation is emitted from the plasma. The sample is placed 6 cm away from the target material. The radiation passes through the Si_3N_4 thin window which is coated with 50 nm Al to filter out some of the unwanted light, such as vacuum ultraviolet. A typical laser

Figure 7. A schematic of the LLNL JANUS laser system

TR1 and TR2 refer to Target Rooms 1 and 2 respectively. 2w refers to the 2ω crystal which acts as a frequency doubler and converts the infrared beam into green light. Drawing courtesy of Jim Swain, LLNL.

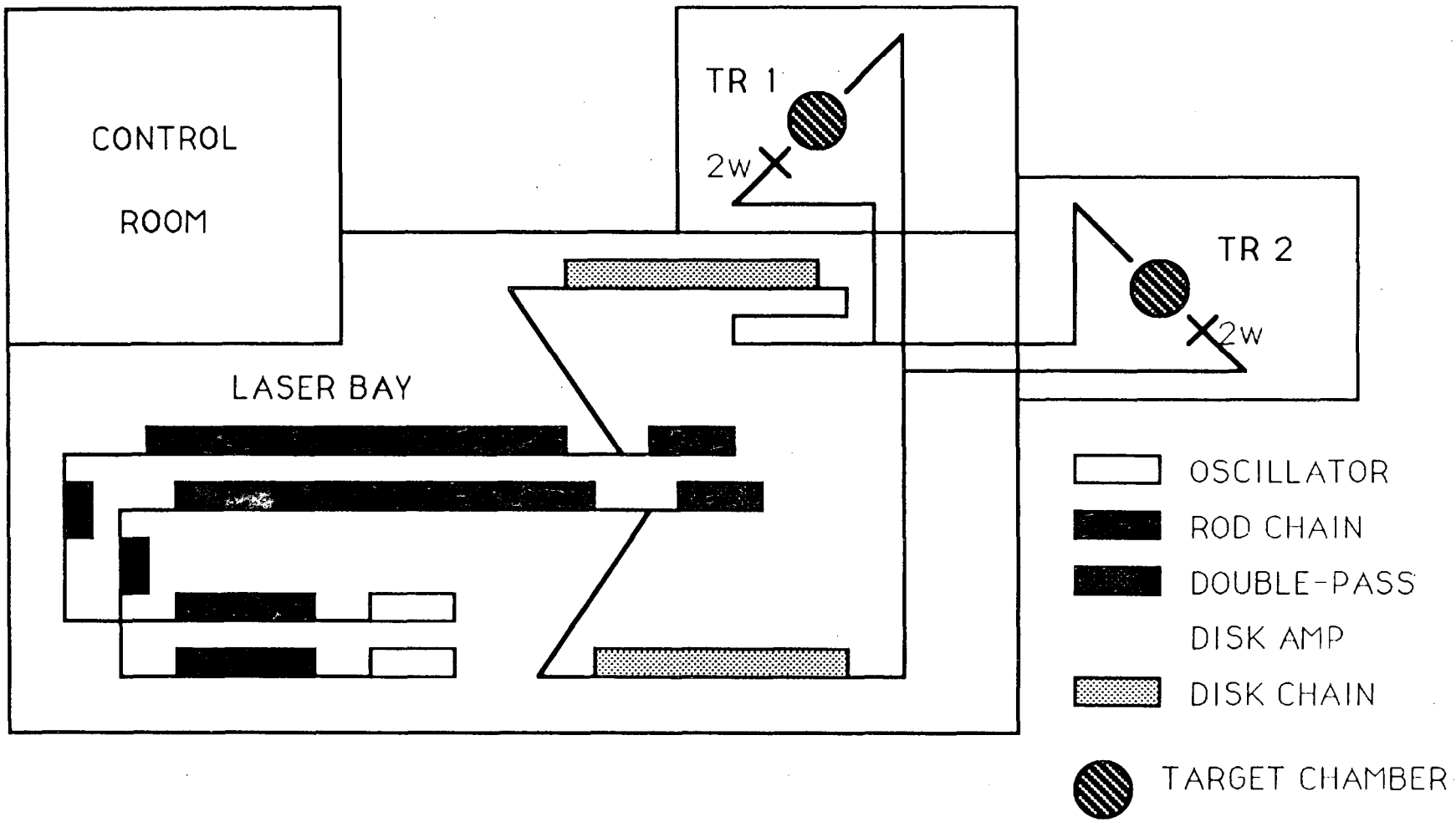
CONTROL
ROOM
TR 1
2w
TR 2
2w
LASER BAY
OSCILLATOR
ROD CHAIN
DOUBLE-PASS
DISK AMP
DISK CHAIN
TARGET CHAMBER

Fig. 7

Figure 8. The laser bay of LLNL JANUS laser system

This view looks down the rod chain on the left, foreground, and right. The oscillator is also on the right. The laser beam(s) enter Target Room 1 through portholes in the left wall near the door next to the rear wall or they may enter Target Room 2 through portholes in the rear wall on the left.

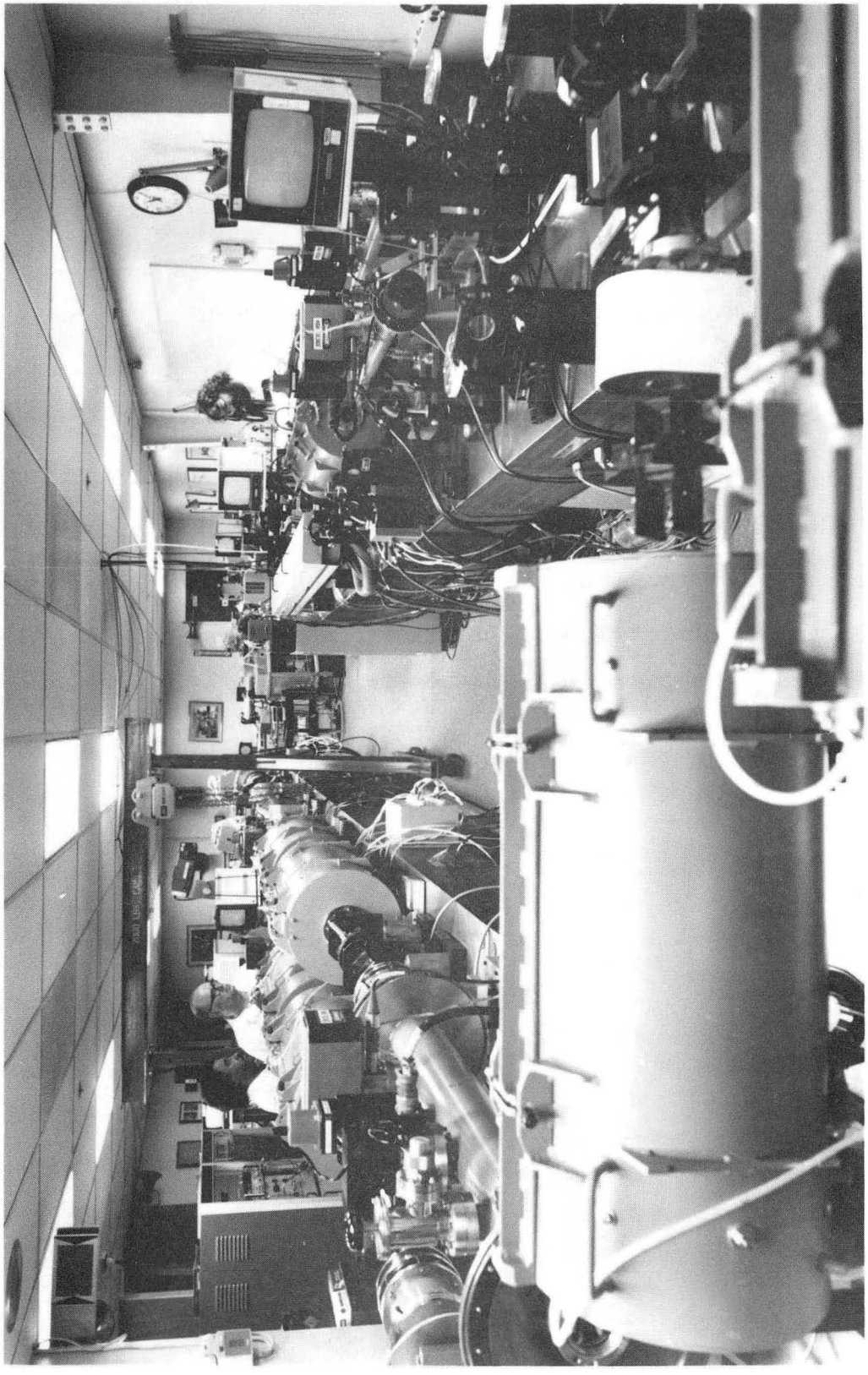

CBB 893-2074

Fig. 8

Figure 9. Target Room 1, LLNL JANUS laser system

The beam enters the room through portholes in the left wall just off the photograph. The beam may be reflected into a set of optics in the corner, where it is again reflected and aligned into the target chamber. The vacuum vessel is the target chamber. The box on the left wall is part of the safety interlock system and provides the experimenter with the status of laser system for the room. A turbomolecular pump is underneath the target chamber. The television camera above the electrical box on the rear wall provides a view of the room which is sent back to the control room. This is another safety measure.

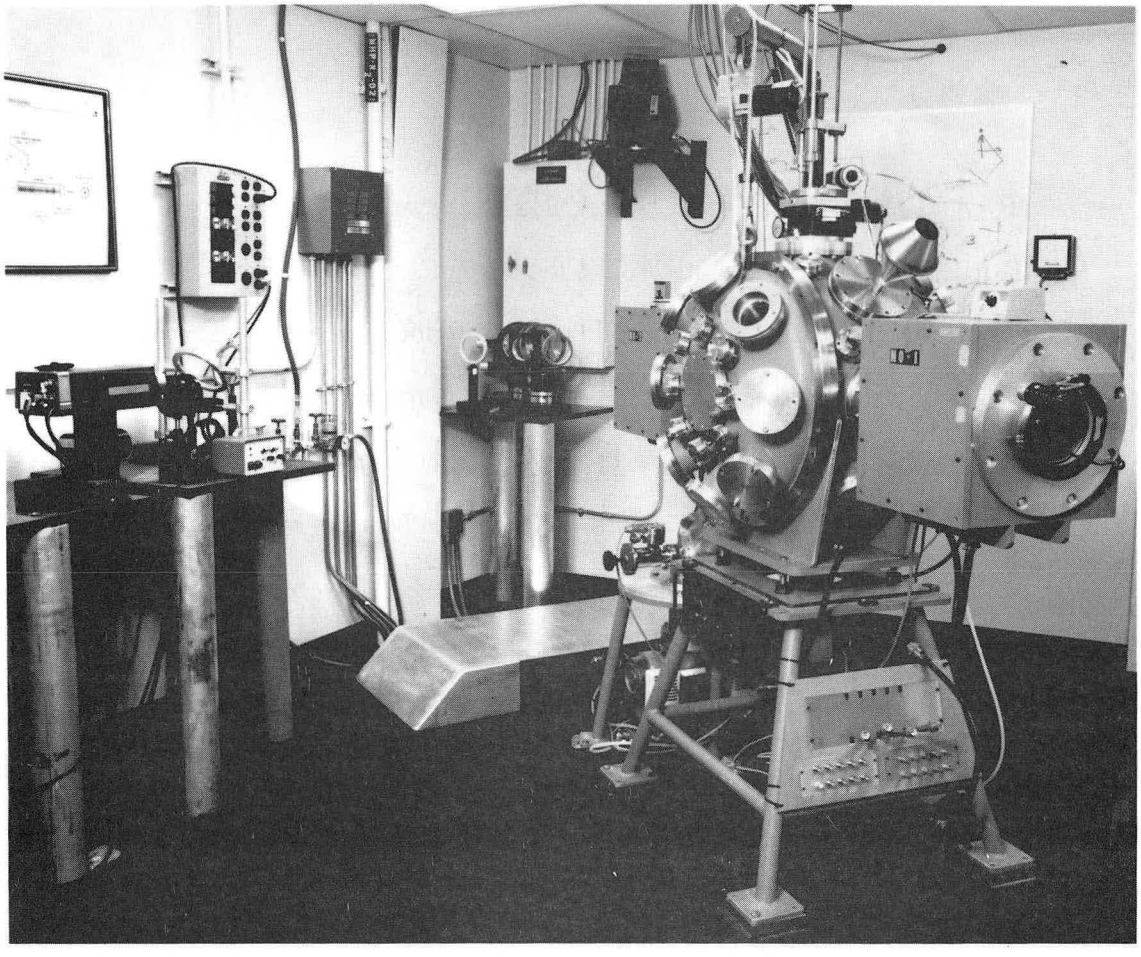

CBB 893-2076

Fig. 9

Figure 10. Target Room 2 of LLNL JANUS laser system

The beam(s) enter the room through the porthole(s) in the rear wall. The paddle, which is covering the portholes, is part of a safety interlock system. The box above the portholes provides the status of the laser system for the room. The laser beam(s) may be reflected by the mirrors on the left table to the right table. The beam is then reflected and aligned into the target chamber, the vacuum vessel. The beam(s) may pass the left table and be reflected by mirrors on a table on the left and out of view of this photograph. Upon reflection, the beam travels through the 2ω (frequency doubler) crystal, where it is converted into green light, and enters the target chamber. Assorted electronics to measure the energy is seen below the target chamber.

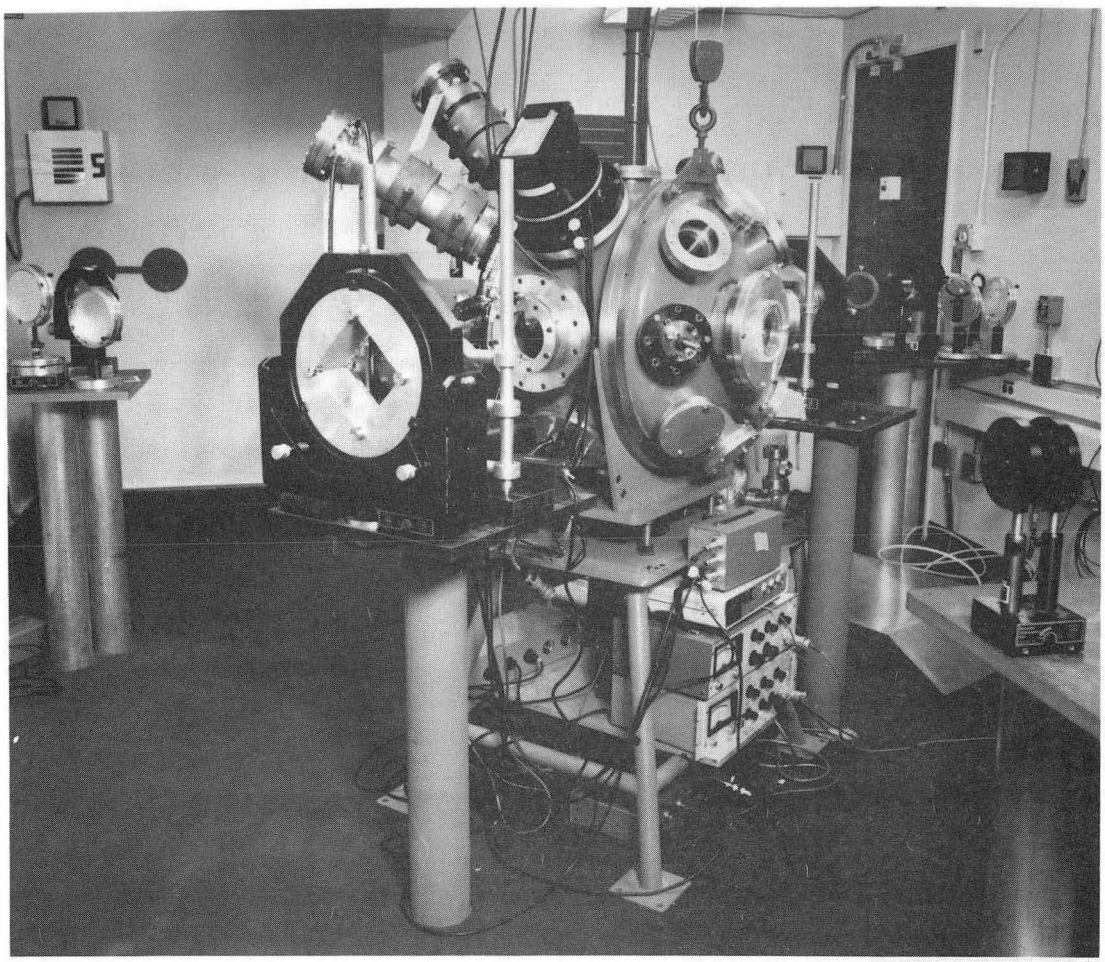

CBB 893-2078

Fig. 10

pulse is 1 nanosecond. Figure 7 diagrams the LLNL JANUS laser system. Figures 8, 9, and 10 illustrate the laser bay of the LLNL JANUS laser, target room 1 and target room 2 respectively.

b). Gas puff z-pinch plasma sources

The operation of a gas puff z-pinch source starts with a fast valve being opened to allow gas to pass through an annular nozzle and form a gas jet. A capacitor bank is discharged and releases an electrical current of 500 kA or more through the annular gas column. A magnetic field is created around the gas. The magnetic field, acting as a magnetic bottle, insulates the plasma from the container walls and radially compresses the plasma. The compressive force is inversely proportional to the plasma radius, which implies that the compressive force increases as the plasma is pinched. This procedure creates a very high temperature plasma which emits thermal radiation in the soft x-ray region. The spectrum and line emission is dependent upon the mass and atomic number of the gas. A typical cylindrical pinched plasma is 0.5 to 4 mm long and has a diameter of 1 mm. Approximately one fifth to one fourth of a kilojoule of energy in the argon continuum has been observed in the 300-500 eV x-ray ultraviolet region. The LEXIS III, an imploding gas jet plasma source manufactured by Maxwell Laboratories, San Diego, CA, provides a 100 ns pulse in the 300-500 eV x-ray ultraviolet region (**Pearlman 1985a, b**). Figure 11 illustrates the imploding gas jet plasma system used in the LEXIS apparatus, manufactured by Maxwell Laboratories (**Riordan 1981**).

3. SYNCHROTRONS

Synchrotrons are sources that provide continuous, high intensity radiation. The typical particle accelerated in today's light sources is the electron. Synchrotron radiation is emitted by relativistic particles, usually electrons, traveling in a circular orbit and following the arc of a dipole magnet. This radiation, sometimes termed magnetic bremsstrahlung (**Landau 1975**), is emitted tangentially to the electron orbit. The shape of the dipole radiation is determined by the velocity and acceleration the electron experiences (**Landau**

Figure 11. The imploding gas jet plasma system used in the LEXIS apparatus

A fast valve is opened and gas passes through the annular cylindrical gas jet to form a gas jet as seen in the end view. A capacitor bank is discharged and releases a current of 500 kA or more through the cathode. The current travels along the cathode into a wire that is at the center of the gas jet. The current returns through the current return post. A magnetic field is created around the gas. The magnetic field, acting as a magnetic bottle, insulates the plasma from the container walls and radially compresses the plasma as seen by the arrows in the end and side views. This procedure creates a very high temperature plasma which emits radiation in the soft x-ray region. LEXIS stands for Low Energy X-ray Illumination System and is manufactured by Maxwell Laboratories, San Diego, CA **(Riordan 1981)**.

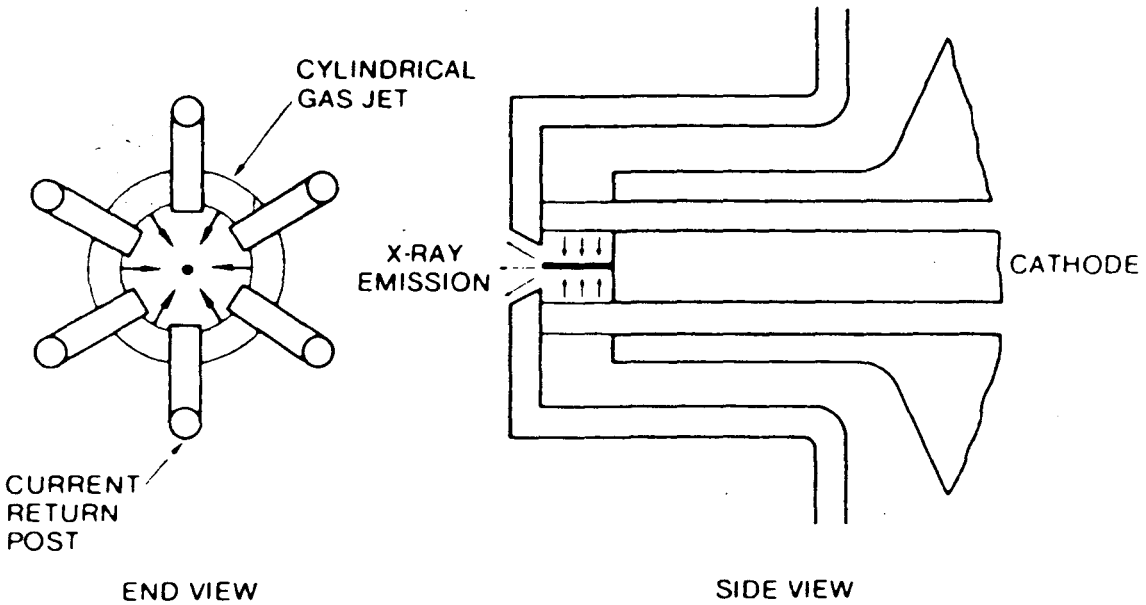
CYLINDRICAL
GAS JET
X-RAY
EMISSION
CATHODE
CURRENT
RETURN
POST
END VIEW
SIDE VIEW

Fig. 11

1975, Jackson 1975). At $v_e << c$, the radiation pattern appears in a dipole form, but as v_e --> c, a highly anisotropic angular distribution occurs with radiation concentrated in the plane of the orbit.

There are two methods to generate synchrotron radiation. The first and most common is to use a bending magnet. As the electron path is bent, the electron experiences a change in direction of its velocity and thus it accelerates. Radiation is emitted tangentially to the bending magnet. A key parameter for bending magnets is the critical wavelength, λ_c. λ_c (nm) = 1.86/B(T)E^2(GeV) where B is the magnetic field strength in units of Tesla and E is the electron energy given in units of GeV. The spectral intensity is relatively constant for $\lambda > \lambda_c$ and drops off rapidly when $\lambda < \lambda_c/3$. The other method is to insert a periodic magnetic structure such as a wiggler into the electron path. A wiggler magnet produces a magnetic field that alternates in polarity and causes an electron to wiggle transversely. Electrons traveling through a wiggler magnet radiate due to the transverse acceleration they experience. The radiated flux per unit solid angle is greater using wigglers than bending magnets. Wigglers may also operate at higher magnetic fields than bending magnets and thus may be used as a source of harder x-rays **(Krinsky 1988).** A characteristic parameter is the maximum angular deviation, K, which is dimensionless. K = 0.934 B_0(T)λ_u(cm), where B_0 is the peak magnetic field strength of the wiggler and λ_u is the magnet period in units of cm. The other periodic magnetic structure is an undulator. An undulator is very similar to a wiggler however K is small (≤ 1) when compared to K of a wiggler (typically ≥ 10) **(Kim 1986).** The spectral brightness is several orders greater than that produced by wigglers or bending magnets. Also undulators are able to generate soft x-rays, 3 - 1000 eV **(Attwood 1988).**

Synchrotron radiation has a broad spectral distribution and monochromators must be used to filter out the desired radiation. A discussion concerning monochromators may be found in the Handbook of Synchrotron Radiation, ed. H. Winick, or the Synchrotron Light Source Handbook by G. Williams, Brookhaven National Laboratory.

4. X-RAY LASERS

An ideal source of coherent x-rays is the x-ray laser. The laser operates in one of two manners. First method, two high energy laser pulses firing from opposite sides strike a thin foil, either selenium, used in this example, yttrium or molybdenum. The thin foil vaporizes to form a plasma. A collisional excitation occurs within the selenium plasma. The photons emitted stimulate a lasing action (**Matthews 1988**). The temperature of the plasma reaches 10^7 ^oK. The dominant emitted wavelengths are 20.6 and 20.9 nm. The pulse length is ~200 psec and the output energy is 0.5 mJ (**Matthews 1985, Rosen 1985**). The other method focuses a CO_2 laser onto a carbon disc, which is located in a strong magnetic field (up to 90 kG). The CO_2 laser produces a maximum energy 1 kJ and a 75 nsec pulse. A long thin plasma is formed. Most of the stimulated emission, which has a wavelength, λ = 18.2 nm , is transmitted along the plasma axis (**Suckewer 1985, Suckewer 1986**). Though x-ray lasers are high intensity sources, 5 $X10^{12}$ W/cm^2, they have yet to reach the wavelengths of interest, the soft x-rays within the "water window".

5. FREE-ELECTRON LASERS

Free-electron lasers, FELs, are expected to become the new high brightness x-ray source, especially in the soft x-ray region. FELs are extremely adaptable, highly efficient, tunable to any wavelength, operate at high power, and produce coherent radiation. FELs operate in the following manner: electrons in the form of a beam are accelerated by a linear accelerator module. The beam passes through a cavity where a periodic magnetic structure produces an alternating magnetic field. Electrons interact with the magnetic field to amplify an incoming light beam. The electron velocity and the magnet period length determine the wavelength of light amplified. Magnitude of transverse electron beam motion produced by the periodic magnetic structure determines the amplification of the light beam by the electrons . Light amplification occurs when an electromagnetic wave traveling through the cavity in the same direction as the electrons receives energy from the electrons. The electrons give up their energy when passing through the alternating magnetic field

(Freund 1989). The principle that led to the theory of FEL operation was originally described by **Motz** (1951), who calculated the emission spectrum of an electron beam in an undulating magnetic field. **Motz** and co-workers (1953) obtained coherent amplification at millimeter wavelengths. In 1971, **Madey** conceived the idea of a FEL operating in the x-ray region. Madey successfully built the first FEL at Stanford using a helical wiggler to generate the magnetic field and an electron beam from a linear accelerator to amplify the output of a 10.6 μm CO_2 laser **(Deacon 1977)**.

D. COMPARISON OF SOFT X-RAY CONTACT MICROSCOPY WITH CHARGED-PARTICLE MICROSCOPY

A comparison of soft x-ray contact microscopy with charged-particle or heavy-ion microscopy (hereafter, called heavy-ion microscopy) will demonstrate the effectiveness of the former technique. The technique of heavy-ion microscopy is very similar to soft x-ray contact microscopy. Biological material is prepared and placed onto a resist material, which is sensitive to heavy ions. The resulting sandwich is exposed to a heavy ion beam, with the biological material in front of the resist. After exposure the biological material is removed, either physically as with tissues **(Yang 1978)** or chemically as with dehydrated cells (typical cell remover was sulfuric acid) **(Kraft 1981)**. The resist is developed in an etching solution to yield a replica of the biological material. Hydrofluoric acid etched mica resists **(Kraft 1981)**, and dicel (cellulose nitrate) resists were etched by a 6.25 N NaOH solution **(Yang 1978)**. This replica is coated with a thin conducting layer such as 10 nm AuPd and read in the SEM. Figure 12 illustrates the technique of heavy-ion microscopy.

The common features of both techniques, soft x-ray contact and heavy-ion microscopy, are the contact methods, use of resist materials, irradiation geometry, etching process and readout methods. Both techniques require some sample preparation and the application of biological material such that the cells are in contact with the resist. The resists, which are usually plastics or polymer chains, must be sensitive to the appropriate

Figure 12. The general technique of heavy-ion microscopy

This diagram illustrates the procedure for obtaining a replica of a biological specimen by the use of heavy ion beams. The replica is then readout by SEM. **(Kraft 1981)**

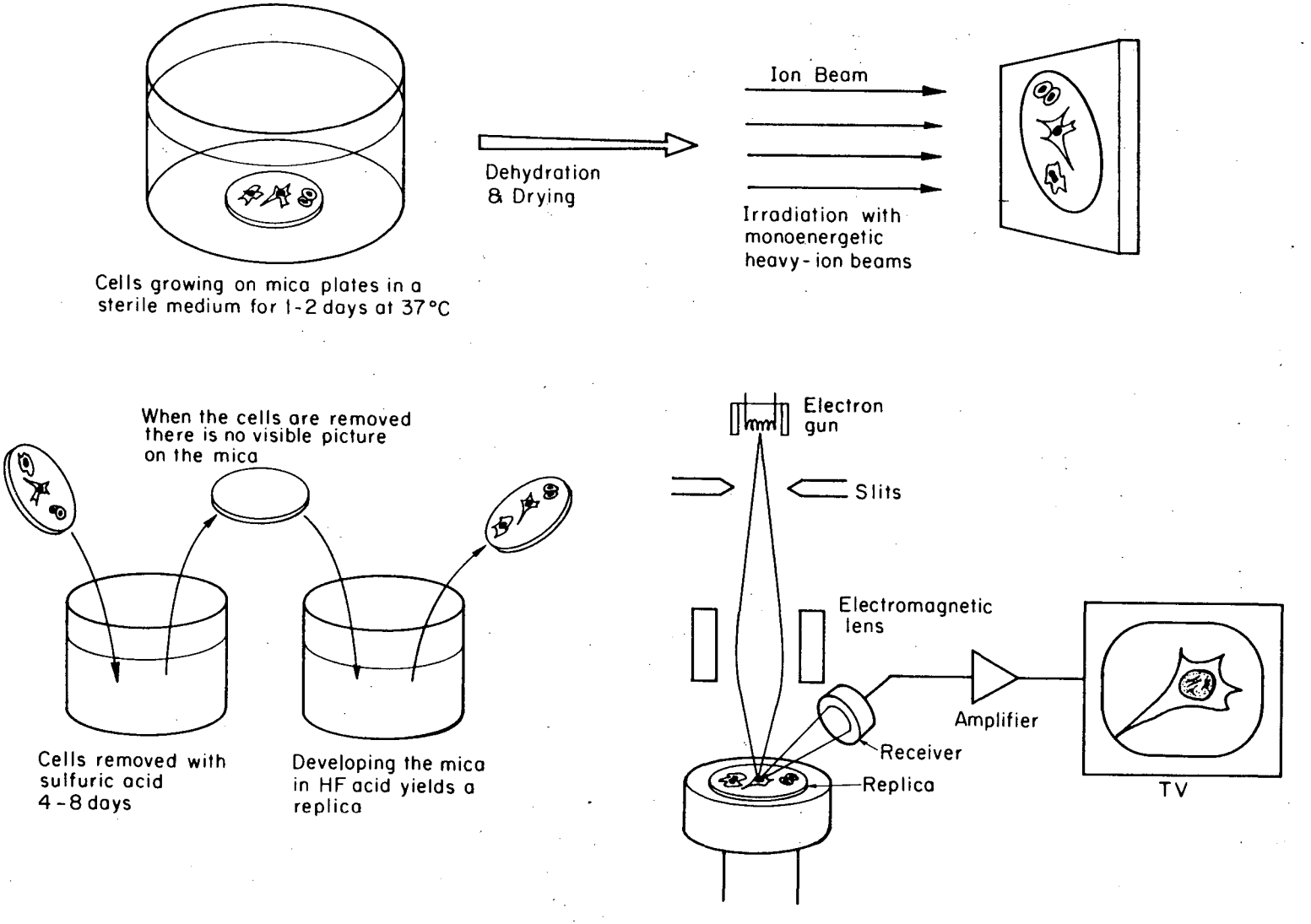
Cells growing on mica plates in a sterile medium for 1-2 days at 37°C
Dehydration & Drying
Ion Beam
Irradiation with monoenergetic heavy-ion beams
When the cells are removed there is no visible picture on the mica
Cells removed with sulfuric acid 4-8 days
Developing the mica in HF acid yields a replica
Electron gun
Slits
Electromagnetic lens
Amplifier
Receiver
Replica
TV
XBL 809-3699

Fig. 12

radiation beams and yield a reasonable resolution. The irradiation geometry is similar for both techniques in that a sandwich of the biological material is created. The beam passes through a window (very thin mylar for heavy-ions and Si_3N_4 for soft x-rays) if we are imaging living or wet cells, the biological material, and interacts finally with the resist material. In both methods, the polymer bonds are broken to yield chains that can be etched away. Once development has occurred, a replica is produced and must be read by electron microscopy **(Kraft, 1981)**.

An interesting aspect is the differences. The most apparent difference lies in the type of radiation used and their interaction with matter; the former defines penetration ability while the latter affects the contrast mechanism, especially the ability to differentiate between carbon, nitrogen and water. Other dissimilarities are the type of resist materials, the etchers or developers, which are dependent upon the resist material, resolution factors, total dose required, and the ability to image living or wet biological specimens. Heavy ions are more energetic than soft x-rays (~1 MeV versus 277 to 525 eV). However, the penetration depth, 10 μm, within biological material is approximately the same for both heavy ions used by **Yang (1978)** and soft x-rays, V_{L_α}. A heavy ion interacts with matter such that the deposition of most of its energy occurs close to a particular depth or range as seen in the Bragg peak graphs. These interactions are almost entirely dependent upon electron density and have no nuclear discrimination. The characteristics of the Bragg peak graphs of heavy ions, at a particular energy, in carbon, nitrogen, or oxygen are very similar. Using these graphs, it is very difficult to find a contrast or attenuation coefficient difference between carbon, nitrogen and water. Soft x-rays interact with the biological material and resist via the photoelectric effect, which is a Z and energy-dependent mechanism **(Dyson 1973)**. The "water window" as previously discussed provides a contrast mechanism to image carbon and nitrogen against water. CR-39, cellulose nitrate or mica appear to be good detectors for heavy-ion microscopy **(Blakely 1982, Phillips 1984)**, however, soft x-ray contact microscopy technique requires the use of a low

molecular weight polymer resist, such as PMMA, copolymer, or terpolymer. Since each microscopy technique uses different resists and the resist governs the appropriate etcher or developer, the action of hydrofluoric acid (for mica) or sodium hydroxide (for cellulose nitrate) used in heavy-ion microscopy is similar to MIBK or ethyl cellulose acetate used in soft x-ray contact microscopy. Resolution factors are beam dependent for heavy-ion microscopy. Longitudinal or depth resolution is dependent upon the range spread of the heavy-ion beam. Lateral resolution is highly dependent upon multiple scattering, one of three important physical factors affecting heavy-ion microradiography image quality (**Yang 1978**). The resolution of soft x-ray contact microradiographs is affected by fresnel diffraction effects of an edge (this is a wavelength dependent feature) and secondary electron travel within the resist. Both of these factors will be discussed later. Heavy-ion microscopy resolution is currently limited by theory to 40 nm whereas soft x-ray contact microscopy has achieved 15 nm for dried specimens and 30-40 nm for wet or living specimens. The total dose required to make an image with heavy-ion microscopy is about 100 megagray (**Yang 1978**) whereas the minimum dose required for soft x-ray contact microscopy is 10 kilogray (discussion about soft x-ray dosimetry appears below). The last difference is the ability to image wet or living biological specimens. At this time, dried or dehydrated cells and very thin wet plant tissues have been imaged by heavy-ion microscopy. One problem in imaging living or wet biological specimens with heavy ions has been the necessity of placing the sample in a vacuum for irradiation. Soft x-ray contact microscopy of living or wet biological specimens has been achieved by the use of Si_3N_4 thin window technology. The Si_3N_4 thin window can withstand vacuum pressure differences and is reasonably transparent to soft x-rays. More discussion about the use of the thin window technology in the sample chamber will follow later.

Heavy-ion and soft x-ray contact microscopy have a number of similarities, especially in the methods but there are very important differences which affect the final product, the readout of the replica. The most important aspect in this comparison is the

ability to image living or wet biological specimens to a high resolution. This aspect has been achieved with soft x-ray contact microscopy.

III TECHNOLOGY DEVELOPMENT - SOFT X-RAY CONTACT MICROSCOPY STATION

LBL's Soft X-ray Contact Microscopy station (SXCM), which is a conventional laboratory tabletop x-ray source, uses a modified Henke x-ray tube. **Henke** (1961,1962) described the theory and operation of the x-ray tube in relation to its use in x-ray microscopy and microanalysis. In 1975, **Henke** described the construction of the x-ray tube and its performance to do low energy x-ray spectroscopy. Feder and co-workers used an electron bombardment evaporation source, manufactured by Vacuum Generators (VG), England, as a modified Henke x-ray tube to generate soft x-rays for x-ray lithography and microscopy (**Spiller 1976a, b**). LBL's SXCM x-ray source, SOXLIS (SOft X-ray LIne Source), is also a VG evaporation source, Model EG2. SOXLIS is used in the same manner as Feder's apparatus to generate soft x-rays.

A. DESCRIPTION OF THE X-RAY SOURCE (SOXLIS)

1. THEORY OF OPERATION

The theory of operation is illustrated in Figure 13. Electrons are boiled off a filament. The surrounding screen and shroud, which is maintained at a high negative voltage, electrostatically focuses the electrons into the target, a water-cooled grounded anode. The electron bombardment of the target material produces x-rays characteristic of this material. The x-rays exit through a 1/2" hole at the top of the screen (**Spiller 1977**). The spot size made in the target material can be focussed by adjusting the level of the screen, shroud and filament assembly in relation to the hearth. Measurement of the distance from the top of the evaporant to the top surface of the screen could be correlated to the focussing of the spot (**VG 1975**). Spot size is an important factor for determining the resolution of x-ray micrographs due to geometry. This geometric factor is called penumbral blurring. Penumbral blurring is defined as

$$S_p = s(w/D) \qquad \text{Eqn III-1}$$

Figure 13. Schematic and theory of operation of a soft x-ray line source

The electrons are boiled off the filament. They follow the electron trajectory lines shown in this figure because they are electrostatically focussed into the target. The screen and shroud surrounding the target are maintained at a high negative potential. The target is a hearth containing evaporant material or a cap that can be evaporated. It is also a water-cooled grounded anode. The x-rays are illustrated by the dashed arrows pointing upward. The slanted lines below the substrate box indicate resist. S_p is the penumbral blurring, a geometric factor limiting resolution in x-ray microscopy and lithography. Penumbral blurring is defined as $S_p = s(w/D)$ where s is the distance of the specimen to the resist and D is the distance of the source to the specimen. w is the diameter of the spot where the electrons are focussed and the x-rays are emitted.

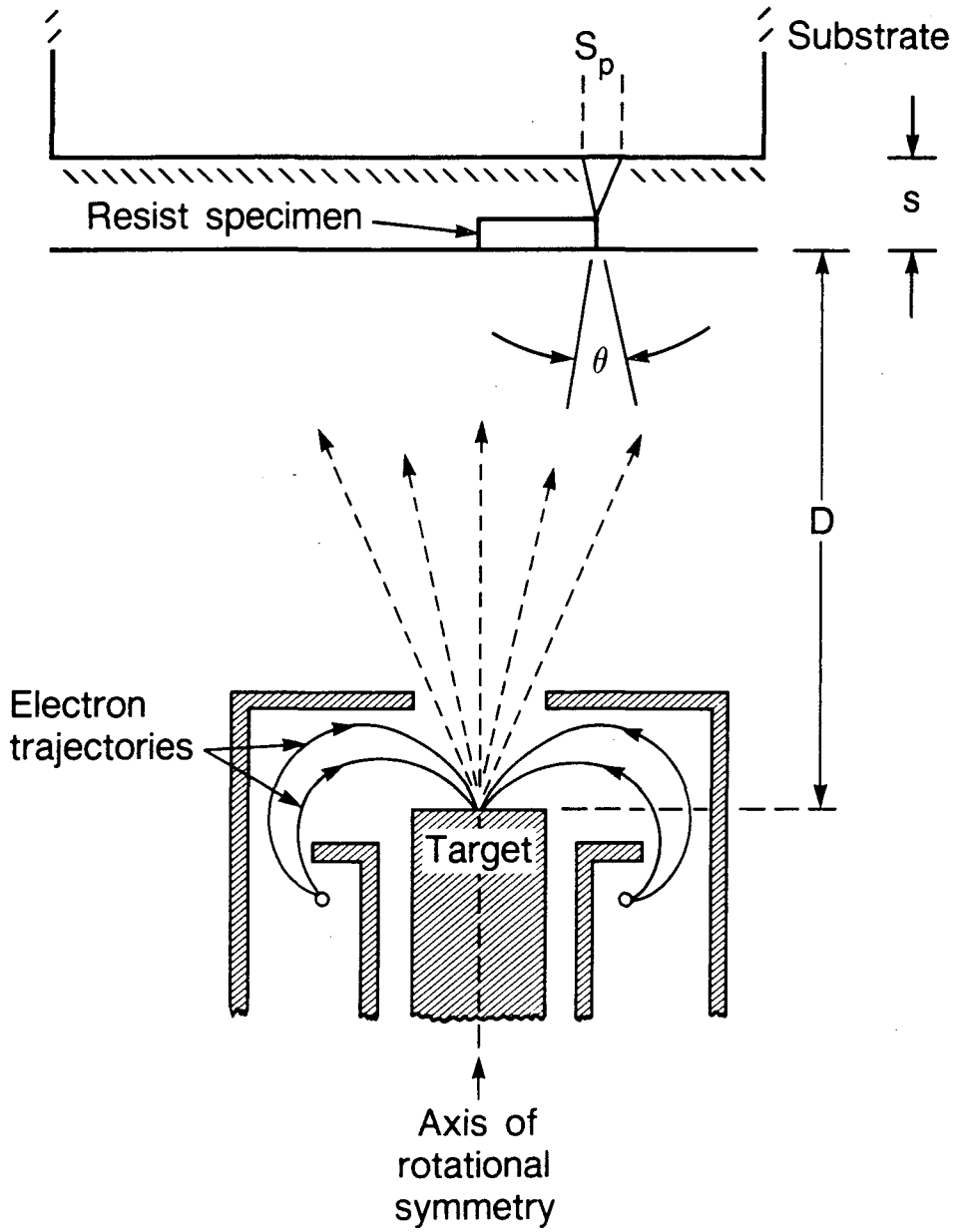
Substrate
S_p
s
Resist specimen
θ
D
Electron
trajectories
Target
Axis of
rotational
symmetry
XBL 867-9850A

Fig. 13

where s is the distance of the specimen to the recording material, in this case, a resist. w is the diameter of the spot size and D is the distance of the source to the specimen. Keeping the anode well-cooled insures that x-rays are produced and evaporation of the target material is kept to a minimum. The power generated by the power supply is kept at constant wattage, with a maximum output of 2 kW. A constant power setting is required so that an evaporant can be evaporated at a constant rate. This condition provides for a stable and constant x-ray flux. The target is a water-cooled grounded anode, that acts as a hearth during evaporation.

2. OPERATING CONDITIONS

The filament is a 0.3 mm (12 mil) diameter thoriated tungsten wire, which is formed into a loop, 1-1/8 in diameter. The maximum rating of the filament is 6 V, 10 A. The emission current is set at 37 mA and the cathode (filament) potential is set at -3500 V when using vanadium as a target material. The cathode potential is set below the energy of the V_{K_α} emission line, 4952 eV **(Vaughn 1986)**. The settings for C_K are 37 mA and -5 kV. The screen and shroud are maintained at least at -1kV and are usually maintained at the same potential as the cathode. The target material, a button, is inserted using silver conducting glue as an adherent into the copper hearth. Sample target materials are carbon, aluminum, and vanadium. The water flow rate to the anode is 6 l/min. Low conductivity water was used in the SXCM. The vacuum pressure is usually maintained at 2 X 10^{-7} torr during evaporation and x-ray generation. This pressure is well below the flashover point, 10^{-5} torr. Flashover, the ignition of any remaining gases within a vacuum vessel, may result in the destruction of SOXLIS by igniting. Figure 17 diagrams the modified SXCM and includes the operating conditions when using a vanadium target. Figure 18 provides a diagrammatic close-up of the evaporation source. Figure 14 is a picture of SOXLIS without the screen in place but with the associated feedthroughs. The focussing mechanism, seen in Figure 14, uses a mini-linear motion feedthrough, (Model No. VF-108, Huntington Mechanical Laboratories, Palo Alto, CA), attached to a support holding

Figure 14.. The soft x-ray line source (SOXLIS) with the screen removed and the associated feedthroughs mounted on a 6" vacuum flange (actual diameter of 8")

Moving left to right on the plate, the first wire from the left electrical feedthrough supplies the filament while the next wire provides a negative potential to the screen and shroud. The next feedthrough is for the focussing mechanism. The focussing mechanism uses a mini-linear motion feedthrough, (Model No. VF-108, Huntington Mechanical Laboratories, Palo Alto, CA), attached to a support holding the filament assembly. The support is two angular aluminum braces with adjustable slots and holes. The center feedthrough is the water-cooled grounded anode. The hearth sits on top of the rod and is cooled by low conductivity water supplied below the plate. The filament is mounted into the filament assembly, which slides on the anode rod and is supported by the focussing mechanism's support. The left wire coming from the right electrical feedthrough acts as a filament current return while the right wire, maintained at - 1 kV or cathode potential, leads to a sample plate that holds the wet cell chamber or specimen. SOXLIS and its associated feedthroughs are mounted on a 6" vacuum flange (with an actual diameter of 8").

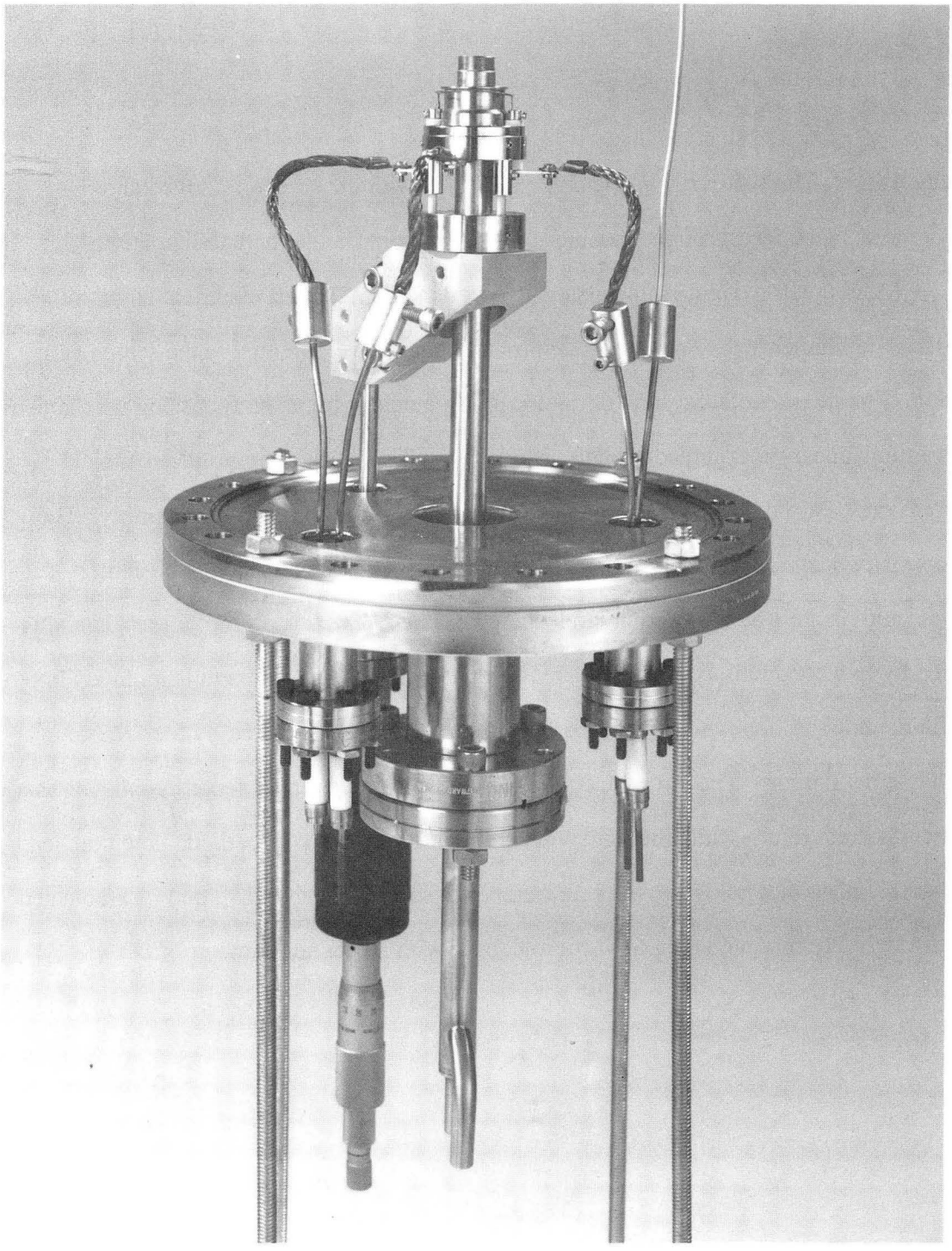

CBB 868-6659

Fig. 14

Figure 15. Interchangeable anodes

The interchangeable anode has a copper hearth at the tip. Left to right, the anodes' hearth is bare, has an aluminum button insert and has a carbon button insert.

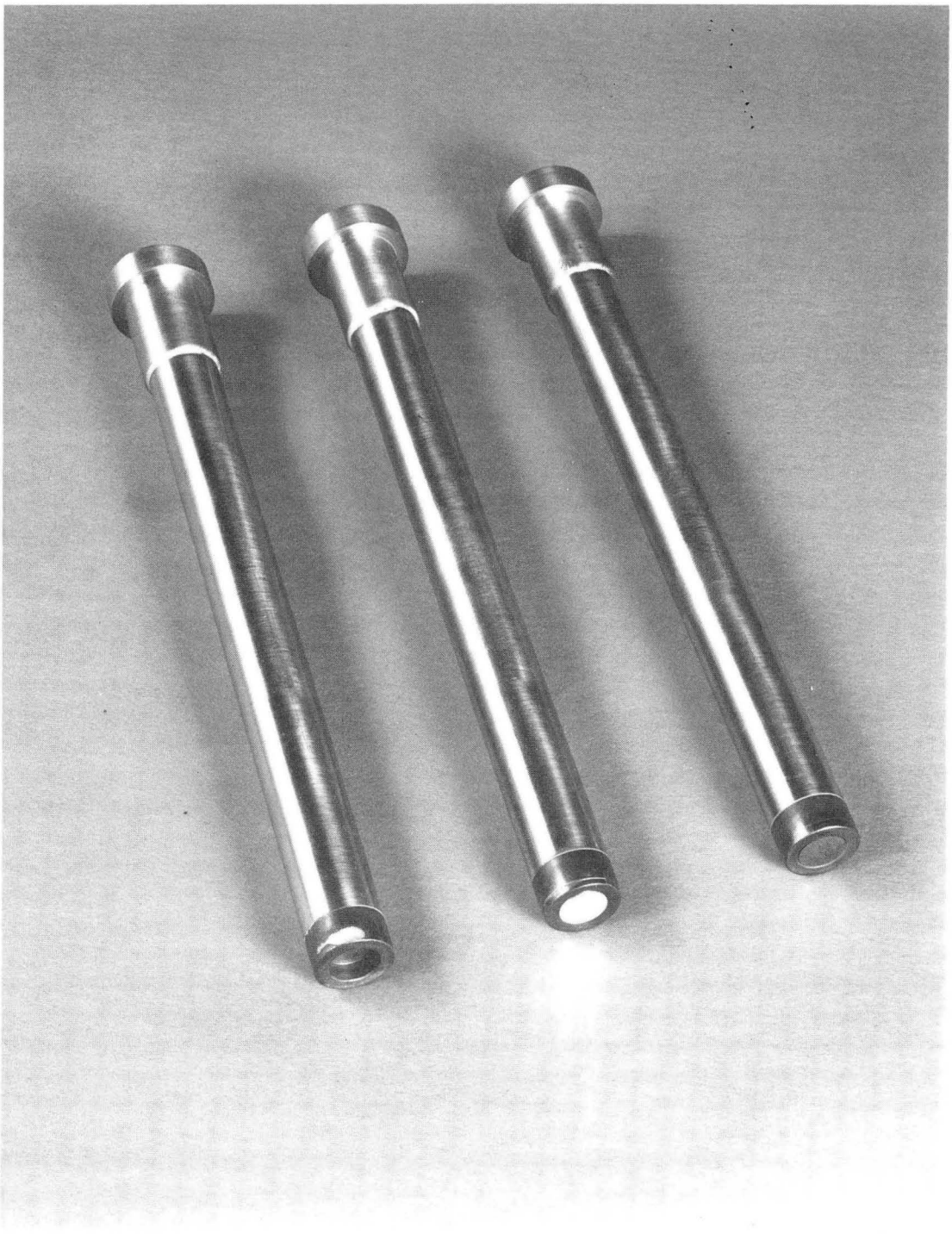

CBB 876-5023

Fig. 15

Figure 16. Modified SOXLIS in operation and modified interchangeable anodes

The viewport shows the hot filament and the screen surrounding the assembly. The target material being used in SOXLIS is vanadium. The other two anodes, left to right, are titanium and copper.

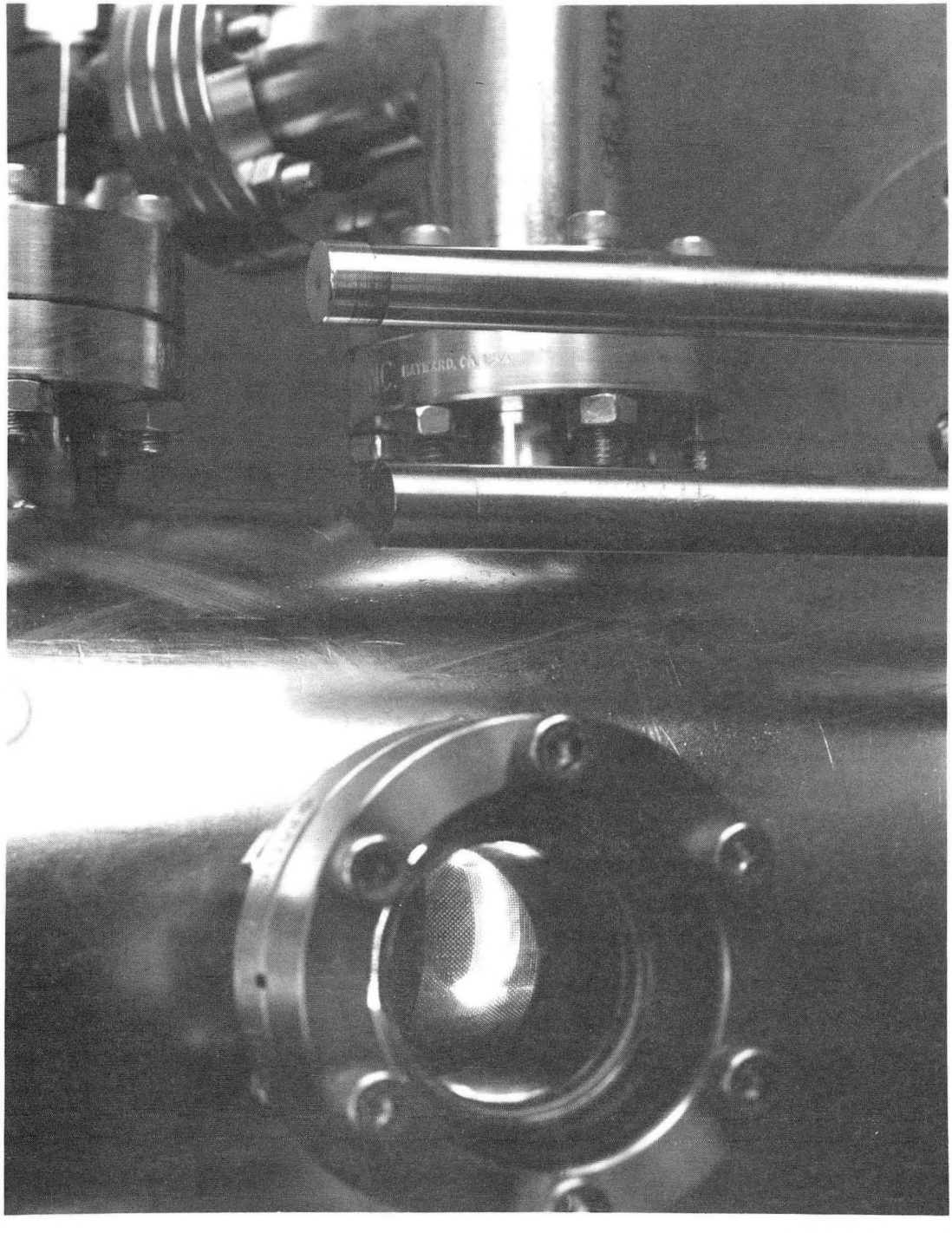

CBB 893-1615

Fig. 16

the filament assembly. The support is two angular aluminum braces with numerous adjustable slots and holes. Figure 19 provides a limited top view of SOXLIS and Figure 15 shows the interchangeable anodes with buttons in their hearths.

3. MODIFICATION OF SOXLIS

SOXLIS was modified to reduce the thermal problems. Heat radiated towards the sample chamber and made the Si_3N_4 thin windows and TEM resists brittle. Reduction of heat radiation was achieved by improving the thermal contact between the target material and the coolant, low conductivity water. New interchangeable anodes were made leaving the copper hearth off and placing a cap that could be screwed onto the rod. The caps were made from vanadium, titanium or aluminum. The seal between the cap and the rod was glued. Figure 16 illustrates the modified anodes and shows SOXLIS in operation.

B. DESCRIPTION OF THE SOFT X-RAY CONTACT MICROSCOPY STATION (SXCM)

SOXLIS is inserted into a cylindrical vacuum vessel, having a diameter, 6", and a length, 15 -1/2 ". The cooling plate is inserted 7-1/4" from the bottom of the vessel. There are four 1-1/2" ports and one 4" port on the vacuum vessel wall. Three of the four small ports are at the same level, giving a view of SOXLIS. The other small port is in-line with one of the small ports but with a view above the cooling plate. A nude Bayard-Alpert ion gauge, Model 580, Varian Inc., Mountain View, CA, is inserted into a tee attached to an elbow that is connected to a small port. A thermocouple is inserted into a flange covering one of the tee's openings. The thermocouple and ion gauge are connected to a Granville-Phillips Series 274 Controller. The large port is for the vacuum pump. The vacuum system is a Balzers TSU170 Turbo-molecular system with a TCF 102 vent valve controller, vent valve and connectors. The turbo-molecular pump has a N_2 volume flow rate (pumping rate) of 170 l/sec and can achieve an ultimate pressure of 10^{-10} mbar. A grounded copper cooling plate is inserted approximately halfway up the vacuum vessel. A 1-1/2" hole is cut into the copper cooling plate to allow x-rays to pass through. The

Figure 17. Schematic of the modified soft x-ray contact microscopy station (SXCM)

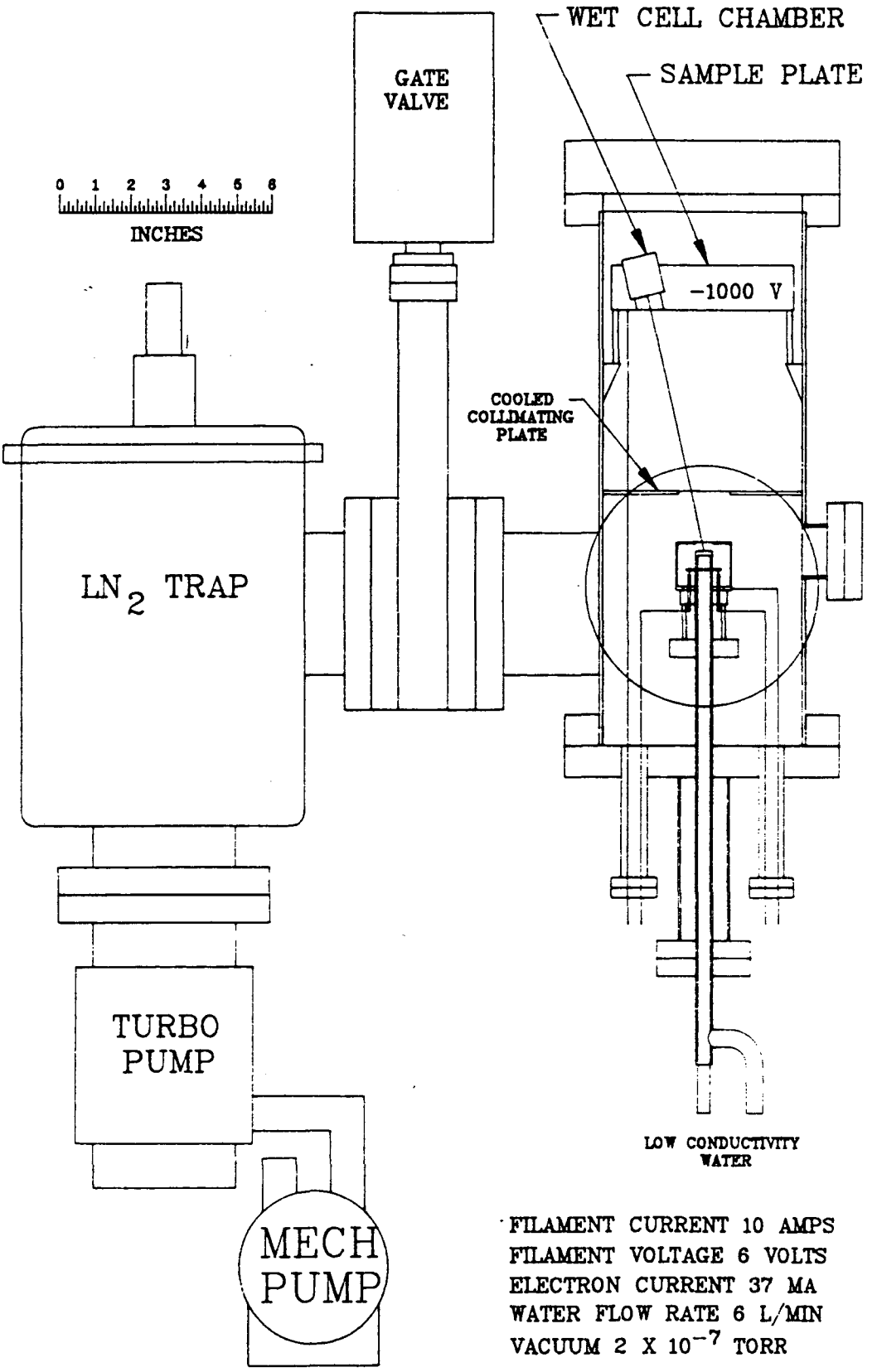
WET CELL CHAMBER
SAMPLE PLATE
GATE VALVE
0 1 2 3 4 5 6
INCHES
-1000 V
COOLED COLLIMATING PLATE
LN2 TRAP
TURBO PUMP
MECH PUMP
LOW CONDUCTIVITY WATER
FILAMENT CURRENT 10 AMPS
FILAMENT VOLTAGE 6 VOLTS
ELECTRON CURRENT 37 MA
WATER FLOW RATE 6 L/MIN
VACUUM 2 X 10-7 TORR

Fig. 17

Figure 18. A close-up schematic of the modified soft x-ray line source (SOXLIS)

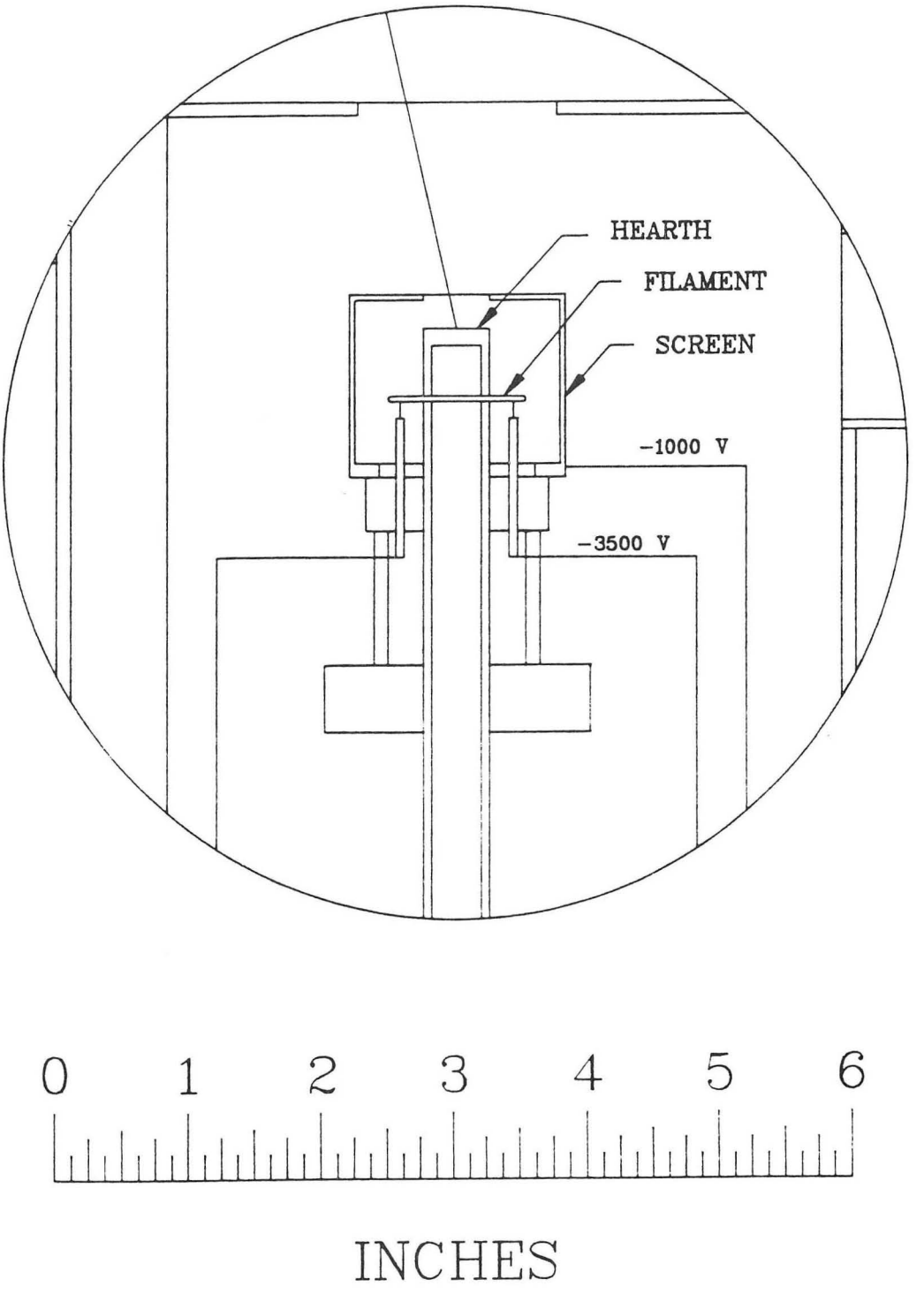

Fig. 18

Figure 19.. Top view of SXCM

This view shows the brackets where the ceramic posts are attached. A ball bolt is inserted into the top of the ceramic post. A sample plate rests on the ball bolt. A copper cooling plate with circular piping is seen below the bracket. A limited view of SOXLIS, the hearth and filament assembly, appears through the hole in the cooling plate.

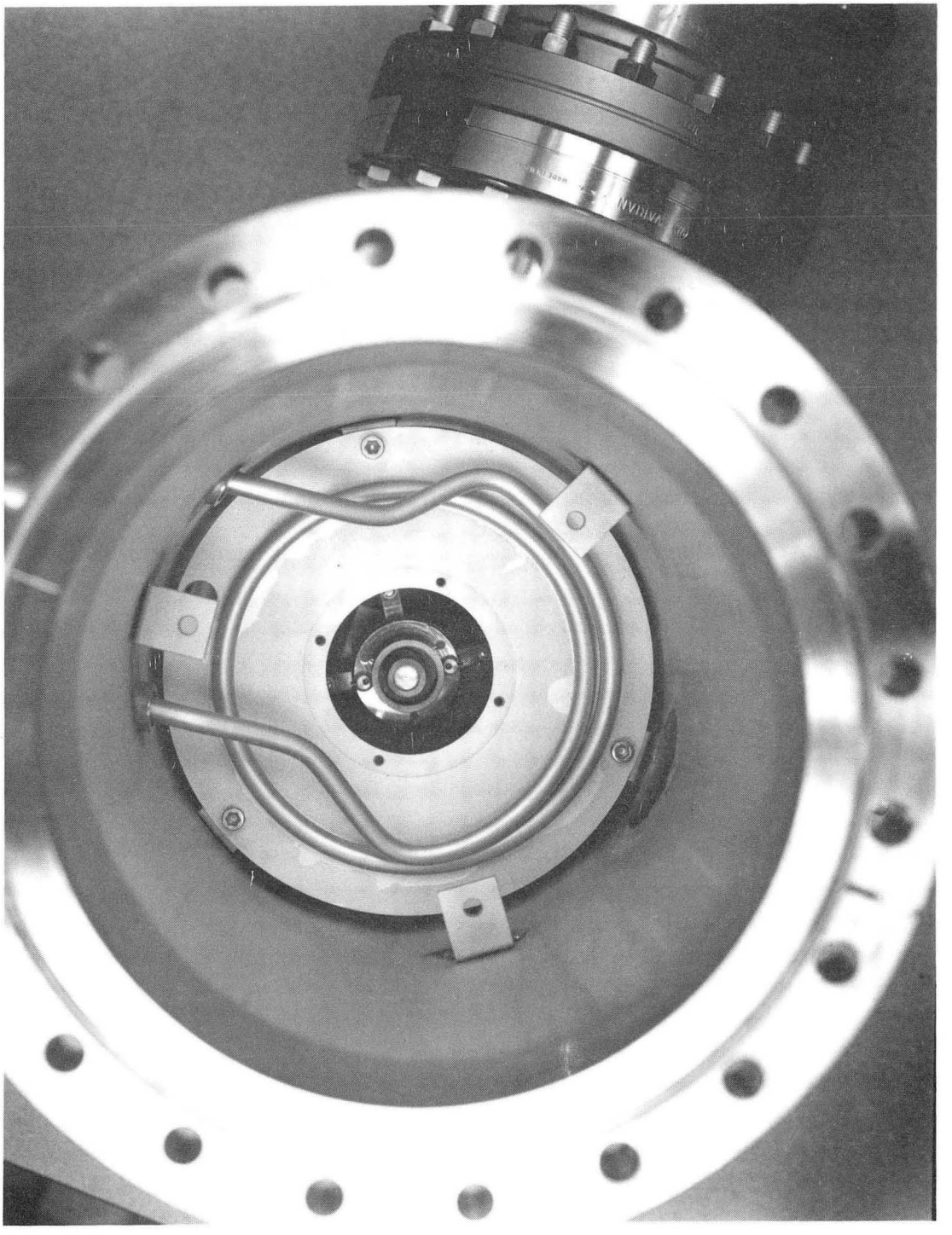

CBB 867-5741

Fig. 19

Figure 20. SXCM in operation

From left to right, the power supply is set for carbon anode operation (5 kV and 37 mA). Next is the safety interlock box. The vacuum vessel, that contains SOXLIS in operation, has the appropriate warning sign and vacuum gauges on the left port. On the right is the vacuum gauge controller. The high voltage leads from the power supply attach to the feedthroughs underneath the vacuum vessel behind the screen door. Low conductivity water is also supplied and returned from the anode via hoses entering beneath the vacuum vessel behind the screen door. The screen door is interlocked with the safety interlock box for safety reasons.

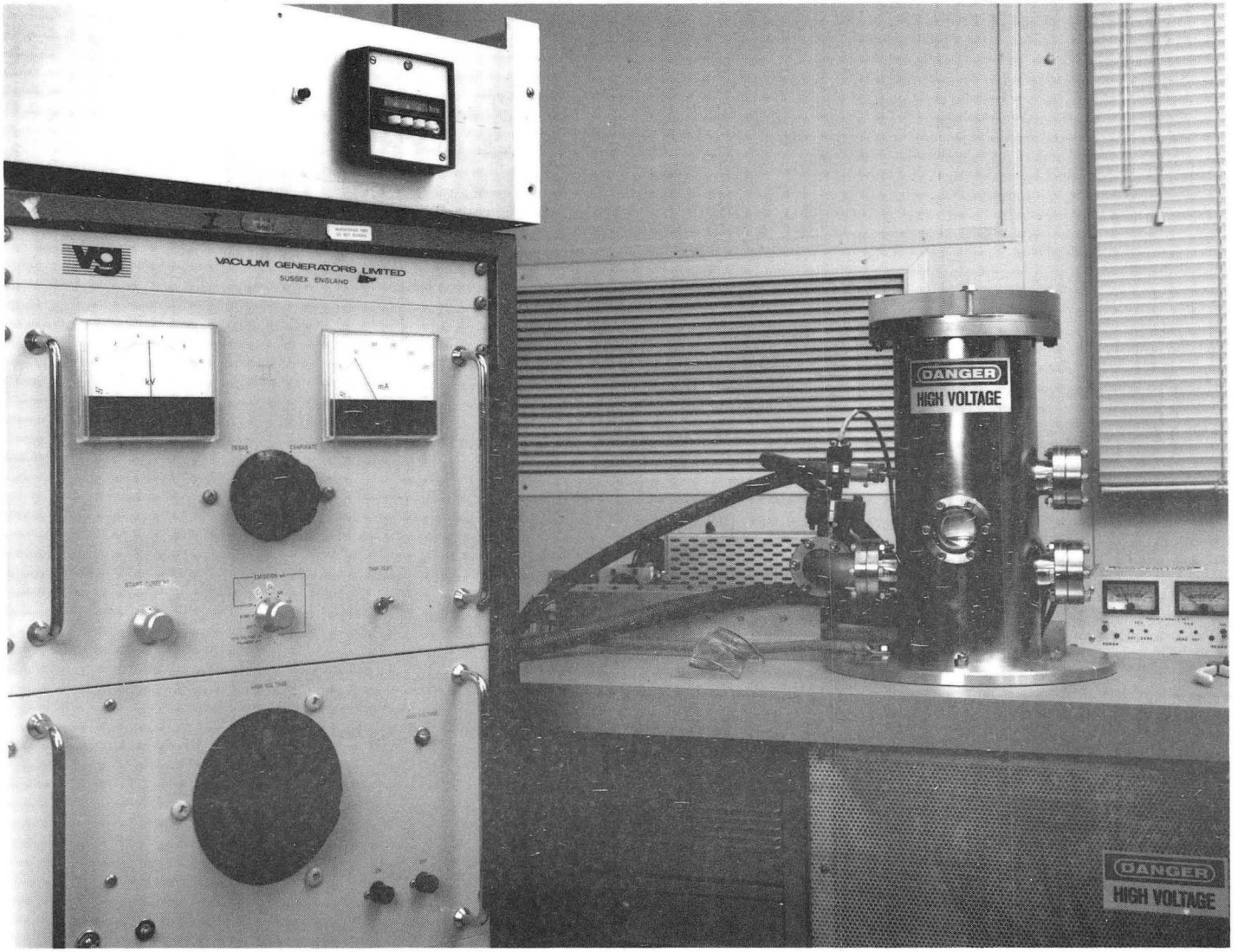

CBB 869-8981

Fig. 20

cooling plate is grounded to attract any electrons that may leave SOXLIS. Figure 19 shows the cooling plate. In order to support a sample plate yet insulate it from the vacuum vessel wall, ceramic posts were bolted onto brackets, set 4-3/4" from the top of the vacuum vessel. The sample plate sat on ball bolts screwed into the ceramic post. A wire, carrying -1 kV or cathode potential, passes through the cooling plate and attachs to the sample plate. Figure 14 shows the wire as part of SOXLIS. The sample plate is maintained at a negative potential to repel electrons that may escape from SOXLIS. Pitting of the resist may occur if electrons are able to impinge upon the resist. Ceramic posts of various lengths could be used to adjust the source-to-specimen distance. To reduce penumbral blurring, the source-to-specimen distance has been maintained at 18 cm.

The safety interlock box is designed to cut off the power to SOXLIS should a breach of safety occur. The connections to the box are from the power supply, the interlock box power supply, a water flow monitor (Model 100C, Proteus Industries, Inc., Mountain View, CA), the back door monitor switch, the front door monitor switch, the vacuum vessel lid monitor switch and the ion gauge controller. The power supply can not be started until all lights are on. This indicates: 1). there is a minimal water flow rate of 6 l/min and a vacuum pressure of 2×10^{-5} torr, 2). the front and back screen doors are closed and 3). the vacuum vessel lid is closed. The first condition is required to prevent flashover of SOXLIS. The second condition prevents electrocution from high voltage wires. The final condition protects the vacuum vessel and SOXLIS. The safety interlock box has a series circuit so that a particular problem can be quickly identified and corrected. As an added safety precaution, all major electrical components of the system are grounded. These components are the power supply, the vacuum vessel, the bottom plate supporting SOXLIS, the safety interlock power supply and the ion gauge controller.

The modifications of the SXCM include an additional roughing pump, a vent valve, a liquid N_2 trap and a gate valve. The gate valve, Series 10, VAT, Switzerland, was inserted between the liquid N_2 trap and the vacuum vessel so that the vacuum system could

Figure 21. The modified soft x-ray contact microscopy station
From left to right, the power supply is set for vanadium, V_{L_α} emission line, anode (3.4 kV and 37 mA). The ion gauge controller sits atop the power supply. Next is the safety interlock box, which is partially covered by the side port holding the thermocouple and ion gauge. The vacuum vessel is safety labelled. A tee is added to the front lower port to accommodate the vent and roughing pump valves. The gate valve and liquid N_2 trap are mounted on the right side of the vacuum vessel. The turbomolecular vacuum pump is mounted beneath the liquid N_2 trap within the screened area.

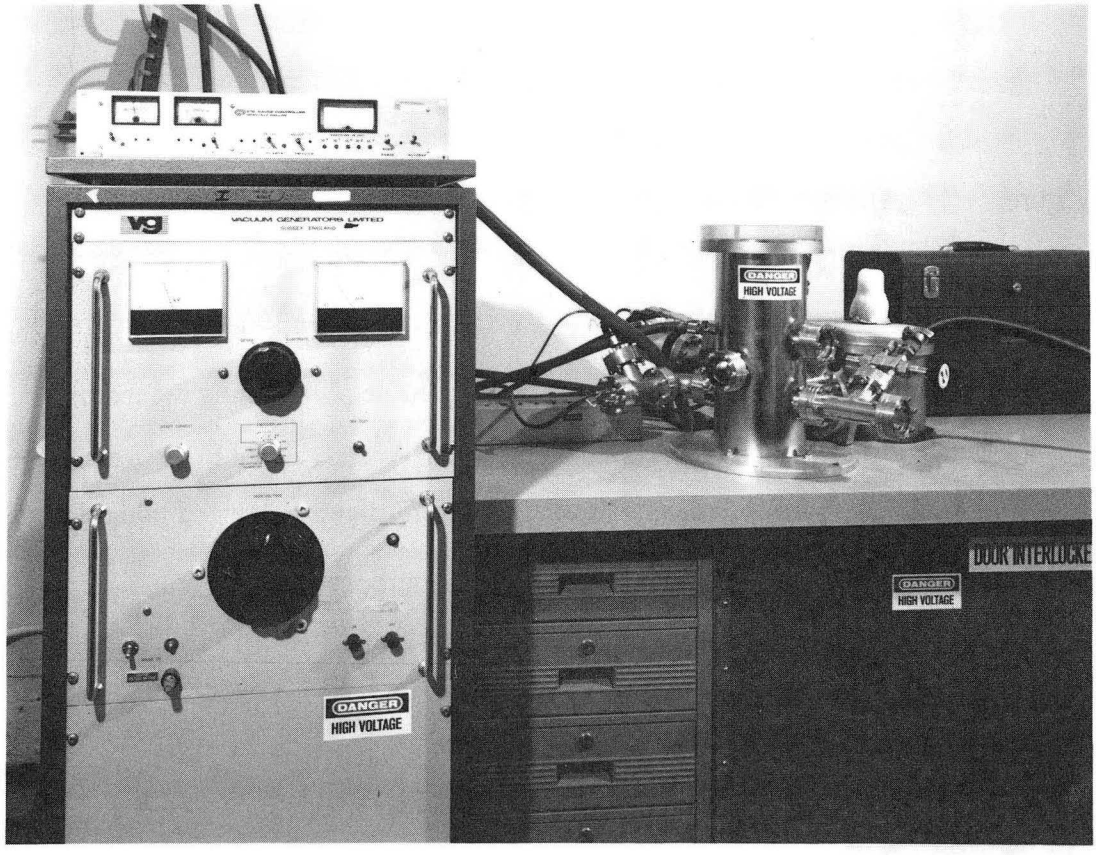

CBB 893-1619

Fig. 21

Figure 22. Close-up of the modified soft x-ray contact microscopy station

From left to right, the side port on the vacuum vessel has a thermocouple and ion gauge. A tee, mounted on the lower front, has a viewing window and a flange holding the vent and roughing pump valves. The black hose goes from the roughing pump valve to the roughing pump. The wire going down the right side of the vacuum vessel from the lid is part of the safety interlock system. The gate valve, which is electro/pneumatically driven, is mounted on the right side of the vacuum vessel and connected to the liquid N_2 trap. The turbomolecular vacuum pump is attached below the liquid N_2 trap.

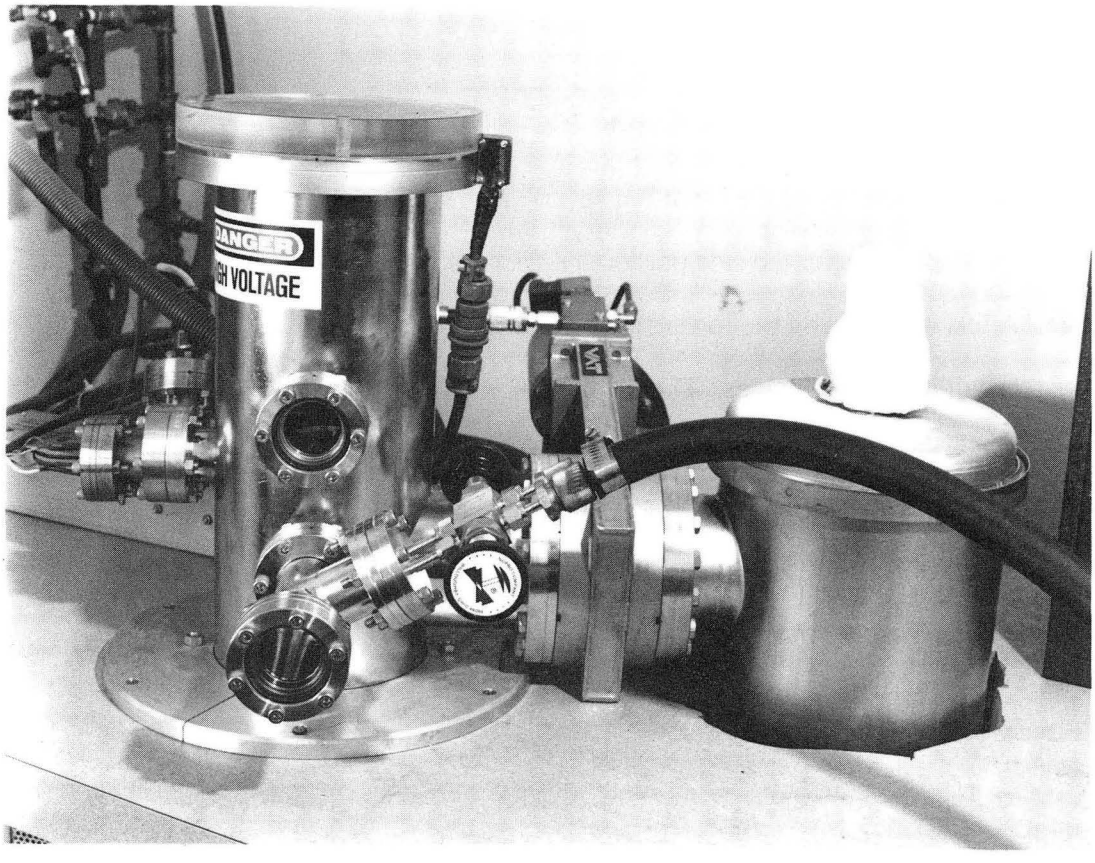

CBB 893-1617

Fig. 22

continue to run without having to be shut down and restarted during a specimen change. To change specimens, the gate valve is closed and the vent valve is then opened slowly to bring the vessel up to air. One changes the specimen and closes the vent valve. The roughing pump valve is opened and the vacuum vessel is pumped down to a pressure of ~50 mtorr. Finally, the roughing pump valve is closed and the gate valve is opened. The vacuum vessel returns to the operating vacuum pressure within 10 minutes. If we add liquid N_2 to the liquid N_2 trap, Nor-Cal, Redding, CA, the vacuum pressure of the system is brought down a whole decade. Also the liquid N_2 trap has an added advantage in that floating oil particulates, mainly carbons, and moisture are removed from the system. Carbons can interfere with the purity of the anode by accumulating on the target. Contaminated anodes help generate a large undesired carbon peak and reduces the intensity of the target material x-ray emission lines sought. An added feature of the liquid N_2 trap is keeping the system cooled, so that the sample plate does not get hot.

C. CHARACTERIZATION OF SOXLIS

The characterization of an x-ray line source consists of the spot size, flux, and spectrum. Measurements of the spot size and intensity were determined using a radiachromic nylon film, which is discussed in Section IV. Penumbral blurring measurements were made using a wire, placed 6 cm from the film and 12 cm from the source. Using Eqn III-1, the spot size was determined to be 2.6 mm. Reduction of the spot size can be achieved by creating a "v" in the target material where the electrons impinge. A spot size of 1.6 mm has been achieved with this method (**Hawryluk 1989**). The flux of SOXLIS is ~3 X 10^8 photons/cm^2-sec. The spectra were recorded by ultraviolet light and x-ray sensitive film, Kodak 101-07, set up in a x-ray diffraction arrangement. In order to record the spectra on the film, the film emulsion is attached to the supporting backing (usually plastic) and not be embedded in a gel, where attenuation will be a problem. The diffraction grating had 1000 lines/mm. The carbon spectrum had a very strong carbon peak with continuum, i. e. peak-to-background ratio was 16.4:1. The

vanadium spectrum had a strong V_{L_α} peak, however, there was a presence of carbon and a continuum, i. e. the V_{L_α} peak: C_{K_α} peak: background was 25.4: 5.2: 1.

IV DOSIMETRY

A. JUSTIFICATION

High doses of soft x-ray radiation are required to make a latent image within a polymer resist, which is then developed and examined by electron microscopy. In order to interpret the resulting image, it is necessary to determine whether the structure of the cell has changed during exposure. This is especially true for long exposure times, i.e. synchrotron exposures of milliseconds or tabletop laboratory source exposures of 6 to 24 hours. The exposure time is not a factor when a z-pinch plasma or laser plasma-induced x-ray source is used. The exposure times for the plasma sources are on the order of nanoseconds. For this latter case and also for other exposures, one would like to know the dose given to the resist so that the appropriate development time and the etching solution concentration can be determined. One would like to know which components of the cell change, how much radiation is necessary to produce the change, and whether the structural changes affect the soft x-ray micrograph. Before these questions may be answered, a dosimetric standard for soft x-ray microscopy must established. The soft x-ray contact microscopy station was calibrated by using radiachromic nylon film which was in turn standardized with a known demountable ultrasoft x-ray cold anode source in Burton Henke's laboratory. The standardization of the film was done in collaboration with Jon Kerner (**Guttmann 1988**).

B. RADIACHROMIC NYLON FILM CALIBRATIONS

The radiachromic nylon film was obtained from Far West Technology, Inc., Goleta, California, USA (Model No. FWT-60-00). It is impregnated with a dye, hexahydroxyethyl aminotriphenylnitrile, which turns blue upon exposure to x-rays or ultraviolet light (**Humphreys 1983**). This film, used primarily within the food industry for calibrating food irradiation machines, has a sensitivity which is well matched to the radiation dose levels (10 to 10^5 gray) typically used in our imaging experiments (**Humphreys 1977**). Figure 23 illustrates this film.

Figure 23. Radiachromic nylon film in a holder

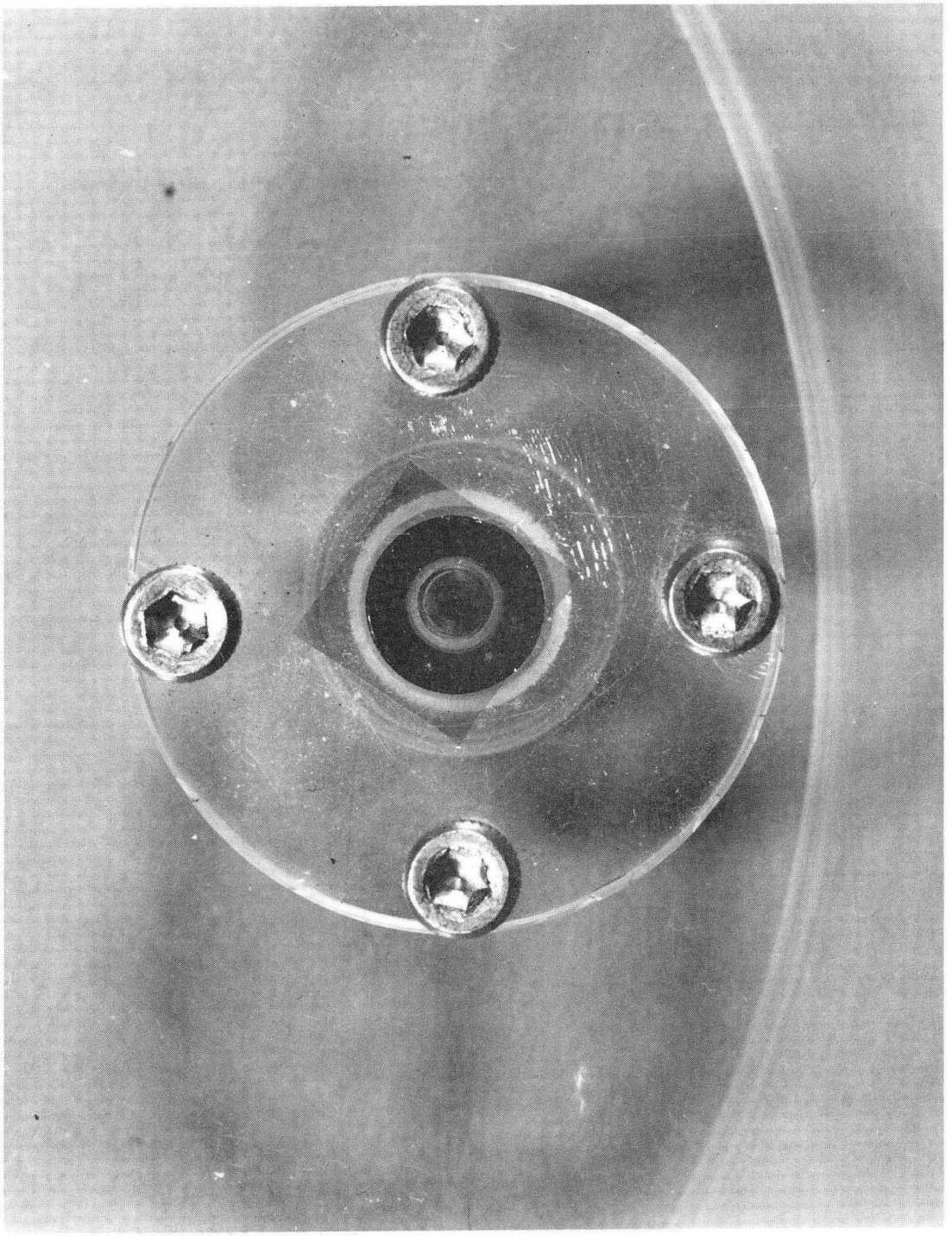

CBB 876-5025

Fig. 23

For calibration, the radiachromic film was exposed to unfiltered characteristic x-ray line radiation from a demountable anode source and the dose was determined using an absolutely calibrated flow-proportional counter (**Henke 1975**). A series of films were placed at different distances from the source and exposed for a fixed time period while the proportional counter measured the integrated flux. Corrections were made for the counter efficiency, transmission of thin windows, and continuum observed in the spectrum of the x-ray line source. The continuum correction was estimated by pulse height analysis.

Two sources of radiation were used. The first was a graphitized copper anode which produced carbon K_α (277eV/4.46 nm) x-rays and a contribution from continuum. The contribution from the continuum for the graphitized copper anode was 20 % of the total dose. The second source was an aluminum anode which produced both oxygen K_α (525 eV/2.36 nm) and aluminum K_α (1487 eV/0.834 nm) lines in an energy flux ratio of 0.2:1, with a continuum contribution amounting to 7 % of the total dose. The anode voltage was maintained at the approximate operating voltage used at the soft x-ray contact microscopy station.

To calibrate the soft x-ray contact microscopy station, the radiachromic nylon film was placed in a holder 18 cm from the x-ray source target. The 18 cm distance is the same as that used to irradiate biological specimens. The films were irradiated for different periods of time to soft x-rays from a carbon source producing carbon K_α x-rays. The operating parameters of the soft x-ray station were 5.0 kV and 37 mA.

The optical density of radiachromic films was read on a densitometer (Model No. FWT-91R, Far West Technology, Inc. , Goleta, CA, USA) before and after irradiation. The film sensitivity required that the optical densities be measured at 510 nm (high scale) and/or 600nm (low scale) (**Humphreys 1977**).

Dose-response curves for the radiachromic nylon film were obtained by plotting the change in optical density at 510nm and 600nm against the absolute dose as seen in Figure 24. The points obtained with the carbon and aluminum anodes virtually fall on

Figure 24. Dosimetry for a radiachromic nylon film

The sources were (■) carbon K_α (277 eV/4.46 nm), (□) aluminum K_α (1487 eV/0.834 nm) and (○) γ rays from ^{60}Co (1.17 MeV and 1.33 MeV). Low (600 nm) and high (510 nm) refer to the wavelength where the film's optical density was measured.

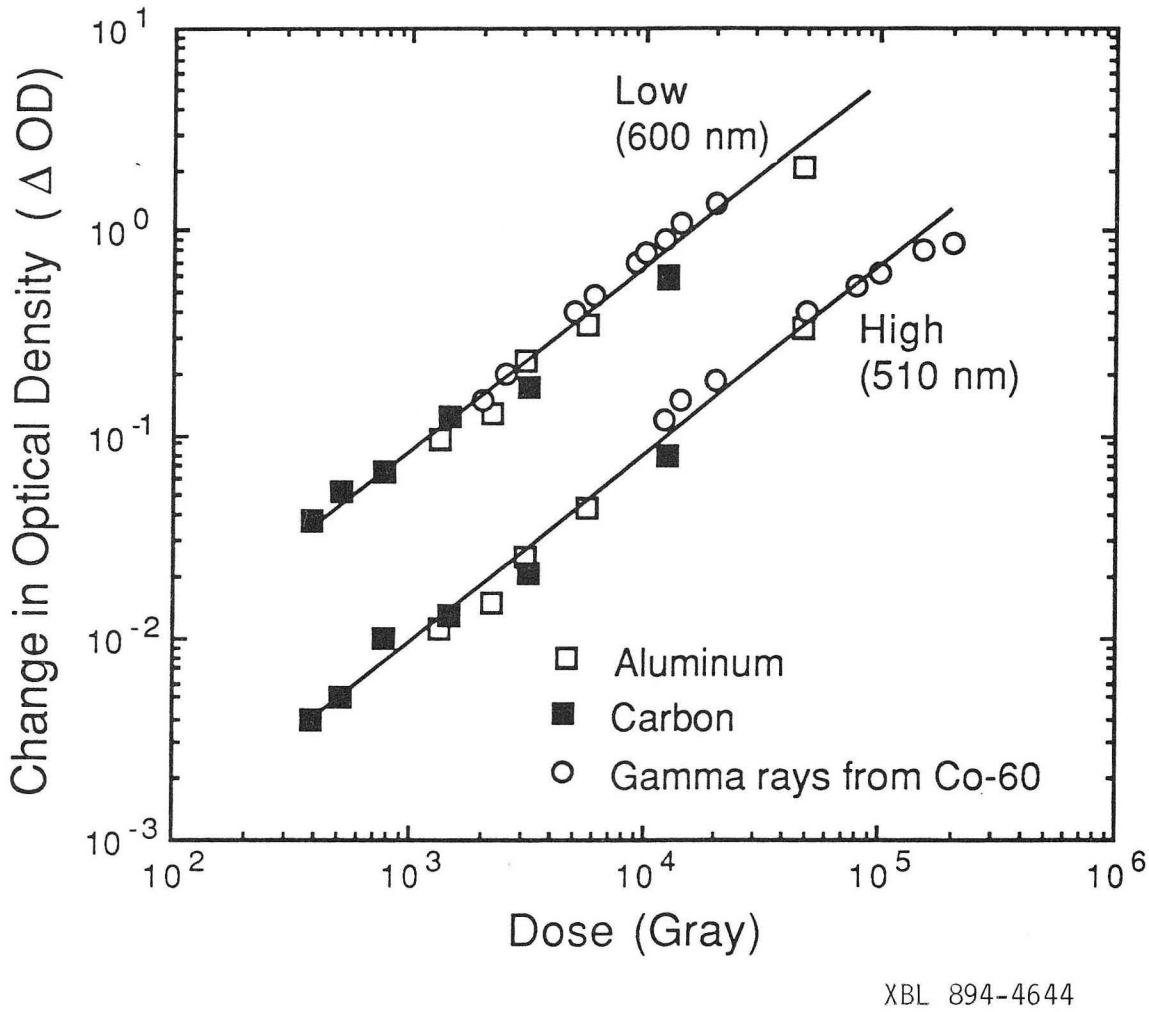
Change in Optical Density (Δ OD)
10^{1}
10^{0}
10^{-1}
10^{-2}
10^{-3}
10^{2}
10^{3}
10^{4}
10^{5}
10^{6}
Dose (Gray)
Low
(600 nm)
High
(510 nm)
Aluminum
Carbon
Gamma rays from Co-60
XBL 894-4644

Fig. 24

Figure 25. The change in optical density of radiachromic nylon film versus exposure time from the soft x-ray contact microscopy station

The source was carbon K_{α} (277 eV/4.46 nm). The apparatus was operated at 5 kV and 37 mA. Low (600 nm) and high (510 nm) refer to the wavelength where the film's optical density was measured. **r** refers to the correlation coefficient. This graph sets the exposure time necessary for a requisite dose. Using Figure 24, the change in optical density may be determined for the dose desired. On this figure, the change in optical density may then be correlated with the time. It is necessary to use the same wavelength at which change in optical density is determined on each graph, (i. e. low (600 nm) on Figure 24 with low (600 nm) on this figure). The dose rate of the soft x-ray contact microscopy station was 1.25 kilogray/hour at 18 cm from the source.

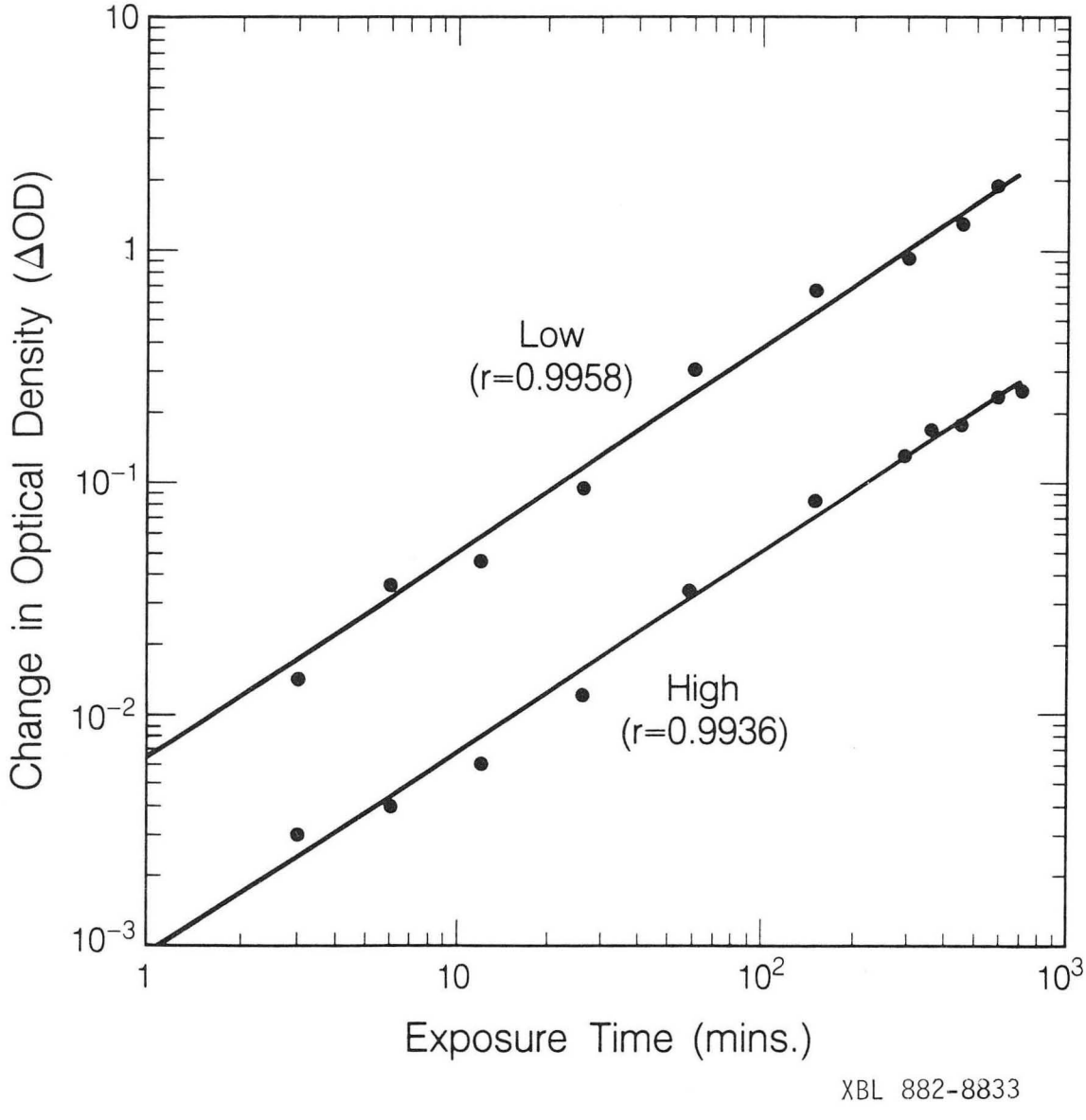
Change in Optical Density (ΔOD)
10
1
10^{-1}
10^{-2}
10^{-3}
1
10
10^2
10^3
Exposure Time (mins.)
Low
(r=0.9958)
High
(r=0.9936)
XBL 882-8833

Fig. 25

the same lines as those obtained by **Humphreys (1977)**. This figure also illustrates the lack of energy dependence in the response of the film.

Figure 25 illustrates the change in optical density of the film at 510 nm and 600 nm for various exposure periods on the soft x-ray contact microscopy source at an operating condition of 5.0 kV and 37 mA using carbon with the C_{K_α} emission line. The length of exposure time can be roughly computed by determining the change in optical density required for a set dose and then comparing the change in optical density with the exposure time. The dose rate of the soft x-ray contact microscopy station was 1.25 kilogray/hour at 18 cm from the source.

A calculation was made to determine if the film absorbed all or part of the dose. The thickness of the film is 51μm; its density is 1.14 g/cm^3, and the elemental composition (mass %) is 65.6 % carbon, 12.8 % oxygen, 11.1 % nitrogen, and 10.5 % hydrogen (**Far West Technology, Inc. 1986**). The film's thickness is equivalent to 18 radiation lengths for carbon K_α x-rays, or 59 for oxygen K_α x-rays, or 4.33 for aluminum K_α x-rays (**Henke 1982**).

C. DOSE REQUIRED TO EXPOSE RESIST AND MAKE A RECORDING

This section discusses the dose required to expose a resist and make a recording or imprint onto the resist. Previous discussion has centered on the properties of the resist material. A correlation between the exposure dose, expressed in J/cm^2, and the dissolution rate is demonstrated and shown to have relevance to the lateral resolution.

Spiller (1977) state that a dose of 10 kilograys are required to adequately expose a resist and make a latent image that may be etched or developed. However, **Shinozaki (1988)** showed that a latent image could be recorded into the resist with only a 2.5 kilogray dose. The latter number was considered to be a low dose exposure and would account for a slow development rate (36 to 50 nm/minute). Other workers have also determined that a resolution of 50 nm is obtained when a resist is exposed to 10 kilogray at

Figure 26.. Dissolution rate versus exposure for PMMA and Copolymer

The PMMA resist was developed in various solutions of MIBK (100% MIBK and MIBK:IPA ratios of 1:1 and 1:3). The Copolymer (90% PMMA and 10% MAA) resist was developed in ethyl cellulose acetate.

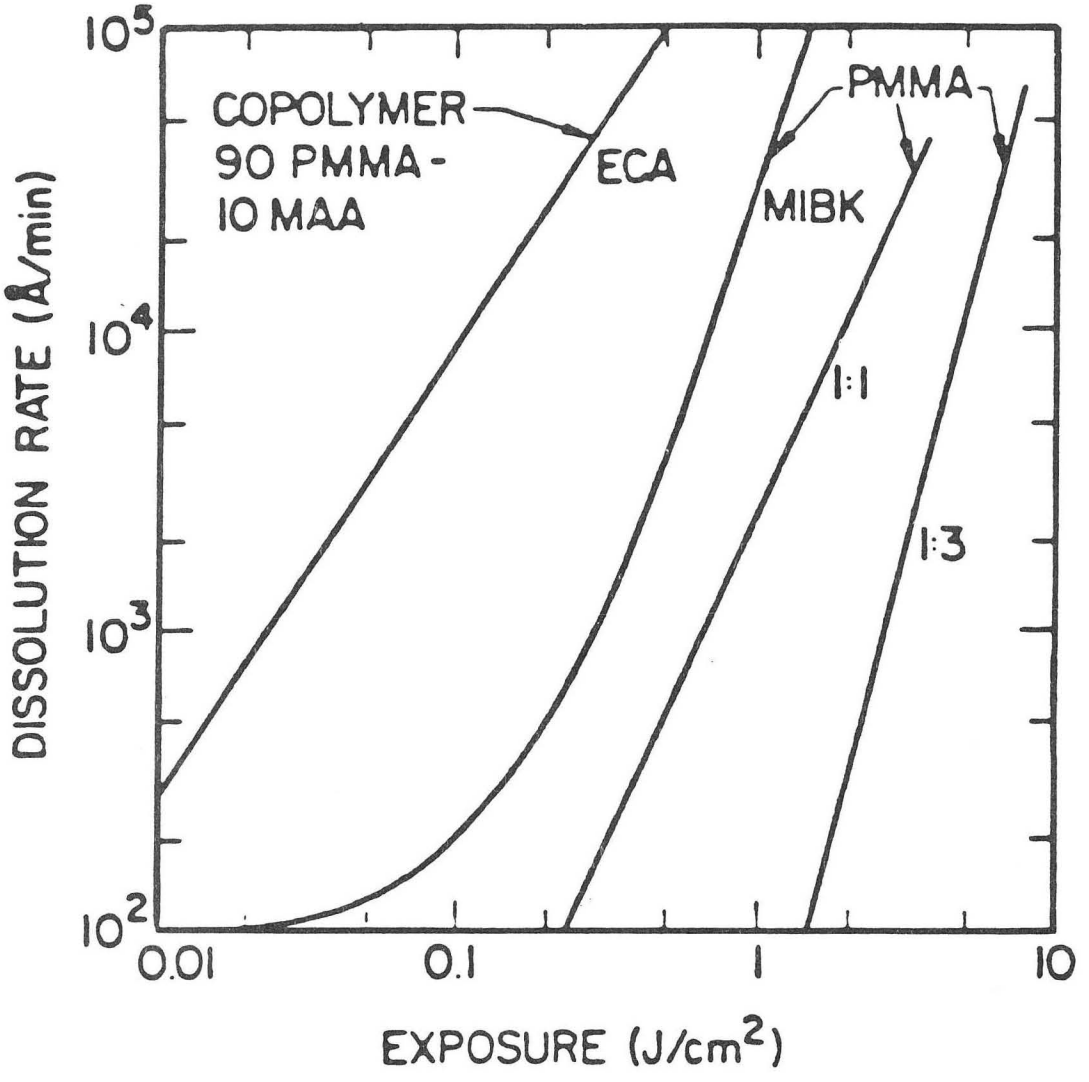
DISSOLUTION RATE (Å/min)
10^5
10^4
10^3
10^2
COPOLYMER
90 PMMA -
10 MAA
ECA
MIBK
PMMA
1:1
1:3
0.01
0.1
1
10
EXPOSURE (J/cm^2)

Fig. 26

λ = 4.3 nm (**Spiller 1977**). Furthermore, it was determined that a dose of 10 megagray was necessary to obtain a resolution of 5 nm. The resists considered are PMMA and copolymer (PMMA and MMA). **Spiller (1976a)** also considered the problem of exposing resists for x-ray lithographic purposes. In particular, they were concerned with determining a dissolution rate (nm/min) versus x-ray exposure relationship using PMMA resists and MIBK as the developer. Their concerns focused on the minimum dose to make an image and the appropiate resolution at various exposure levels. Further work by **Spiller and Feder (1977)** demonstrated that dissolution rate was a function of exposure as previously discussed. Figure 26 is a graph relating the dissolution rate to exposure for PMMA using MIBK and various dilutions in IPA as developers and Copolymer (90% PMMA and 10% MAA) using ethyl cellulose acetate as a developer. **Gudat (1982)** suggested that photo-resist sensitivity and contrast can be defined by the dissolution rate. **Haelbich (1984)** demonstrated that increasing the radiation dose to the resist reduced the effects of sidecutting. Sidecutting reduces the effective resolution. For $\lambda \approx 1$ nm photons, PMMA resist will have etched walls with slopes of 55° at an exposure of 0.05 J/cm^2 and slopes of 85° at an exposure of 0.51 J/cm^2. **Sayre and Feder (1979)** adopted an arbitrary standard such that the development depth approximates 5 times the width of the smallest feature of interest. Use of this arbitrary standard ensures that sidecutting does not reduce the desired resolution. For this work, the required exposure to make an image in the resist is considered to be 10 kilogray when using the conventional laboratory soft x-ray source. Exposures as low as 2.5 kilogray may be used to make an image in a resist when using a flash source such as the JANUS laser plasma source at LLNL. **Spiller and Feder** were concerned with the ablation of the resist when using a flash source and proposed an exposure consisting of a short series of pulses. **Sayre and Feder** make special considerations for flash sources in view of the fact that a possible temperature rise on the order of 2400°C may occur. This temperature rise is calculated on the basis that a

required exposure of 10 kilograys, which is equivalent to 10^4 J/g or 2400 calories/g, is deposited into a resist material having a specific heat capacity of approximately 1 cal/°C-g.

A minimum dose of 10 kilogray, especially in PMMA, is considered to be necessary to make a latent image. Data presented in this dissertation have been acquired successfully using doses of 2.5 kilogray as will be shown in the Biological Applications Section. **Spiller and Feder** have shown a correlation between the exposure dose and the dissolution rate and also how this correlation, defined as γ in an earlier section, is related to resolution. Ablation was thought to be a problem when using flash sources, however, data presented herein and by **Feder (1985a)** indicate that this aspect in practice may not be a factor. Data obtained for this work from laser-induced plasma sources does show the effects of ablation in some resists.

V LIMITS OF RESOLUTION

Any microscopic or optically-based technique has advantages and disadvantages. The advantages have been discussed. The disadvantages of soft x-ray contact microscopy are found in the limits of resolution and the resist properties. The resist properties were discussed earlier. The limits of resolution are based theoretically on the Fresnel diffraction effects, the geometry, the absorption properties of the biological sample and resist, and the effects of secondary electrons within the biological sample and the resist. Experimentally, the limit of resolution is based on the readout device, which may be an electron microscope (SEM, TEM or STEM), the scanning tunneling microscope or the atomic force microscope.

A. THEORETICAL CONSIDERATIONS

1. DIFFRACTION EFFECTS

The limit of resolution based on wave properties of soft x-rays is Fresnel or near-field diffraction. The example, that illustrates the experimental geometry best, is Fresnel diffraction along a straight edge. Figure 27 illustrates the geometry for Fresnel diffraction along a biological sample edge, the intensity pattern of the Fresnel diffraction fringes and the resist surface profile generated by this geometry. The derivation of the Fresnel integrals and their representation by the Cornu spiral may be found in optics texts such as **Born and Wolf** (1980), **Hecht** (1987) and **Jenkins and White** (1976). An exact solution for diffraction by a perfectly conducting semi-infinite plane screen was calculated by Sommerfeld in 1896 (**Born 1980**). The amplitude and intensity patterns for Fresnel diffraction by a straight edge are derived and illustrated in these optics texts.

Using notation similar to **Born**, the limit of resolution as defined by the Rayleigh criterion may be derived from the following equation:

$$w = x \cos \delta \sqrt{\frac{2}{\lambda}\left(\frac{1}{R} + \frac{1}{d}\right)} \qquad \text{Eqn. V-1}$$

where w is the length of the arc from the origin obtained from the Cornu spiral. The origin is defined as the edge of the shadow projected to the level of the straight edge. x is the distance of the straight edge from the origin. The plane of the straight edge is usually perpendicular to the display screen, however any deviation from the normal is defined by δ. R is the source-to-straight edge distance and d is the straight edge-to-display screen distance. The wavelength is defined by λ. The projection of the fringes, given by l, onto the display screen require an inversion of Eqn. V-1 and the multiplication of a geometrical projection factor, (R + d)/ R. Eqn. V-1 becomes

$$x \cos \delta = w \sqrt{\frac{\lambda}{2}\left(\frac{Rd}{R+d}\right)} \qquad \text{Eqn. V-2a}$$

$$l = x \cos \delta \left(\frac{R+d}{R}\right) = w \sqrt{\frac{d\lambda}{2}\left(\frac{R+d}{R}\right)}. \qquad \text{Eqn. V-2b}$$

The Rayleigh criterion requires that two adjacent fringes be distinguishable from each other. For light microscopic purposes, the angular limit of resolution is $\alpha = 1.22\ \lambda/D$ where D is the diameter of the objective lens. The factor, 1.22, and the diameter may be replaced by a lens characteristic called numerical aperture. When applying the Rayleigh criterion to the straight edge Fresnel diffraction pattern, the maxima and minima must be determined from the Cornu spiral. Equation V-2b must be differentiated first to determine the distance between fringes:

$$\partial l = \partial x \cos \delta \left(\frac{R+d}{R}\right) = \partial w \sqrt{\frac{d\lambda}{2}\left(\frac{R+d}{R}\right)} \qquad \text{Eqn. V-3}$$

The geometrical conditions of soft x-ray contact microscopy allow for the following assumptions: 1). the biological sample edge has the same behavior as a straight edge. 2). the sample edge and resist are considered to be parallel thus $\delta = 0$, $\therefore \cos \delta = 1$. 3). the source-to-sample distance, R, ranges from 6-18 cm and the sample-to-resist distance, d, is

Figure 27. Fresnel diffraction effects in soft x-ray contact microscopy

Figure A illustrates the geometry for Fresnel diffraction along a biological sample edge. The sample-to-resist distance is d. The intensity of the incident radiation is I_0 while the intensity of the transmitted radiation, having passed through the supporting film (formvar or Si_3N_4), is I. Figure B shows the intensity pattern of the Fresnel diffraction fringes and figure C demonstrates the resist surface profile generated by this geometry.

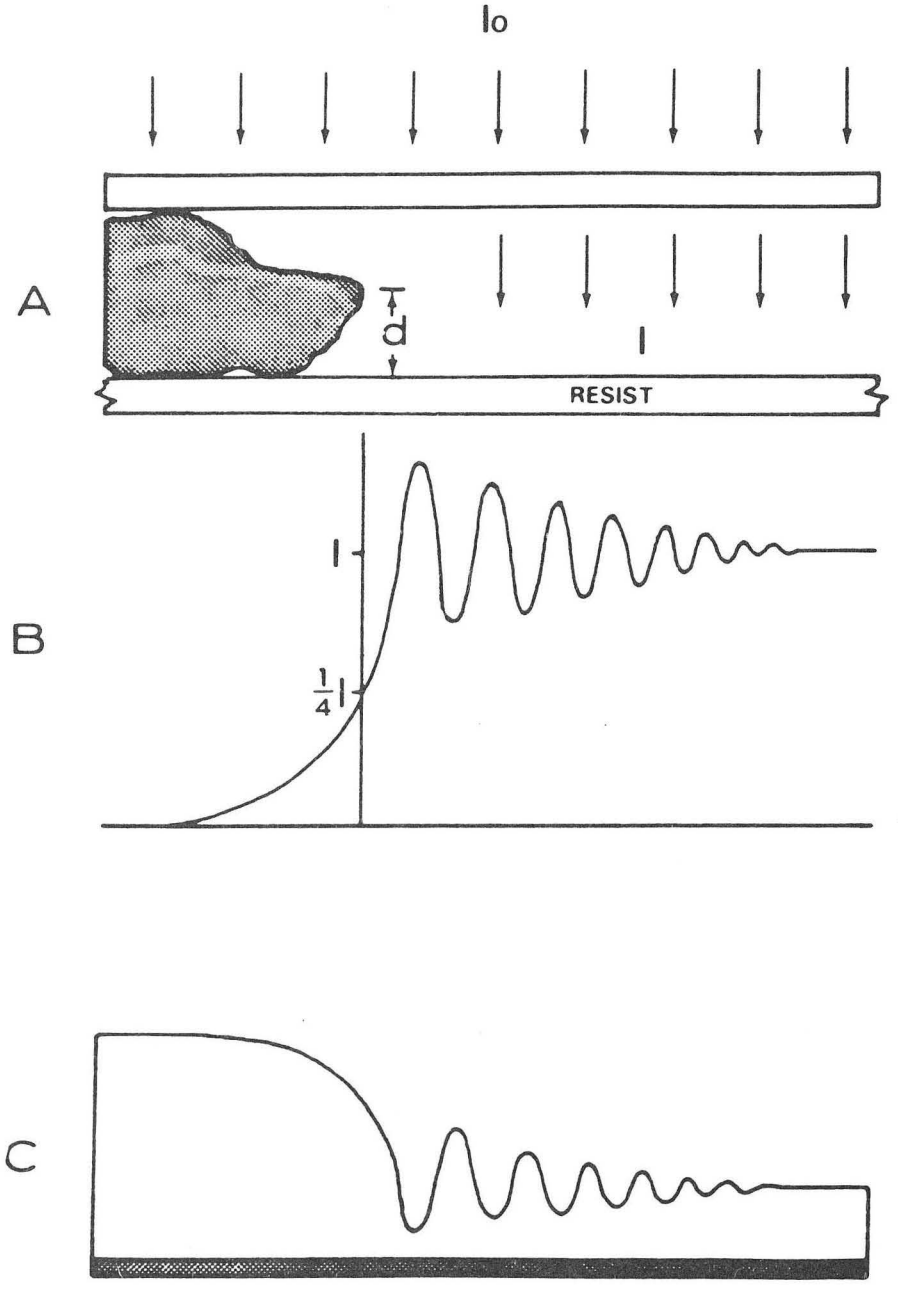

Fresnel-type diffraction in contact microscopy. A: The object and resist distance is *d*. The intensity of the incident light is I_0, and the light transmitted through the supporting film is *I*. B: Fresnel diffraction fringes. C: Resist surface profile.

Fig. 27

~1 μm, ∴ R >> d. and 4). soft x-rays are treated classically as plane waves, i. e. the same properties as visible light. Equation V-3 may be rewritten as follows:

$$\partial l = \partial x = \partial w \sqrt{\frac{d\lambda}{2}} \qquad \text{Eqn. V-4a}$$

$$\frac{\partial l}{\partial w} = \sqrt{\frac{d\lambda}{2}} \qquad \text{Eqn. V-4b}$$

The limit of resolution due to Fresnel diffraction effects is defined by Eqn. V-4b. This result implies that the resolution of the soft x-ray contact micrographs are wavelength dependent. The lowest resolution achievable within the "water window" using a wavelength, λ = 2.5 nm, and a contact distance, d = 1 μm, would theoretically be 25 nm. Experimental results using electron microscope grids are shown later in this section.

2. GEOMETRICAL EFFECTS

The geometrical effect limiting resolution is penumbral blurring. Figure 13 diagrams the geometry relating to penumbral blurring. The source spot size is one of the important factors for determining the size of the penumbra. The penumbra is defined as

$$S_p = s(w/D) \qquad \text{Eqn III-1}$$

where s is the distance of the biological sample to the recording material, in this case, a resist. w is the diameter of the spot size and D is the distance of the source to the sample.

Calculated values of the penumbra for the two sources are dependent upon source spot size, w, and source-to-sample distance, D. The sample-to-resist distance, s, is assumed to be 1 μm. For the LBL conventional source used in this work, w = 2.6 mm and D = 180 mm, the calculated penumbra, S_p, is 14.4 nm. At the experimental setup at LLNL JANUS laser facility, w = 100 μm and D = 6 cm, the calculated penumbra, S_p, is 1.67 nm.

3. ABSORPTION EFFECTS

Absorption effects are concerned with the interaction of radiation with matter (i. e. the biological sample and the resist). To understand absorption effects, one must start with

a look at low energy x-ray scattering. At the microscopic level, Thomson scattering and the atomic scattering factor have important roles in defining the atomic photoionization cross section. On the macroscopic level, the atomic scattering factor becomes a part of the complex dielectric constant, the complex refractive index and the linear absorption coefficient. Using this approach, one may consider the doses required to image biological samples for various forms of x-ray microscopy. A knowledge of soft x-ray interactions can provide an understanding of the radiobiological effects at the molecular level. Low energy x-ray scattering is an important factor in defining the limits of resolution within the resist due to secondary electron travel. Secondary electron travel will be discussed in the next subsection. The topic of absorption effects within the resist in this subsection will be limited to the comparison of resist profile and development.

Figure 28 is a schematic of low energy x-ray scattering. This interaction may be defined as coherent scattering and photoelectric absorption because incoherent scattering is negligible. The general case is scattering at long wavelengths by dipoles induced in small scatterers. The incident wave induces electric and magnetic multipoles that oscillate in a definite phase relationship to the incident wave. The electric and magnetic multipoles radiate energy in directions other than the direction of incidence. Since the incident x-ray wavelength is much greater than the scattering diameter, only the lowest multipoles, usually electric and magnetic dipoles, are considered (**Jackson 1975**). In this case, the x-ray is incident on an atom, however, Thomson scattering is assumed thus the atom is initially treated as a free electron. The sequence of Thomson scattering continues when the electron is set into a vibratory motion at the forcing frequency, causing it to behave as an electric dipole. The electron then radiates electromagnetic energy with an angular and intensity distribution determined by its electric dipole behavior (**Dyson 1973**).

Low energy or soft x-ray scattering is described by a complex scattering amplitude, which is the single electron scattering amplitude multiplied by the atomic scattering factor, $f_1(\lambda) + if_2(\lambda)$. The single electron scattering amplitude is assumed by replacing the atom

Figure 28. Schematic of low energy x-ray scattering (**Henke 1981**)

$\mathcal{E}_o$ is the amplitude of the incident electric field. r_o is the classical electron radius, which is $\left(\frac{e^2}{mc^2}\right)$ and has a value, 2.82×10^{-15} m. R is the radial distance from the atom to the point where $\mathcal{E}(\theta, \lambda)$, the amplitude of the electric field scattered by the atom, is measured. $P(2\theta)$, a polarization factor, is 1 or $\cos 2\theta$ depending upon the orientation of the incident electric field, i. e. is it perpendicular or parallel to the scattering plane.

LOW ENERGY X-RAY SCATTERING

$\lambda >>$ ATOMIC DIAMETER

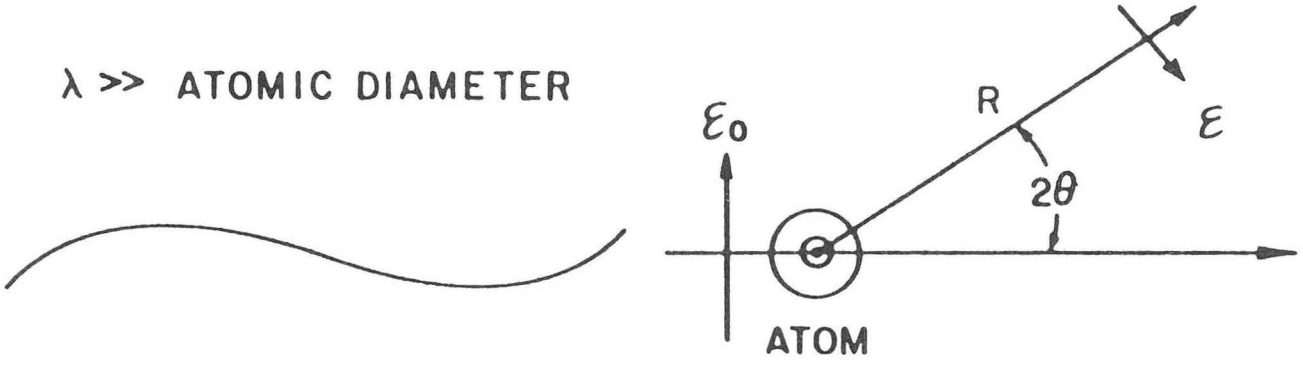

SINGLE ELECTRON SCATTERING AMPLITUDE X ATOMIC SCATTERING FACTOR

$$\mathcal{E}(\theta,\lambda) = -\left[\mathcal{E}_0\left(\frac{r_0}{R}\right)P(2\theta)\right](f_1(\lambda) + if_2(\lambda))$$

Fig. 28

with a free, Thomson electron (**Henke 1981**). The mathematical formulation of Thomson scattering can be found in numerous texts (**Panofsky 1962, Dyson 1973, Landau 1975 and Jackson 1975**). The result is the Thomson scattering cross section,

$$\sigma = \frac{8\pi}{3}\left(\frac{e^2}{mc^2}\right)^2 \qquad \text{Eqn. V-5}$$

which generates the classical electron radius, $r_e = \left(\frac{e^2}{mc^2}\right)$ with a value, 2.82 X 10^{-15} m. mc^2 is the rest mass energy of the electron. The Thomson scattering cross section is 0.665 X 10^{-24} cm^2 or 0.665 barns. The differential cross section is as follows,

$$\frac{d\sigma}{d\Omega} = \frac{r_e^2}{2}\left(1 + \cos^2\theta\right) \qquad \text{Eqn. V-6}$$

To determine the effect of coherent scattering, it is necessary to determine the atomic scattering factor. Following the notation of **Landau** (1977), the atomic scattering factor may be derived from the Born approximation of the scattering amplitude,

$$f = -\frac{2\pi m}{h^2}\int U(\mathbf{r})\, e^{-i\,\mathbf{q}\cdot\mathbf{r}}\, d\Omega \qquad \text{Eqn. V-7}$$

where U(**r**) is the potential, **q** is the wave vector between the incident and scattered waves, h is Planck's constant and $d\Omega$ is a volume element. Vectors are denoted in bold typeface. The absolute magnitude of **q** is

$$q = 2k\,\sin\frac{\theta}{2} \qquad \text{Eqn. V-8}$$

where θ is the scattering angle. The validity of using the Born approximation in low energy x-ray scattering is shown by allowing k --> 0. Thus q--> 0 and $e^{-i\,\mathbf{q}\cdot\mathbf{r}} \approx 1$ in Eqn. V-7, which becomes

$$f = -\frac{2\pi m}{h^2}\int U(\mathbf{r})\, d\Omega \rightarrow f = -\frac{8\pi^2 m}{h^2}\int_0^{\infty} U(r)\, r^2\, dr \qquad \text{Eqn.V-9}$$

Two other conditions prevail. First, the amplitude of the scattered wave is much less than that of the incident wave ($\psi_{coh} << \psi_o$) and second, the phases are small and calculable from Schroedinger's equation when the potential energy is regarded as a perturbation. The treatment of the scattering field as a perturbation, i. e. the Born approximation, may be found in numerous texts (**Saxon 1968, Landau 1977 and Shankar 1980**). Equation V-7 may also be restated to consider the atom in the potential term,

$$f = -\frac{1}{e}\int \rho(\mathbf{r})\, e^{-i\,\mathbf{q}\cdot\mathbf{r}}\, d\mathbf{r} \qquad \text{Eqn. V-10}$$

where $\rho(\mathbf{r})$ is the charge density distribution defined by the number of electrons occupying each orbital of the atom (**Ashcroft 1976**). Equation V-10 may take the following form,

$$f = f_1(\lambda) + if_2(\lambda). \qquad \text{Eqn. V-11}$$

f_1 and f_2 are independent of the scattering angle because the condition, $\lambda >>$ the atomic diameter, assumes that all electrons scatter in phase for all but the largest scattering angles (**Henke 1981**). Equation V-10 suggests that

$$|f| \approx Z \qquad \text{Eqn. V-12}$$

where Z is the charge of the nucleus. The differential (Eqn. V-13a) and total (Eqn. V-13b) coherent scattering cross sections may be defined as

$$\frac{d\sigma_{coh}}{d\Omega} = \frac{r_e^2}{2}\left(1 + \cos^2\theta\right)|f_1 + if_2|^2 \qquad \text{Eqn. V-13a}$$

$$\sigma_{coh} = \frac{8\pi}{3} r_e^2 \left(f_1^2 + f_2^2\right). \qquad \text{Eqn. V-13b}$$

The total cross section is defined by the optical theorem,

$$\sigma_{tot} = \frac{4\pi}{k}\,\mathrm{Im}\, f = 2\lambda r_e f_2. \qquad \text{Eqn. V-14}$$

The absorption cross section may be approximated to the total cross section, $\sigma_{abs} \cong \sigma_{tot}$,

because $\sigma_{abs} >> \sigma_{coh}$ (**Henke 1981**). The ratio of the coherent scattering cross section to the absorption cross section is

$$\frac{\sigma_{coh}}{\sigma_{abs}} = \frac{4\pi}{3}\frac{r_e}{\lambda}\frac{(f_1^2 + f_2^2)}{f_2} = \frac{1.18 \text{ X } 10^{-5}}{\lambda(\text{nm})}\frac{(f_1^2 + f_2^2)}{f_2} \quad \text{Eqn. V-15}$$

In the soft x-ray region, $Z \geq f_1 \geq f_2$, the ratio of cross sections, Eqn. V-15, becomes

$$\frac{\sigma_{coh}}{\sigma_{abs}} \approx \frac{1.18 \text{ X } 10^{-5}}{\lambda(\text{nm})} Z \quad \text{Eqn. V-16}$$

This ratio is approximately $3 \text{ X } 10^{-5}$ when $\lambda = 2.5$ nm and $Z = 6$ (carbon). In the soft x-ray region it has been demonstrated that coherent scattering is not a substantial factor.

The components of the atomic scattering factor, f_1 and f_2, have been computed and **Henke** (1981) presents the results which are based on other referenced calculations. The relativistic quantum dispersion theory for atomic scattering gives the semi-classical Kramers-Kronig relations. The real part, f_1, requires two correction terms. The imaginary part, f_2, is related directly to the atomic photoionization cross section, which is a measurable quantity. Thus,

$$f_2(E) = \frac{E\mu_a(E)}{2\pi r_e hc} \quad \text{Eqn. V-17}$$

where E is the x-ray energy and $\mu_a(E)$ is the atomic photoionization cross section. The Kramers-Kronig relations may be used to calculate f_1 from the values of f_2. Another assumption is the electrons within the atom scatter in all directions in the same phase as they would in the forward direction because $\lambda >>$ atomic diameter. So,

$$f_1(E) = Z + \frac{1}{\pi r_e hc}\int_0^\infty \frac{\varepsilon^2 \mu_a(\varepsilon)\, d\varepsilon}{E^2 - \varepsilon^2} + \Delta f_r \quad \text{Eqn.V-18}$$

where

$$\Delta f_r = \frac{5}{3}\frac{E_{tot}}{mc^2} - \frac{Z}{2}\left(\frac{E}{mc^2}\right)^2. \qquad \text{Eqn. V-19}$$

The last term of Eqn. V-18 is a relativistic correction, which is negligible for low energy x-rays except near absorption edges. The first term of Eqn. V-19 is expressed in terms of Z,

$$\frac{5}{3}\frac{E_{tot}}{mc^2} = 2.19 \text{ X } 10^{-6} Z^3 - 1.03 \text{ X } 10^{-4} Z^2 \qquad \text{Eqn. V-20}$$

where E_{tot} is the total energy of the atom and is negative. Inputting f_2 from Eqn. V-17 into Eqn. V-18,

$$f_1(E) = Z + \frac{2}{E}\int_0^{\infty} \frac{\varepsilon^2 f_2(E)\, d\varepsilon}{E^2 - \varepsilon^2} + \Delta f_r \qquad \text{Eqn. V-21}$$

where f_1 is dependent upon Z, f_2 and E. However, the anomalous scattering or dispersion term represented by the integral becomes very large and negative near the ionization thresholds or absorption edges. The application of a damping term to the integral could correct this problem.

Henke (1981) proposes that the low energy photoionization cross section and the corresponding atomic scattering factors are atomic-like in the chemical and solid-states too except near the absorption edges. The "Henke" tables (**Henke 1982**) demonstrate that the atomic scattering factors are first, uniquely defined by the photoionization cross section; secondly, they are independent of scattering angle except at large scattering angles; and finally, they are independent of the atomic system's state except near the absorption edge.

The condition that the wavelengths of soft x-rays are greater than the scatterer dimensions may apply on the macroscopic level. The molecular or macroscopic parameters can be related to the material constants, K, which is the dielectric constant, and n_r, which is the refractive index. The atomic scattering factors are directly related to the macroscopic parameters (α, γ, δ and β) of the complex dielectric constant and the complex refractive

index. These parameters are unit decrements, i.e. much less than one ($\alpha, \gamma, \delta, \beta << 1$). In the low energy x-ray region, the complex dielectric constant is

$$K = 1 - \alpha - i\gamma \qquad \text{Eqn. V-22}$$

and the complex refractive index is

$$n_r = 1 - \delta - i\beta. \qquad \text{Eqn. V-23}$$

The macroscopic parameters are

$$\delta = \frac{r_e \lambda^2}{2\pi} n\overline{f_1} = \frac{\alpha}{2} \qquad \text{Eqn. V-24}$$

and

$$\beta = \frac{r_e \lambda^2}{2\pi} n\overline{f_2} = \frac{\gamma}{2} \qquad \text{Eqn. V-25}$$

where the average atomic or molecular scattering factors per unit volume, $n\overline{f_1}$ and $n\overline{f_2}$, are given by

$$n\,\overline{f_1} = \sum_Z n_Z f_{1,Z} \qquad \text{Eqn. V-26}$$

$$n\,\overline{f_2} = \sum_Z n_Z f_{2,Z} \qquad \text{Eqn. V-27}$$

The number densities, n_Z and n, are the atomic density of type-Z and the molecular density, respectively. The general formula is

$$n = \frac{N_A}{A} \rho \qquad \text{Eqn. V-28}$$

where N_A is Avogardo's number (6.02×10^{23} atoms or molecules/mol), A is the atomic or molecular weight and ρ is the specific gravity.

The linear absorption coefficient, μ_l, may be derived from electromagnetic theory concerning the boundary value solution for the Poynting vector describing transmitted energy flow. The intensity of a plane wave, $\psi = e^{-i k n_r z}$, in the forward direction yields

$$I = \psi^* . \psi = \left(e^{i kz}\, e^{-i k\delta z}\, e^{-k\beta z}\right).\left(e^{-i kz}\, e^{i k\delta z}\, e^{-k\beta z}\right)$$

$$= e^{-2k\beta z} = e^{-4\pi\beta z/\lambda}. \qquad \text{Eqn. V-29}$$

The exponential term in Eqn. V-29 may be defined by the linear absorption coefficient, μ_l, multiplied by z. The result is

$$\mu_l = \frac{4\pi\beta}{\lambda} = 2r_e\lambda n\overline{f_2} \quad . \qquad \text{Eqn. V-30}$$

The atomic or molecular photoionization cross section, μ_a, is μ_l /n.

The photoionization cross section may be inputted into the following attenuation equation

$$I = \sum_{E=E_{min}}^{E_{max}} I_o(E)e^{-\mu(E)t} \qquad \text{Eqn. V-31}$$

where t is the thickness of the material imaged or etched. The absorption of soft x-rays by the biological material is defined by the thickness of the material, its elemental composition and the photoionization coefficient. The etched image in the resist will have a limitation that restricts one's ability to see fine features and large structures of the cell image at the same time.

4. SECONDARY ELECTRON TRAVEL

Secondary electron travel within the resist, especially PMMA, has not been well defined. Empirical models have been proposed. Figure 29 illustrates the results of an experiment to measure secondary electron travel (**Spiller 1977**). The PMMA resist was coated with a thin film of erbium and exposed to x-rays from a conventional laboratory source. The three emission lines used were C_{K_α} (0.277 keV), Al_{K_α} (1.48 keV) and Rh_{L_α} (2.7 keV). Faster development occurs in the resist because there is added exposure from the secondary electrons from erbium. The kinks observed in the lines of the graph are caused by the transition from secondary electron travel to x-ray exposure, thus the height of the kink yields the change in thickness or secondary electron range. The range (δ) was found to be 5 nm, 35 nm, and 65 nm for C_{K_α} (0.277 keV), Al_{K_α} (1.48 keV) and Rh_{L_α} (2.7 keV), respectively (**Spiller 1977**). Figure 30 illustrates the region of best resolution by comparing the effective range of secondary electrons and the wavelength with x-ray

Figure 29.. Estimation of secondary electron travel in PMMA at various x-ray energies

The PMMA resist was coated with a thin film of erbium and exposed to x-rays from a conventional laboratory source. The three emission lines used were C_{K_α} (0.277 keV), Al_{K_α} (1.48 keV) and Rh_{L_α} (2.7 keV). Δ is the change in thickness from the initial time of development. Faster development occurs in the resist because there is added exposure from the secondary electrons from erbium. The kinks observed in the lines of the graph are caused by the transition from secondary electron travel to x-ray exposure, thus the height of the kink yields the change in thickness or secondary electron range. This range (δ) was found to be 5 nm, 35 nm, and 65 nm for C_{K_α} (0.277 keV), Al_{K_α} (1.48 keV) and Rh_{L_α} (2.7 keV), respectively (**Spiller 1977**).

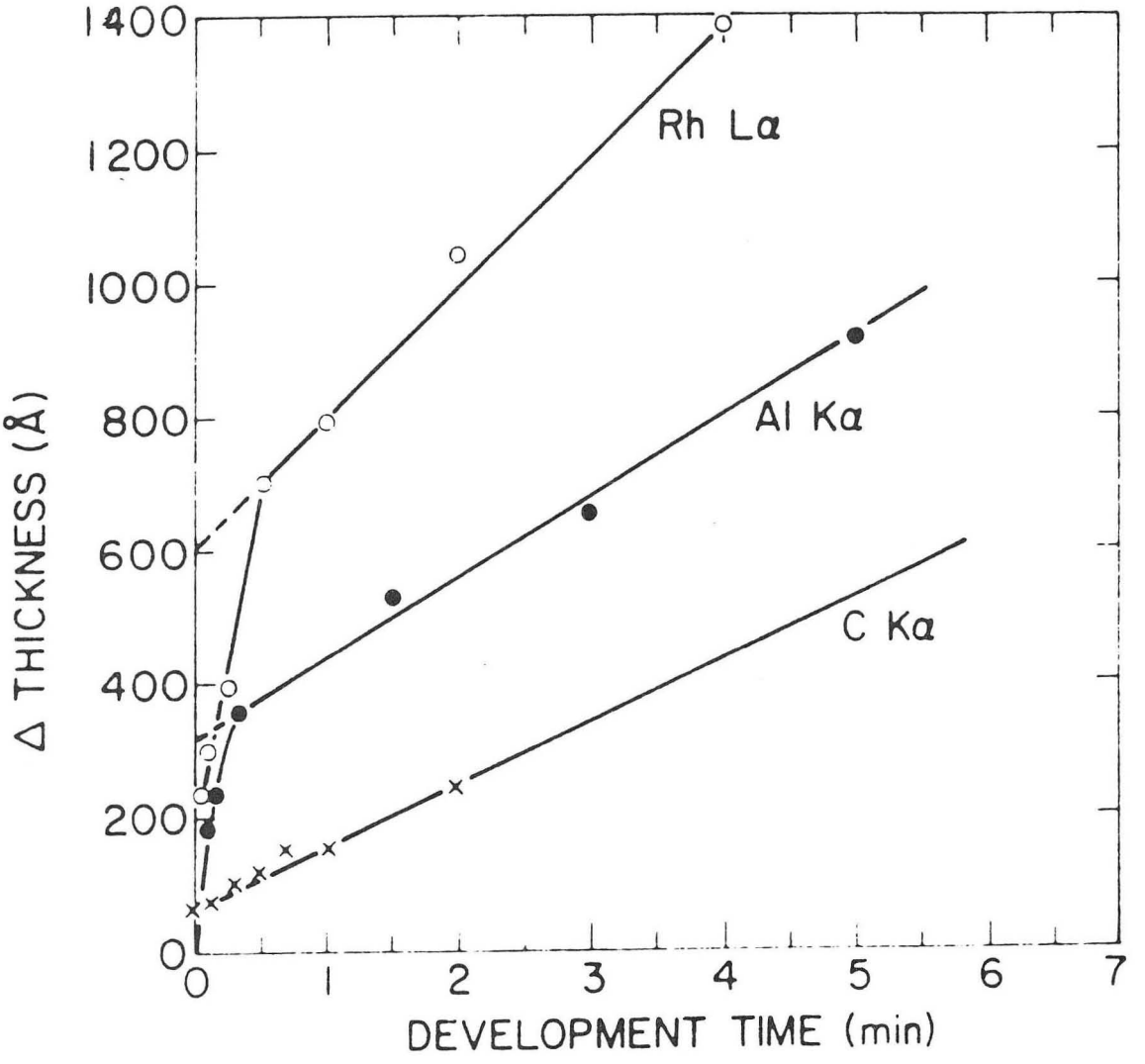
1400
1200
1000
800
600
400
200
0
Δ THICKNESS (Å)
0
1
2
3
4
5
6
7
DEVELOPMENT TIME (min)
Rh Lα
Al Kα
C Kα

Fig. 29

Figure 30. The region of best resolution for soft x-ray microscopy

The region of best resolution is determined by comparing the effective range of secondary electrons (δ) and the wavelength (λ) with x-ray energy. This region is the range of x-ray energies approximately 150-500 eV. The point of intersection of the range of secondary electrons and wavelength is close to 277 eV, which is the C_{K_α} emission line **(Spiller 1979).**

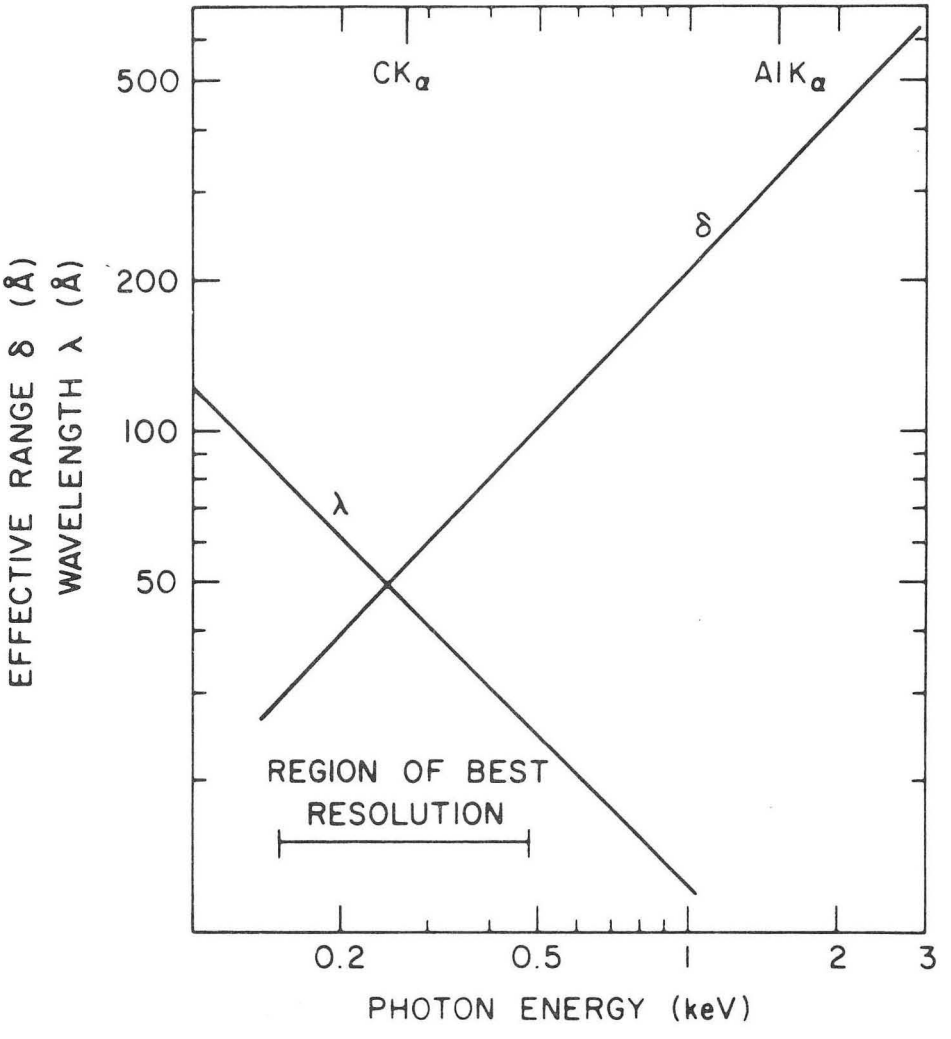
EFFECTIVE RANGE δ (Å)
WAVELENGTH λ (Å)
500
200
100
50
CKα
AlKα
δ
λ
REGION OF BEST
RESOLUTION
0.2
0.5
1
2
3
PHOTON ENERGY (keV)

Fig. 30

energy (**Spiller 1979**). This region is the range of x-ray energies approximately 150-500 eV. The point of intersection of the range of secondary electrons and wavelength is close to 277 eV which is the emission line for C_{K_α}.

B. EXPERIMENTAL ASPECTS

1. READOUT TECHNIQUE

The method of reading or looking at the etched resists by a microscope is termed readout. Currently, the readout technique uses electron microscopy, both scanning and transmission. A discussion of SEM and TEM principles and techniques may be found in numerous texts (**Agar 1974, Goldstein 1981, Chescoe 1984, Reimer 1984 and 1985**). Currently, a resist is coated or shadowed at a 7° angle with approximately 10-15 nm AuPd after development. The development is monitored by reflective light microscopy using differential interference contrast (DIC) with Nomarski optics. The shadowing of resists to enhance the signal of small surface modulations is calculated by **Bjorklund** (1974). **Goldstein** and **Reimer** (1985) discuss shadowing or coating techniques in the practical and theoretical aspects, respectively. Viewing of the resist in the SEM is usually done at a 75° angle from the horizontal. Another readout method is replication of the resist using an organic monomer (**Shinohara 1986**) or carbon (**Cheng 1986a**) for TEM viewing or a metal for SEM viewing (**Goldstein 1981**). Future readout techniques may include scanning tunneling microscopy or atomic force microscopy. Atomic force microscopy (AFM) appears to be a better method because the resist does not have to be coated to be conductive. AFM images are apparently more useful than the STM images (**Feder 1987**).

2. RESPONSE TO AN AMPLITUDE STEP

The amplitude step response experiment used two EM grids, one placed atop the other, as the mask. The EM grids were placed at an angle to each other such that an overlapping image of an EM grid was made on the TEM resist, which was copolymer 480 nm thick. The spacing of the second EM grid was 2 mils (50.8 μm) from the resist. The

resist was exposed for 24 hours to a V_{L_α} emission line, which is 511 eV. The filament settings were at a potential of 3kV and a current of 36 mA. The dose delivered to the resist was ~35 kgrays. The resist was developed for 15 seconds in a solution of MIBK:IPA (1:1). The resists were shadowed at a 7° angle to the horizontal with ~13 nm AuPd. The readout of the resists was done on a Zeiss EM 109 TEM.

The results of the amplitude step response test are shown in Figures 31-36. The shadowing material used on the resist depicted in Figure 31 was ~15 nm Au. A comparison between Figures 31 and 32, which are at the same magnification of 27500X, shows the difference in grain size between Au and AuPd shadowing, respectively. A larger grain size is observed when shadowing with Au. Figure 33, which has a magnification of 4200X, illustrates the effect of shadowing and the surface roughness that may be induced by soft x-ray exposure from a conventional laboratory source. **Shinozaki** (1986, 1988) has considered the effect of surface roughness within the resist when exposed to soft x-rays and unexposed. Shallow development and replication may reduce surface roughness (**Shinozaki 1986**). The cause of surface roughness is attributed to the long and short chains of the polymer and their alignment (**Shinozaki 1988**). Surface roughness on both the unexposed and exposed sides of the EM grid edge and heating of the edge of the contact EM grid is seen in Figure 34, which has a magnification of 7400X. The first fringe due to Fresnel diffraction is seen in Figures 35 and 36. Figure 36, magnification 12800X, is a higher magnification of Figure 35, which is at 4200X. The first fringe appears ~70 nm from the penumbral edge and ~360 nm from the beginning of the penumbra. The latter measurement compares with an expected value of 352 nm for a sample-to-resist distance, d = 50.8 μm when the resolution, $r = \sqrt{\lambda d}$.

Figure 31. TEM of the x-ray resist image of an EM grid edge shadowed with Au (Magnification 27500X)

This resist was shadowed with Au. Note the grain size. The scale on this micrograph is 1 cm: 159 nm (micrograph: actual)

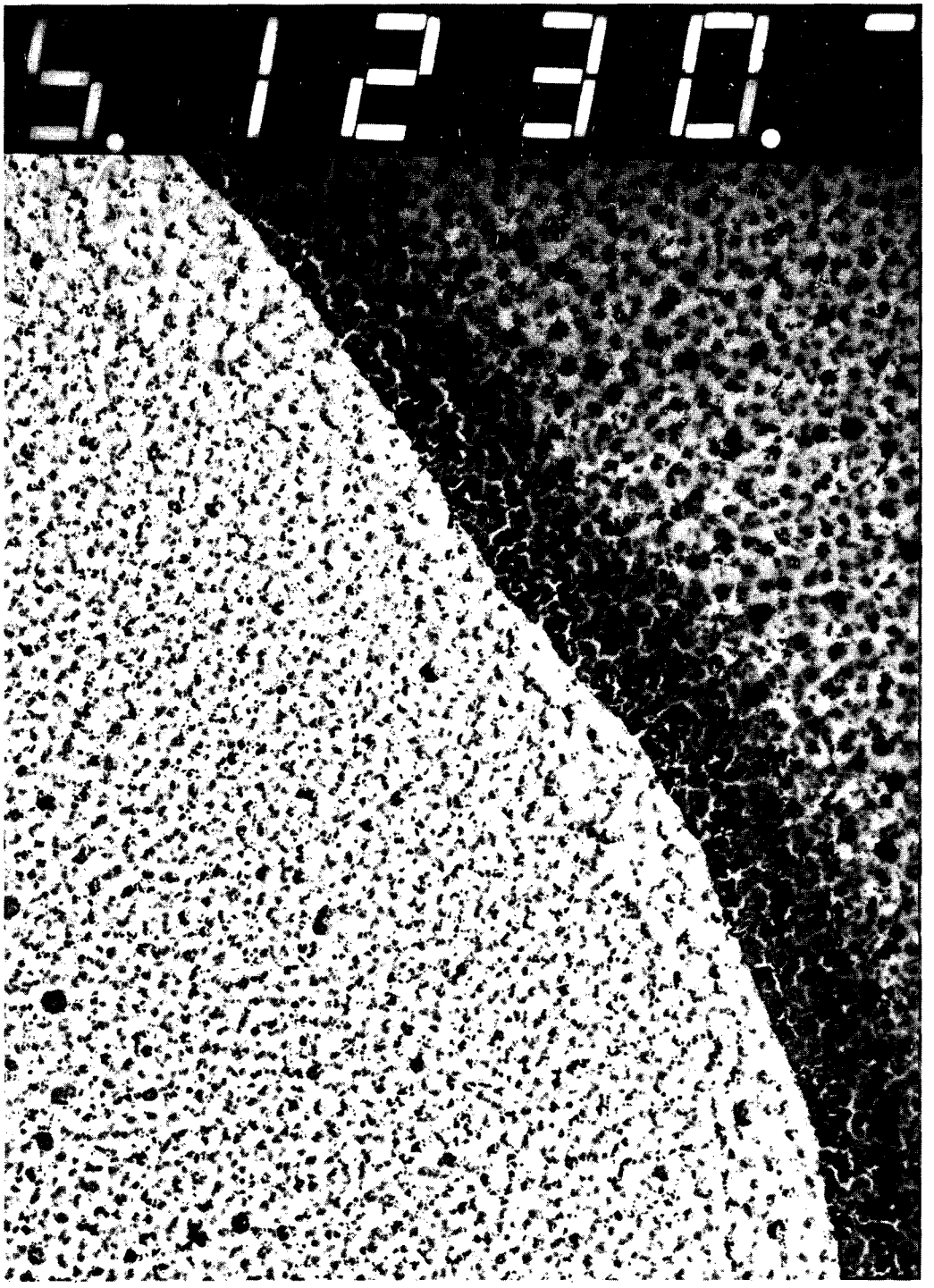

XBB 895-4101

Fig. 31

Figure 32. TEM of the x-ray resist image of an EM grid edge shadowed with AuPd (Magnification 27500X)

This resist was shadowed with AuPd. Note the grain size. The scale on this micrograph is 1 cm: 159 nm (micrograph: actual)

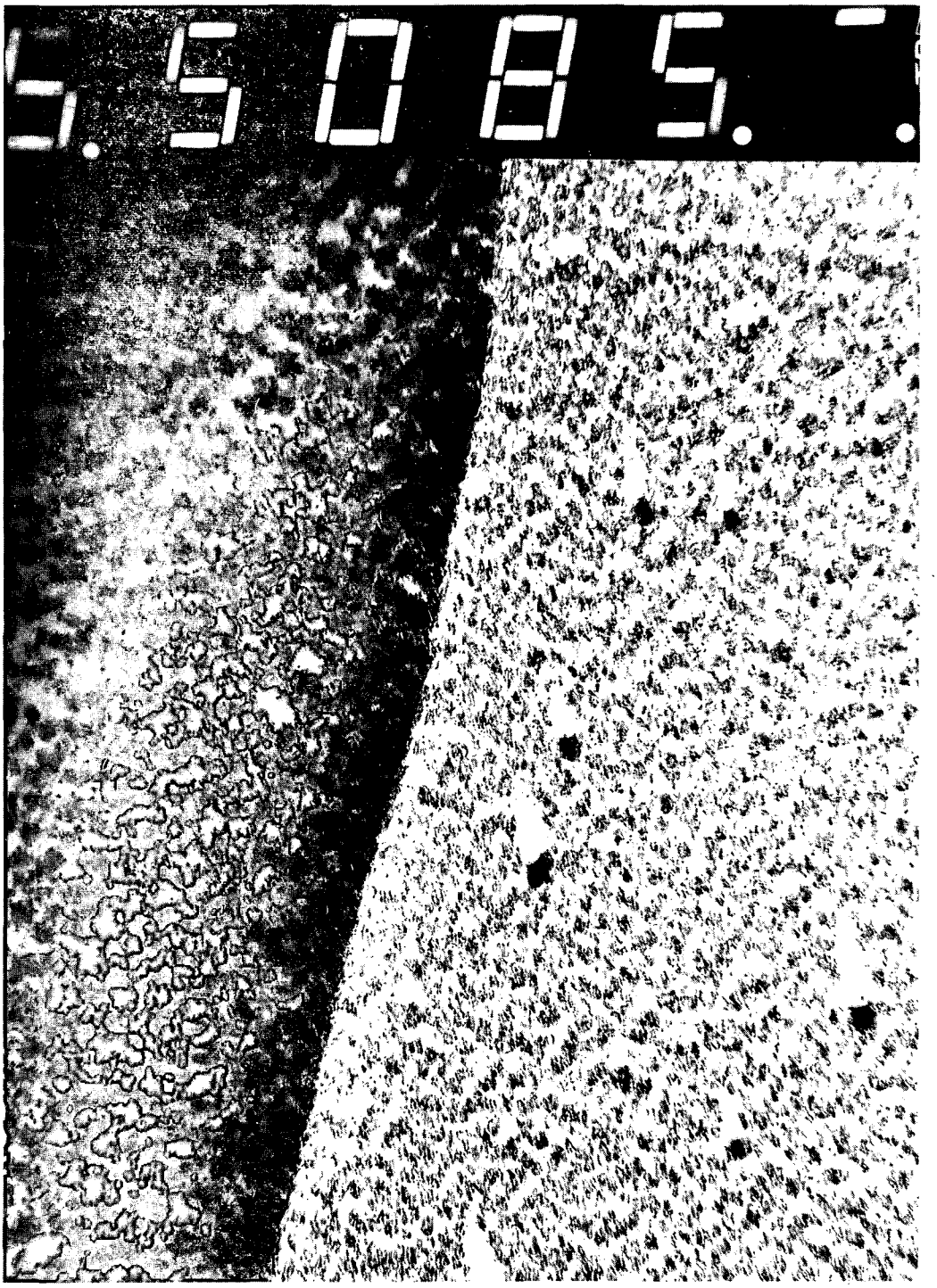

XBB 895-4102

Fig. 32

Figure 33. TEM of the x-ray resist image of an EM grid edge shadowed with AuPd (Magnification 4200X)

Note the clear shadows in the exposed area. The scale on this micrograph is 1 cm: 1.04 μm (micrograph: actual)

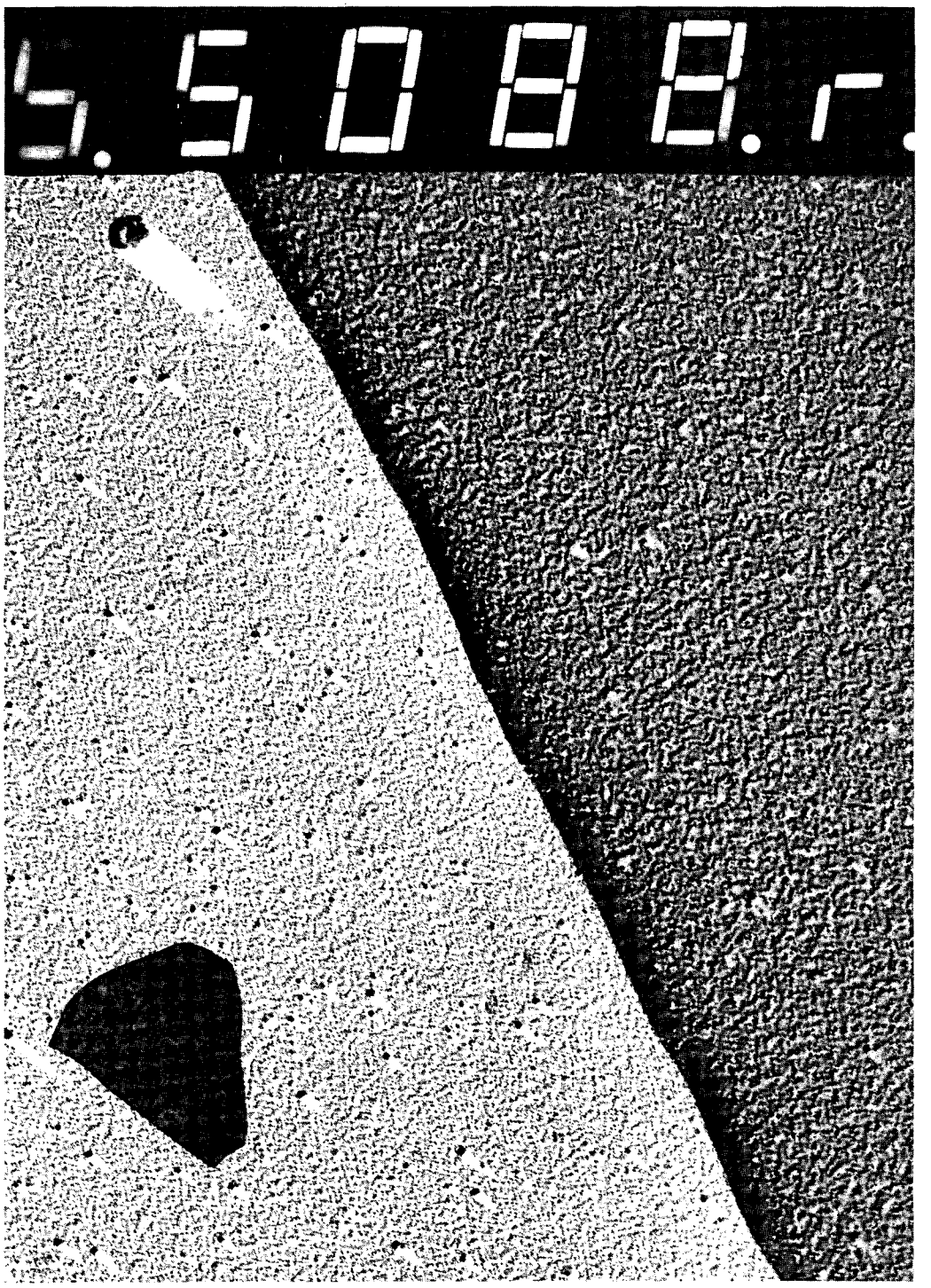

XBB 895-4103

Fig. 33

Figure 34. TEM of the x-ray resist image of an EM grid edge shadowed with AuPd (Magnification 7400X)

The scale on this micrograph is 1 cm: 0.6 μm (micrograph: actual). Surface roughness and heating of the edge of the contact EM grid is seen.

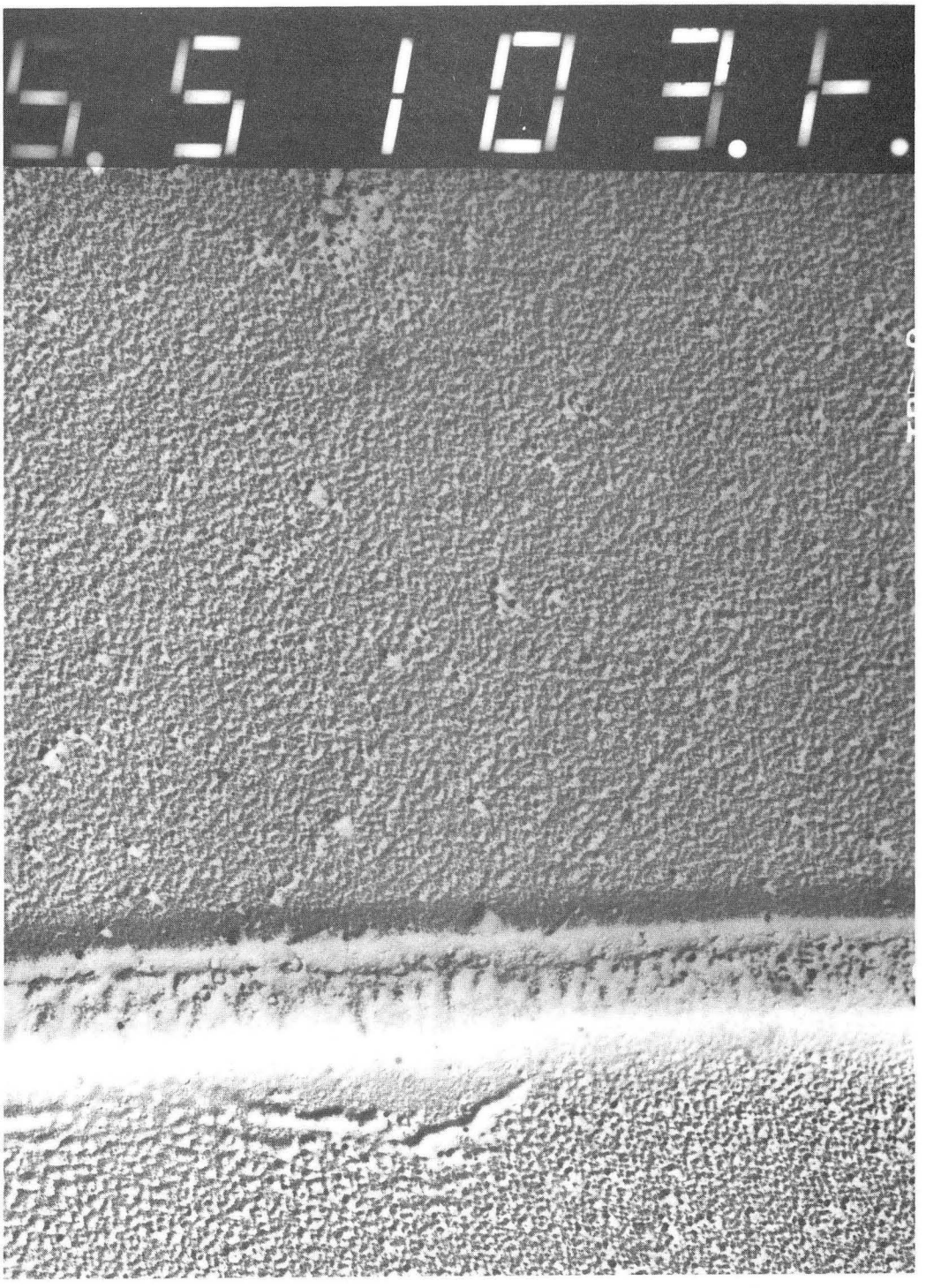

XBB 895-4106

Fig. 34

Figure 35.. TEM of the x-ray resist image of an EM grid edge shadowed with AuPd illustrating the first Fresnel diffraction fringe (Magnification 4200X)

The scale on this micrograph is 1 cm: 1.04 μm (micrograph: actual). The first Fresnel diffraction fringe is ~80 nm from the penumbra edge and ~350 nm from the beginning of the penumbra.

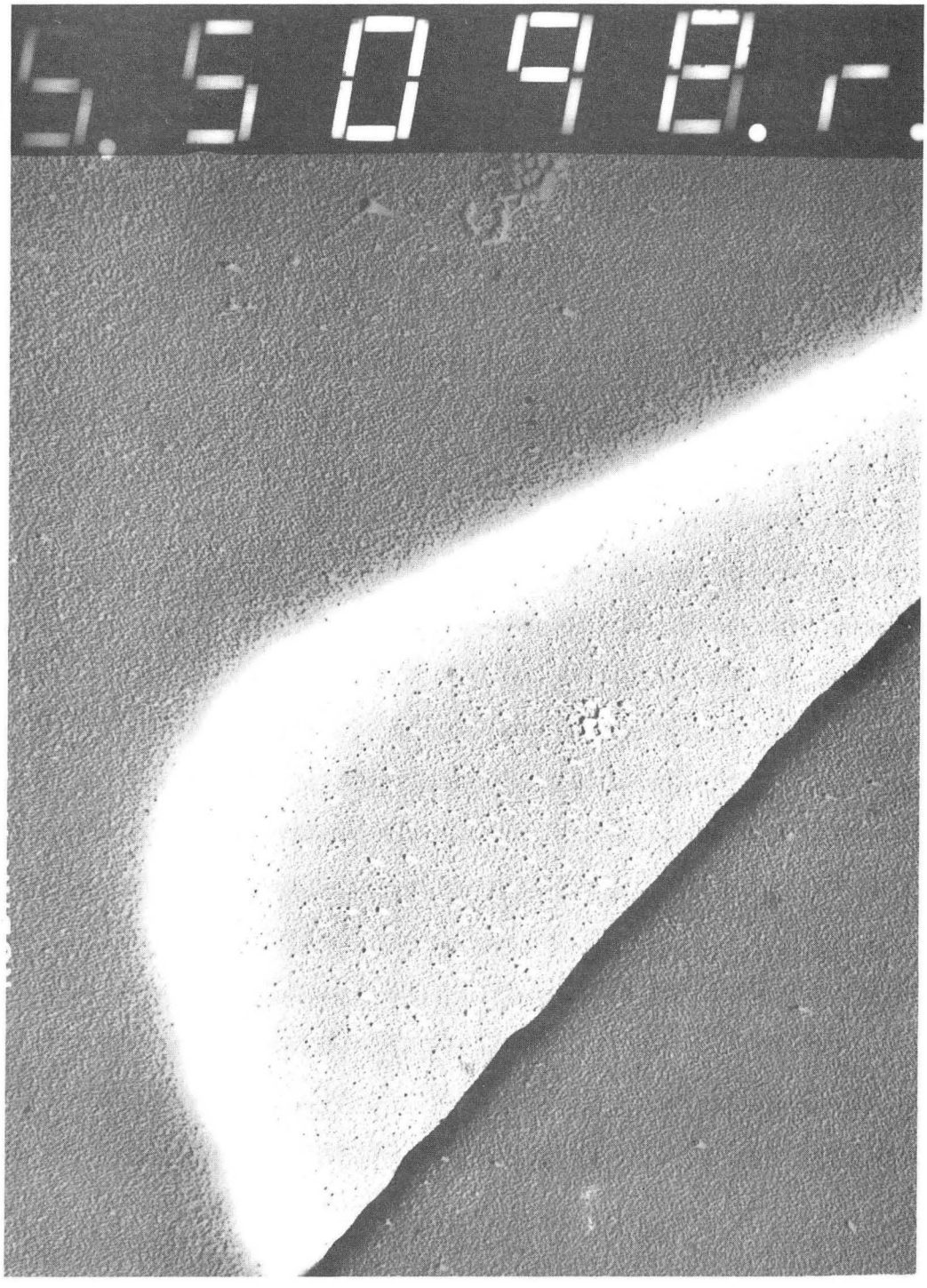

XBB 895-4104

Fig. 35

Figure 36. Higher magnification TEM of Figure 35 (Magnification 12800X)

The scale on this micrograph is 1 cm: 342 nm (micrograph: actual). At higher magnification, one is able to obtain a more exact measurement. The first fringe appears ~70 nm from the penumbral edge and ~360 nm from the beginning of the penumbra. The latter measurement compares with an expected value of 352 nm for a sample-to-resist distance, d = 50.8 μm.

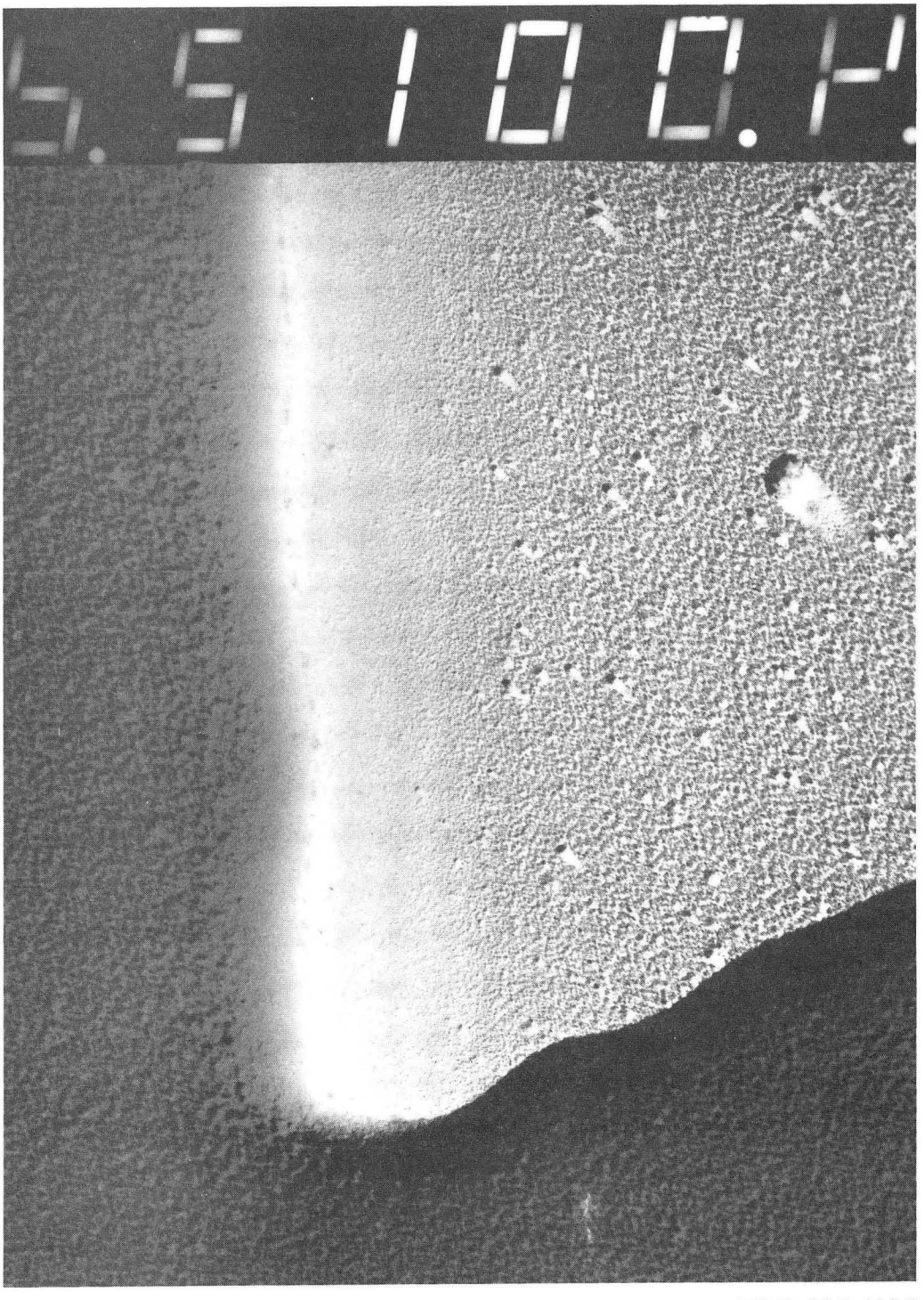

XBB 895-4105

Fig. 36

VI WET CELL CHAMBER (WCC)

A. DESIGN OF FEDER'S CHAMBER

The philosophy leading to the design of the IBM chamber was to provide an environment in which the specimen would stay alive at atmospheric pressure while the chamber was in a vacuum. **Feder** (1985a) imaged living platelets using a first iteration chamber design. A Si_3N_4 window was glued onto a substrate holder. The platelets were placed into a honeycombed structure of wells etched in PMMA and sitting on a Si_3N_4 window. The wells within the PMMA were 1 μm deep and had a 10 μm^2 area. After the resist had been placed on top of the platelets, the substrate holder was attached to the body of the chamber using an o-ring seal. A spring mechanism held the resist in place and a chamber top was attached using an o-ring seal.

The last iteration of the IBM WCC design provided for an ease of changing samples and an assurance of maintaining contact between the resist and the sample. Figure 37 illustrates the components of the IBM WCC. A plain Si_3N_4 window was glued onto a sample plate. After the biological sample had been placed onto the Si_3N_4 window, the sample plate was placed into a recessed bottom, which had a hole to allow x-rays to pass through to the Si_3N_4 window and an o-ring seal. The resist was placed atop the biological sample and the chamber body attached to the bottom with another o-ring seal maintained against the sample plate. A spring mechanism held the resist in place and a chamber top was attached using an o-ring seal. One had to use care with the spring mechanism to prevent breakage of the Si_3N_4 window and to assure even distribution of contact between the resist and the biological sample. The three o-ring design allowed for quicker sample change. Figure 38 shows an assembled IBM WCC ready for an exposure.

B. LBL DESIGN

1. EVOLUTION FROM FEDER'S DESIGN

Development of the LBL WCC was based on a desire to image living biological samples in the SXCM and to do x-ray holography with zymogen granules at Brookhaven's

Figure 37.. The components of the IBM wet cell chamber

From left to right are the chamber top, chamber body, recessed bottom, sample plate, spring mechanism and spring compressor. Si_3N_4 window is glued onto the sample plate over the hole. After placement of the biological sample and resist on the Si_3N_4 window, the sample plate is put into the recessed bottom. The chamber body is attached to the recessed bottom. The spring mechanism is gently dropped through the top of the chamber body onto the resist. The spring compressor is screwed into the chamber body to insure the effectiveness of the spring mechanism. The chamber top is then attached to the chamber body.

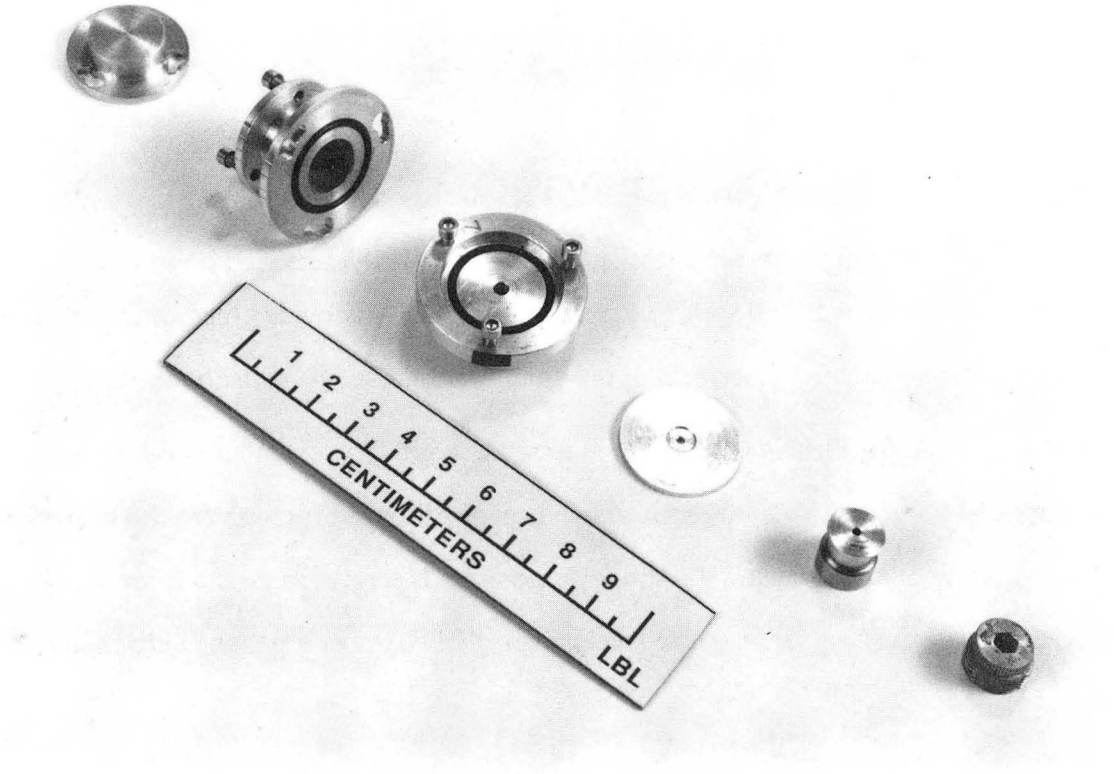

XBB 893-1976

Fig. 37

Figure 38. The IBM wet cell chamber assembled and ready for exposure
The scale in this photograph is in centimeters.

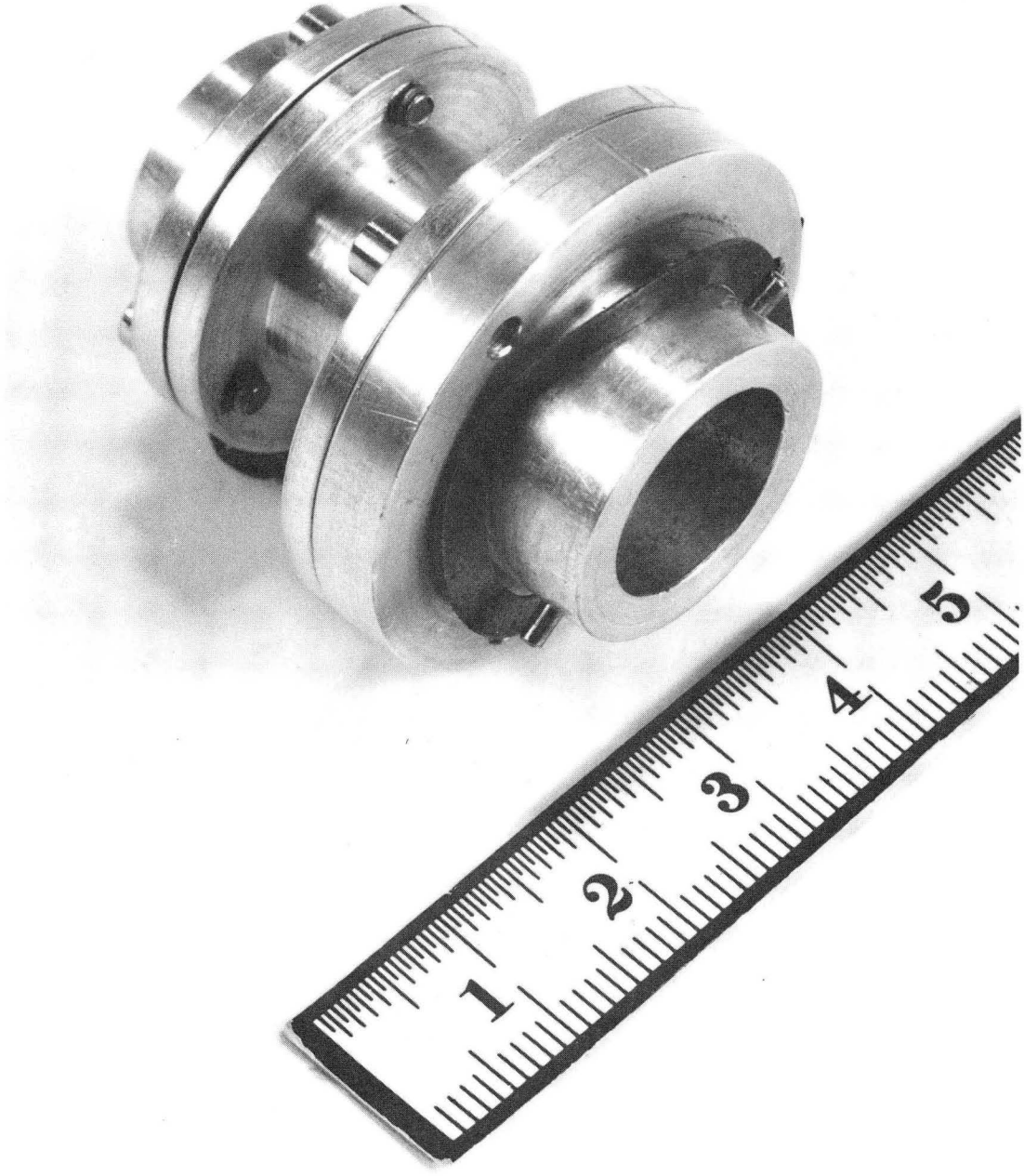

XBB 893-1977

Fig. 38

National Synchrotron Light Source. The use of the WCC to do flash soft x-ray contact microscopy on living CHO-SC1 cells and 9L glialsarcoma cells at LLNL's JANUS laser facility was an afterthought. The requirements of these experiments necessitated that the WCC be simple, allow easy sample change, provide a moist, atmospheric environment for the biological sample and insure contact between the resist and the sample without breaking the Si_3N_4 window. The x-ray holography experiments required a spacer for multiple TEM resists. In 1987, Phil Batson and the author developed the design concept for the WCC, which later became the LBL WCC design. To simplify the WCC and improve the ease of operation, the number of o-ring seals was reduced from three to one. The sample plate became an integral part of the WCC. It had an o-ring groove for the o-ring, knobs to hold the spacer in place and threaded screw holes for attachment of the sample cap and chamber cap. To allow quick sample changes and provide as many opportunities as possible for imaging, numerous sample plates were manufactured. A moist environment was provided by sponges attached to sample and chamber caps. The sample cap sponge also applied pressure to the resist against the biological sample without breaking the Si_3N_4 window.

2. DESIGN OF THE LBL WET CELL CHAMBER

Figure 39 shows a schematic of the LBL WCC. Figure 40 depicts the following: 1). the LBL WCC mounted on an optics support ready for exposure, 2). the sample cap and spacer mounted onto the sample plate ready for placement of the chamber cap, and 3). the pieces of the LBL WCC. The sample plate has a thickness of 0.3 cm, a diameter of 1.91 cm, an o-ring groove, two recessed areas with common 0.63 cm diameter, two knobs for the spacer, four threaded screw holes for 2-56 NC screws and a 0.12 cm hole to allow x-rays to pass through to the Si_3N_4 window. The o-ring groove provides for an o-ring with a thickness of 0.15 cm and an inside diameter of 1.25 cm. The recessed area within the chamber has a depth of approximately 1 mil (~25 μm) so that the Si_3N_4 window can be glued in place over the hole. The biological sample may be placed on the Si_3N_4 window over the area of the hole. The spacer, which has a thickness of 0.15 cm, an outside

Figure 39. Schematic of the LBL wet cell chamber

From left to right are the chamber cap, sample cap, spacer, and sample plate. The sample plate is shown in both side and top views. D refers to diameter.

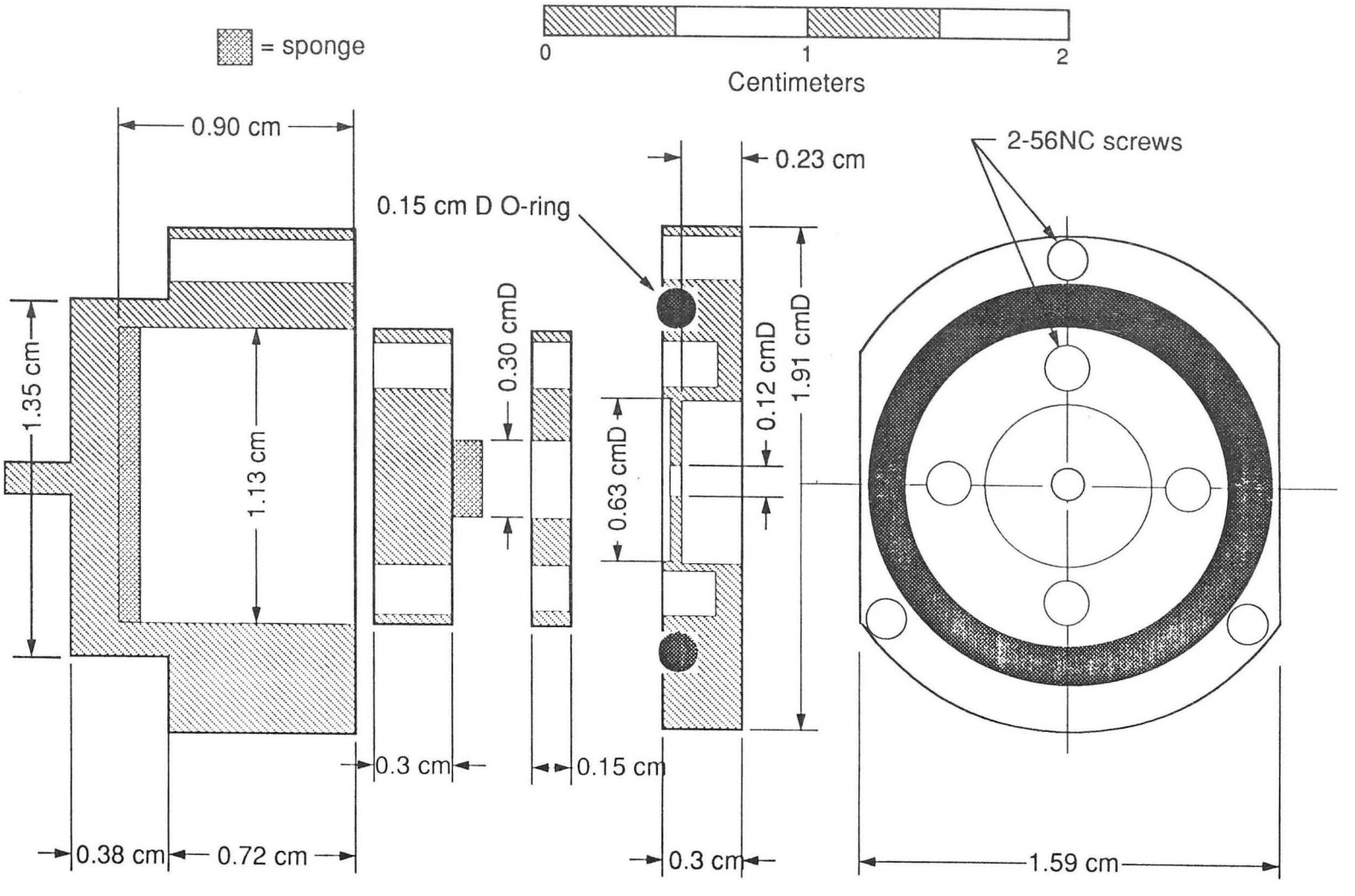

WET CELL CHAMBER

XCG 894-4645

Fig. 39

Figure 40. The LBL wet cell chamber and components

From top to bottom are the LBL wet cell chamber mounted on an optics support ready for exposure, the sample cap and spacer mounted onto the sample plate ready for placement of the chamber cap, and the components of the LBL wet cell chamber. The components are from left to right the three screws to attach the chamber cap to the sample plate, the chamber cap, the two screws to attach the sample cap and spacer to the sample plate, the sample cap with sponge showing, the spacer, and the sample plate. The sample plate has a Si_3N_4 window glued in place, an o-ring to provide a seal with the chamber cap and knobs to keep the spacer in place. The scale is in centimeters.

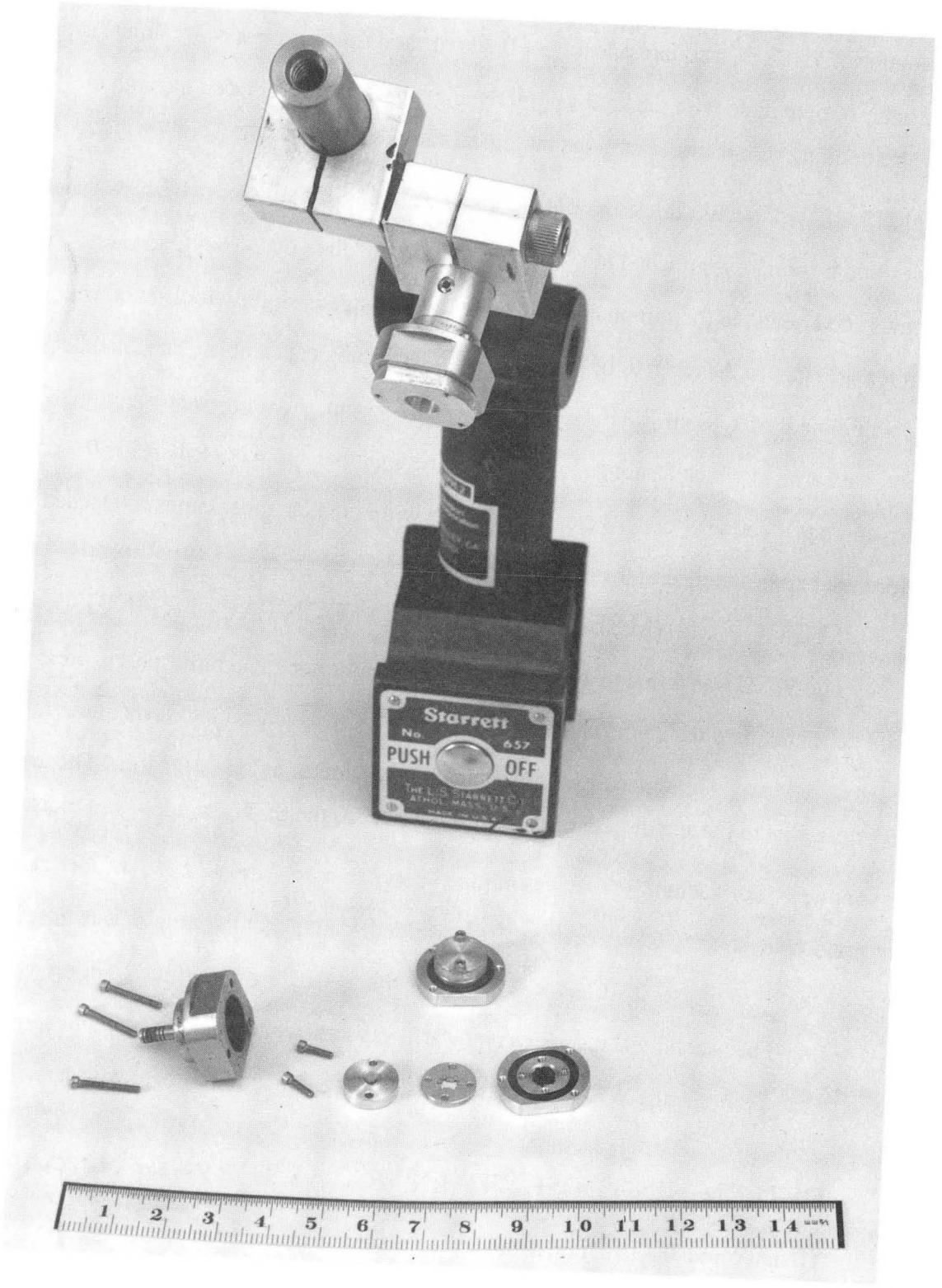

CBB 888-7471

Fig. 40

diameter of 1.10 cm, a square opening of 0.30 cm^2 and four screw spacing holes, is placed onto the sample plate with the knobs properly aligned. A resist is placed through the square opening of the spacer atop the biological sample sitting on the Si_3N_4 window . A sample cap, which has a thickness of 0.30 cm, a diameter of 1.10 cm, two screw spacing holes and a sponge, is attached to the spacer and sample plate by 2-56 NC screws. These screws "dead-end" in the sample plate. The sample sponge is slightly moistened and applies pressure to the resist to be in contact with the biological sample. The chamber cap has a thickness of 1.10 cm, an outside diameter of 1.91 cm, three screw spacing holes and a recessed area in which a sponge is attached. The chamber cap recessed area is 0.9 cm deep and has a diameter of 1.13 cm. The sponge within the chamber cap is moistened before the cap is attached to the sample plate by 2-56 NC screws.

C. TEST OF CHAMBER'S ABILITY TO MAINTAIN ITS INTEGRITY

The WCC was tested to determine if a moist environment at atmospheric pressure could be maintained inside the chamber while the WCC was placed into a vacuum. In use, the vacuum vessel would need to attain a vacuum pressure of at least 10^{-5} torr. The test procedure was to place a droplet of cells in solution onto the Si_3N_4 window and moisten the sponges. The vacuum vessel was pumped down to a pressure of 2×10^{-7} torr. Upon returning to air, the WCC was opened and it was determined that the droplet was intact and the sponges were moist. This test was repeated with SOXLIS running for 24 hours within the SXCM. The second test results were a warm yet somewhat moist droplet and sponges. It is very apparent that the WCC can hold a moist atmospheric environment within itself when it is placed into a high vacuum.

D. DETERMINING DOSE WITHIN WCC AT THE Si_3N_4 WINDOW

To determine the radiation dose inside the sample chamber, one may use the **Henke** (1982) tables to determine the x-ray absorption effects of a 120 nm Si_3N_4 window. The theoretical value may be derived from the following equation:

$$I(E) = I_0(E)e^{-\mu(E)t} \qquad \text{Eqn. VI-1}$$

where I(E) (number of photons at a particular energy/cm^2-sec) is the flux after passing through a material with thickness, t (g/cm^2), and photoabsorption cross section, $\mu(E)$ (cm^2/g). $I_o(E)$ is the flux entering the material. E is the energy of the photons. A condition of using monoenergetic x-rays has been assumed. The total photoabsorption cross section is as follows:

$$\mu(E) = \sum_Z m_z \mu_z(E) \qquad \text{Eqn. VI-2}$$

where m_Z is the mass percent of an element and μ_Z is the photoabsorption cross section for an element at a particular energy. To consider all energies, Equation VI-1 must be summed over all energies:

$$I = \sum_{E=E_{min}}^{E_{max}} I_o(E)e^{-\mu(E)t} = \sum_{E=E_{min}}^{E_{max}} I_o(E)e^{-\sum_Z m_z\mu_z(E)t} \qquad \text{Eqn. VI-3}$$

E_{max} and E_{min} are the upper and lower limits of the energy range.

Experimentally, the dose within the WCC at the Si_3N_4 window was simulated by placing a Si_3N_4 window over a piece of radiachromic nylon film. This combination was taped to the bottom of the SXCM sample plate or when doing laser-induced plasma shots, the bottom of the WCC sample plate. When using the SXCM with a vanadium target on SOXLIS to generate V_{L_α} x-rays, the ratio of the dose determined from a film covered by the Si_3N_4 film to that from an uncovered film was ~85% of the expected theoretical value. $\mu_{Si_3N_4} = 1.30 \times 10^4$ cm^2/g when using the V_{L_α} x-rays. For laser-induced plasma sources, the ratio could not be easily determined.

E. WATER LAYER PROBLEM

The water layer problem occurs when a layer of water covering the cell or cell organelle is too thick, i.e. >10 μm. A droplet of cells or cell organelles suspended in water or phosphate buffered solution (PBS) is placed on the Si_3N_4 window. The cells or cell organelles are allowed to settle. Water or PBS is wicked away very slowly with this process being monitored by a differential interference contrast microscope. As the solution

is wicked away, interference fringes become noticeable on the frame of the Si_3N_4 window. Once these fringes are seen, a spacer is put in place on the WCC sample plate and a resist placed atop the cells or cell organelles. The procedure continues very quickly until the WCC is ready for placement in the vacuum vessel. This method seems to work very effectively in taking care of the water layer problem. A key factor is putting in just enough water on the sponges to keep the WCC environment moist. Results from the x-ray micrographs of living CHO-SC1 cells indicate the water layer problem is surmountable and may be kept to ~1 μm thickness.

VII BIOLOGICAL APPLICATIONS

The biological specimens imaged by the author using soft x-ray contact microscopy were red blood cells, zymogen granules from the rat pancreas, 9L glialsarcoma cells and CHO-SC1 cells. The red blood cells and zymogen granules were fixed in glutaraldehyde. The 9L glialsarcoma cells were grown on formvar coated electron microscope (EM) grids and then critical point dried. The CHO-SC1 cells were imaged in the living state after treatment with colchicine. The progression of soft x-ray contact micrographs illustrates the development of readout techniques of the etched resists by electron microscopy. Also, these micrographs show the course of biological soft x-ray imaging starting with dried or fixed specimens and ending with living cells. The resolution of soft x-ray contact microscopy is between the limits of light microscopy and those of electron microscopy, whether in scanning or transmission mode. For this reason, some structures seen in electron microscopy may not be imaged by soft x-ray contact microscopy, however discussion of these structures has been included.

A. RED BLOOD CELLS

1. MATERIALS AND METHODS

The red blood cells were obtained from a human blood sample. When the blood sample was drawn, an appropriate amount of anticoagulent (blood-to-anticoagulent ratio is 9:1) was added. This mixture was washed in phosphate buffered solution (PBS) and then fixed for 2 hours with a solution of 2.3% glutaraldehyde in a 0.05 M sodium cacodylate buffer, which had a pH of 7.4 $\pm$ 0.05 and an osmolarity of 360 mOsm $\pm$ 5. The fixative volume-to-blood volume solution was 6:1. This preparation was rinsed in double distilled water three times and then centrifuged for ~5 min at 500 g. At this point, 1.5 cc of red blood cells were obtained. A second group of cells was stained by electron dense materials, which were osmium tetroxide, uranyl acetate and lead citrate. To continue this procedure, 0.25 cc of red blood cells were stained with 5 cc of 1% osmium tetroxide in distilled water for 2 hours. The sample was rinsed in double distilled water three times and

then centrifuged for ~5 min at 500 g. Now, 5 cc of a solution containing uranyl acetate in methanol was added for 20 minutes in a dark room at room temperature. The solution of uranyl acetate in methanol was dispensed by syringe through a 0.22 μm nucleopore filter to strain precipitate. The cells were dispersed. This solution was rinsed in double distilled water three times. Lastly, 5 cc of Reynold's lead citrate, which was passed through a 0.22 μm nucleopore filter, was added for 10 minutes. Again, this solution was rinsed in double distilled water three times. Extreme care and proper disposal must be maintained when handling electron dense stains, because these materials are toxic. For the soft x-ray contact microscopy experiments, both the stained and unstained red blood cells were placed on Pella formvar coated EM grids. The distilled water was wicked away and the EM grid was inserted into a holder. The recording resist, which was 900 nm thick copolymer on a solid silicon substrate, was placed on top of the EM grid. The holder was put into the SXCM sample plate. The red blood cells were prepared by Jacob Bastacky, LBL.

The soft x-ray exposures were 6 hours long. The radiation emission line was V_{L_α} which has an energy of 511 eV. The power supply was operated at 37 mA and 2.5 kV, which implies a continuum of higher energy soft x-rays contributed to the total radiation emitted.

2. RESULTS

After the 6 hour exposure to V_{L_α} x-rays, the resists were developed in a solution of methyl isobutyl ketone (MIBK) and isopropyl alcohol (IPA) (MIBK:IPA 1:5). The development time ranged from 6' 30" to 9' 15". Development of the resist was monitored by reflective light microscopy, which was differential interference contrast (DIC) with Nomarski optics. Figure 41 illustrates the x-ray resist image of unstained red blood cells at 200 x magnification using DIC while Figure 42 shows a higher magnification of 1000 x of the same field. A piece of thread is seen to cover some cells in Figure 42. At the light microscopic level, there are typical red blood cells and some poikilocytes, which are a normal feature if excess numbers are not found.

Figure 41. Light micrograph of the x-ray resist image of normal red blood cells (Magnification 200X)

The scale on this micrograph is 1 cm: 40 μm (micrograph: actual)

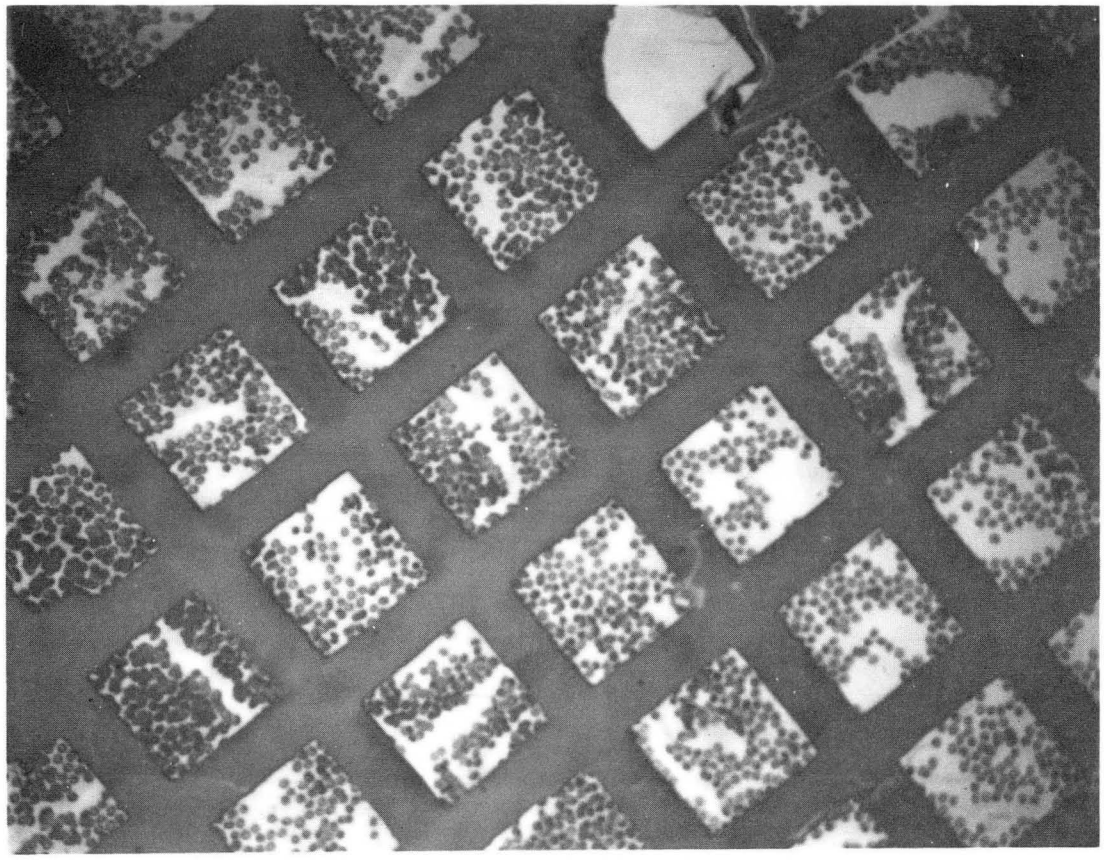

XBB 876-5290

Fig. 41

Figure 42. Higher magnification light micrograph of Figure 41 (Magnification 1000X)
The scale on this micrograph is 1 cm: 8 μm

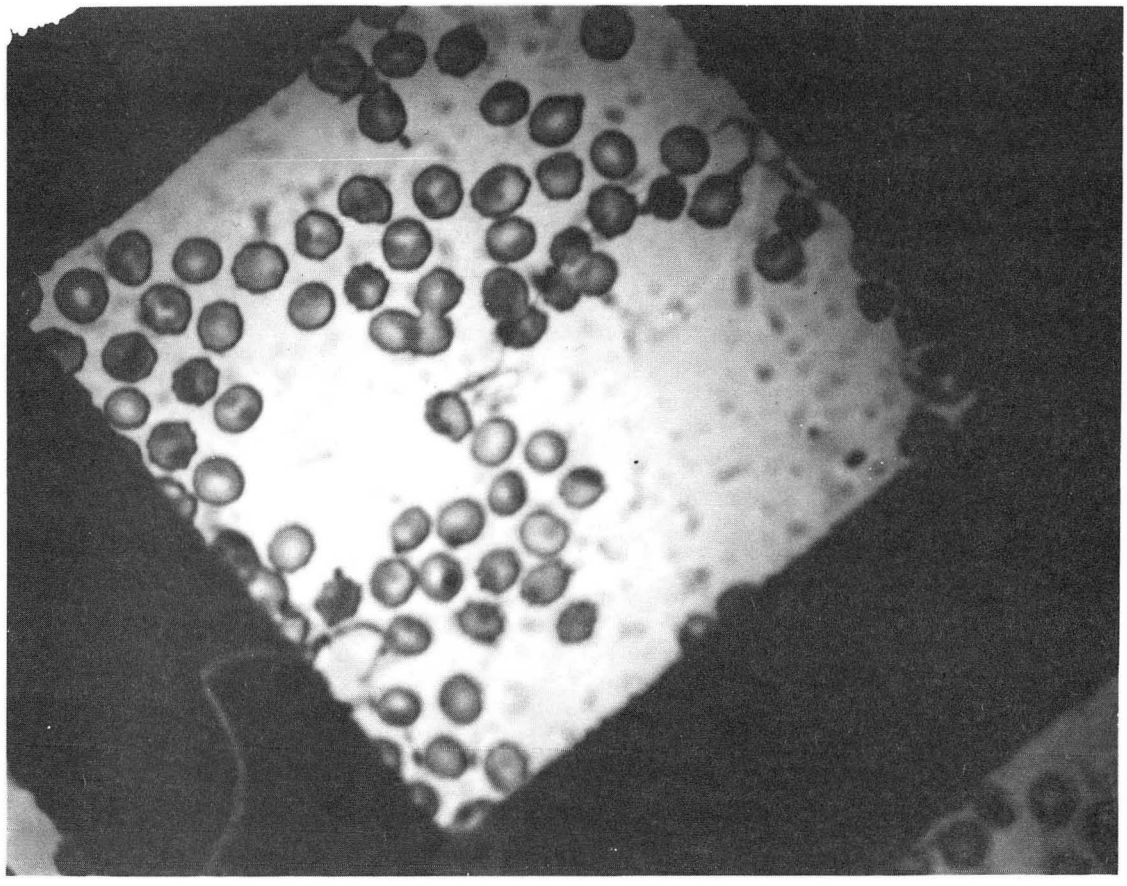

XBB 876-5288

Fig. 42

Figure 43. SEM of the x-ray resist image of normal red blood cells (Magnification 5000X)

The scale is given on the micrograph. The viewing angle is 75° from the horizontal. Note the resolution of the piece of thread.

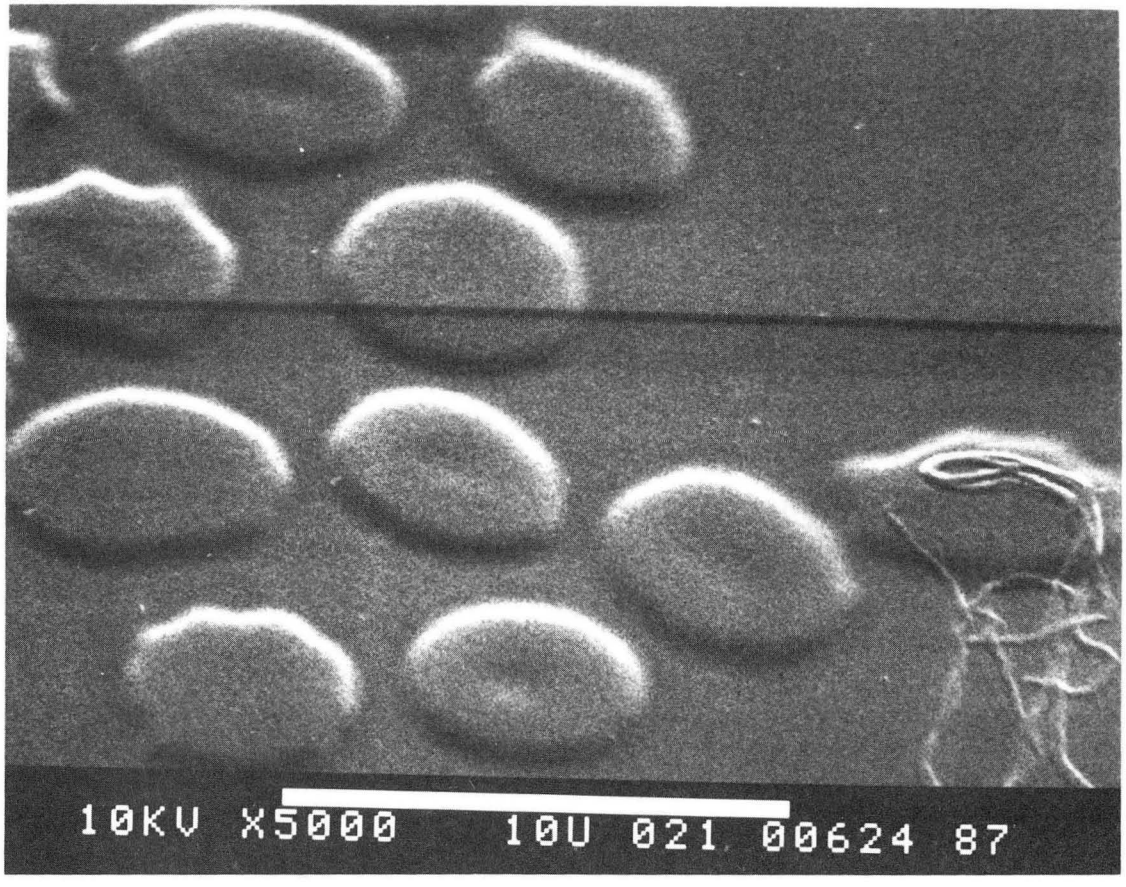

XBB 876-5296

Fig. 43

Figure 44. SEM of the x-ray resist image of normal red blood cells (Magnification 10000X)

The scale is given on the micrograph. The viewing angle is 75° from the horizontal.

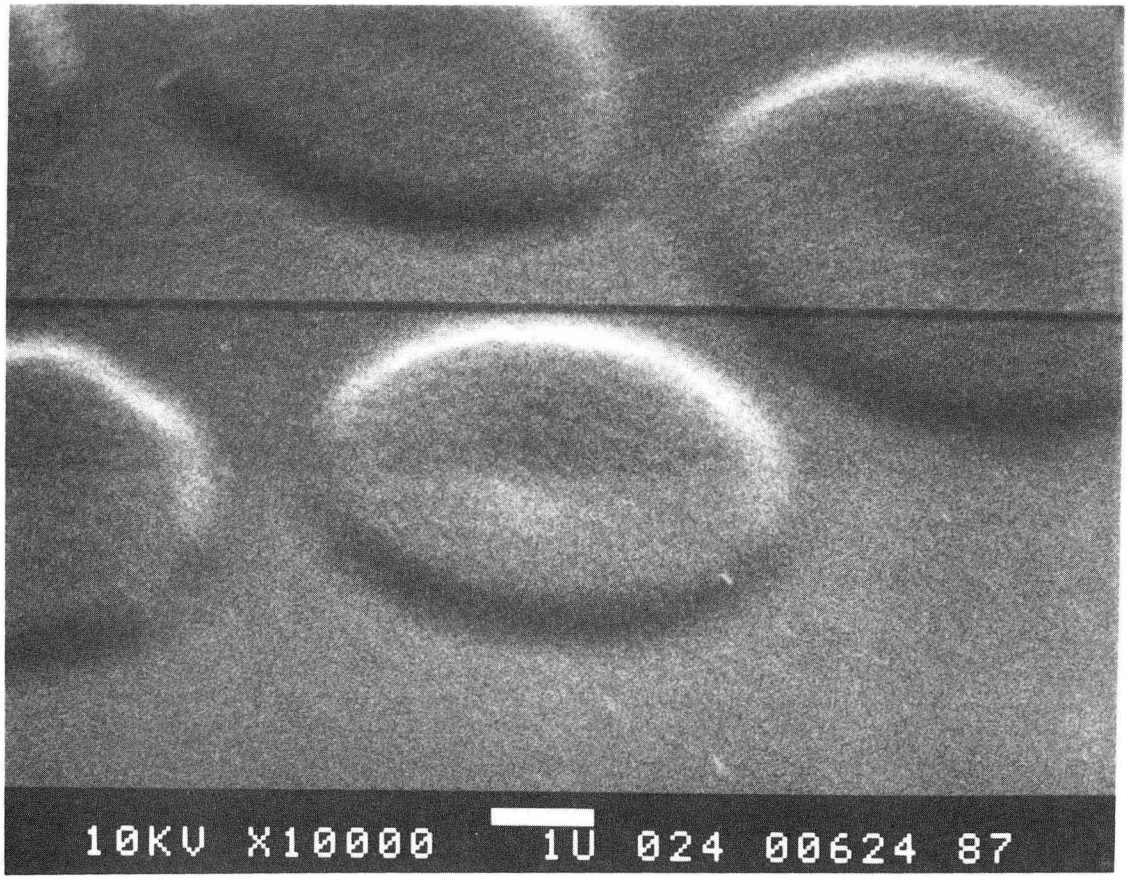

XBB 876-5297

Fig. 44

Before viewing the resists by SEM, a coat of ~10 nm thick Pt-C was applied by sputtering. The resists were viewed at ~75^{o} angle from the horizontal in the SEM, which is an Amray model located at Donner Laboratory, LBL. Figure 43, a SEM picture at 5000X magnification, illustrates some of the red blood cells seen in the light microscope field in Figure 42. The sharpness of the thread demonstrates the resolution of the SEM and the level of focussing attained in this micrograph. Dimpling in the red blood cells are a normal feature, seen also in SEMs. At higher magnification, which is shown in Figure 44, the dimpling feature is still prominent.

Hemoglobin, a macromolecule, is the characteristic protein that is the oxygen carrier within the erythrocyte. It is also involved in the transport of carbon dioxide and hydrogen ions **(Stryer 1981)**. The best way to view hemoglobin, which was the goal of this experiment, is to use synchrotron radiation. An important aspect of synchrotron radiation is the capability to generate a coherent polarized x-ray beam. If exposures are made using the polarized beam, one can detect the polarization or orientation of the hemoglobin. A mapping of hemoglobin orientation would facilitate a better understanding of hemoglobin related diseases, such as sickle cell anemia.

No internal cytoskeletal architecture was observed in the soft x-ray contact micrographs of red blood cells. Current knowledge indicates that mammalian red blood cells maintain their shape with a submembraneous meshwork of actin and spectrin . Actin, a monomeric protein, is a major constituent of thin filaments within muscle cells and microfilaments in nonmuscle cells. Spectrin is a key actin-binding protein, that is anchored to ankyrin, which in turn also anchors the integral membrane proteins. The actin-spectrin association is thought to stabilize and regulate the shape of the red cell membrane **(Fulton 1984, Stryer 1981)**.

3. COMPARISON OF SOFT X-RAY CONTACT MICROGRAPHS WITH LIGHT MICROGRAPHS, TEMs AND SEMs

The soft x-ray contact micrographs of the red blood cells correlate very well with current literature illustrating light micrographs, SEMs and TEMs (**Leeson 1981**). It has been indicated that the soft x-ray contact micrographs show dimpling in the erythrocytes or that the cells are biconcaved discs. The goal of this experiment was to image hemoglobin, however polarized x-rays are necessary to determine the orientation of the hemoglobin. This requirement may be easily met by using a synchrotron radiation source. The x-ray images also demonstrate a lack of large internal cytoskeletal structures, such as stress fibers. These features are also lacking in the light micrographs, SEMs and TEMs.

B. ZYMOGEN GRANULES

1. MATERIALS AND METHODS

The zymogen granules were obtained from a rat pancreas. The rat pancreas was enzymatically digested and broken into cells. The cell membrane was broken and the solution centrifuged. The zymogen granules were removed and maintained in a sucrose solution. To prepare the granules for transport and storage, they were washed two times with a buffered solution and kept on ice until they were ready for exposure. For soft x-ray contact microscopy, the zymogen granules were placed on Pella formvar coated EM grids. The solution was wicked away and the EM grid was inserted into a holder. The recording resist, which was 900 nm thick copolymer on a solid silicon substrate, was placed on top of the EM grid. A sealed spring mechanism was placed on top of the substrate to ensure contact between the resist and the sample. The holder was put into the SXCM sample plate. The preparation of the zymogen granules was done by Ken McQuaid, UCSF.

The duration of the soft x-ray exposure was 18 hours 34 minutes long. The radiation emission line was V_{L_α} which has an energy of 511 eV. The power supply was operated at 37 mA and 2.5 kV, which implies a continuum of higher energy soft x-rays contributed to the total radiation emitted.

Figure 45. SEM of the x-ray resist image of rat pancreatic zymogen granules (Magnification 1800X)

The scale is given on the micrograph. The viewing angle is 75° from the horizontal.

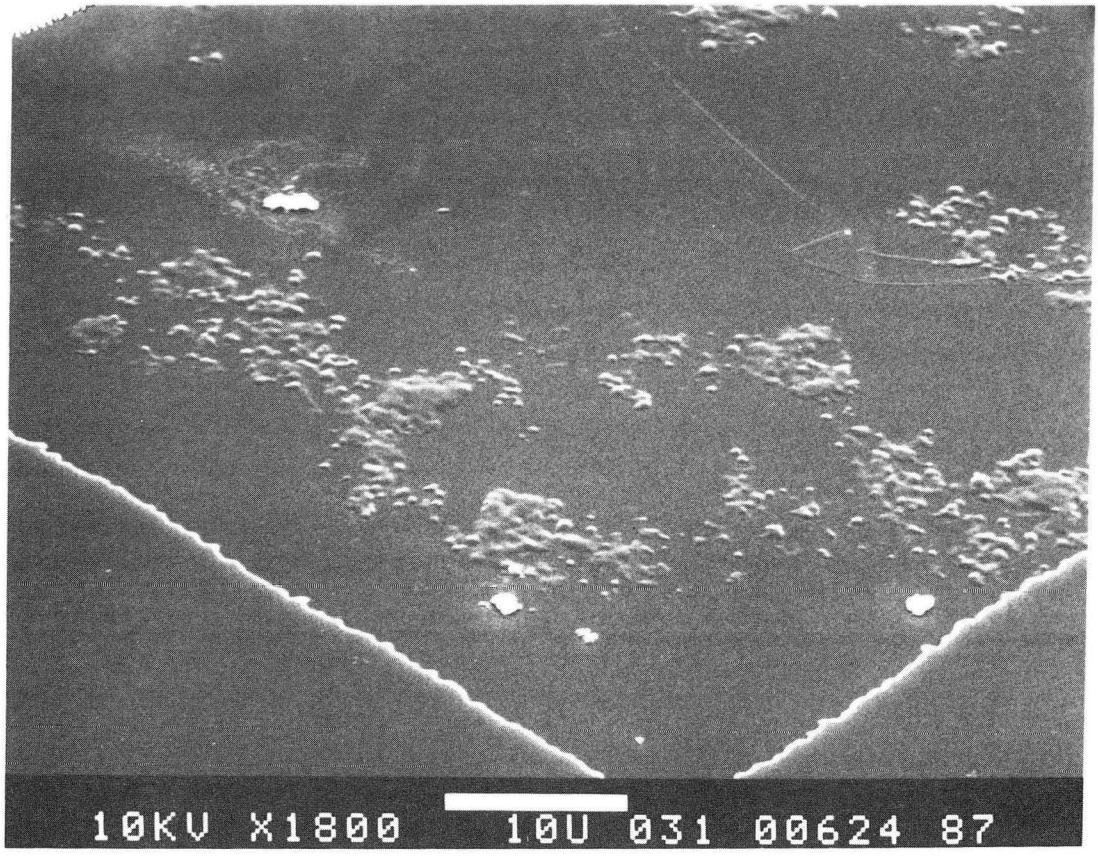

XBB 876-5286

Fig. 45

2. RESULTS

The exposed resists were developed in a MIBK: IPA (1:5) solution for 1 minute. Development of the resist was monitored by DIC and Nomarski optics. Before viewing the resists by SEM, a coat of ~10 nm thick Pt-C was applied by sputtering. The resists were viewed at about a 75° angle in the SEM, which was an Amray model. Figure 45 illustrates a soft x-ray contact micrograph of zymogen granules viewed by SEM at a magnification of 1800X. The zymogen granules, which are a specialized form of secretory vesicles found in the pancreas, are about 1 μm in diameter and contain zymogens, such as trypsinogen, chymotrypsinogen, procarboxypeptidase and proelastase. Zymogens, also known as proenzymes, are inactive precursors, which upon proteolytic cleavage outside the secretory cell become active digestive enzymes. Thus, trypsinogen becomes trypsin; chymotrypsinogen --> chymotrypsin; procarboxypeptidase --> carboxypeptidase and proelastase --> elastase **(Stryer 1981, Alberts 1983)**.

3. COMPARISON OF SOFT X-RAY CONTACT MICROGRAPHS WITH LIGHT MICROGRAPHS, TEMs AND SEMs

The soft x-ray contact micrographs of the zymogen granules were inconclusive in depicting the density mapping within a single zymogen granule. Current TEMs indicate that zymogen granules are solid uniform dense masses **(Stryer 1981, Alberts 1983)**. **Rothman** (1988) demonstrated the possibility that zymogen granules may not be homogeneous but have a heterogeneous density composition.

C. 9L GLIALSARCOMA CELLS

1. MATERIALS AND METHODS

The 9L glialsarcoma cells were grown on Si_3N_4 windows on formvar coated Pella EM grids. The cells were grown in a culture medium, which was MEM with 15% calf serum. The following is a list of ingredients that make up the MEM with 15% calf serum media:

1). 433 ml triple filtered sterile water

2). 50 ml 10X concentrated MEM (Gibco #410-1700, modified, autoclavable and without L-glutamine

3). 10 ml 100X concentrated L-glutamine (Gibco #320-5030, density 29.2 mg/ml)

4). 16 ml $NaHCO_3$ (Gibco #670-5080, 7.5% solution)

5). 22 ml fetal calf serum (Irvine Science #3000, sterile filtered)

6). 66 ml heat inactivated (30 min. @ 56°C) newborn calf serum (Gibco #200-6010)

7). 5 ml fungizone (Gibco #600-5295, lyophilized)

8). 1 ml gentamycin (Gibco #600-5750)

or 9). 5 ml pen-strep solution (Gibco #600-5070)

or 10). 5 ml 100X concentrated kanomycin sulfate solution (Gibco #600-5160).

After two days, the cells appeared to have attached to the EM grids. At this time, the grids and attached cells were placed in ethyl alcohol baths of increasing concentrations. The cells were exposed to the alcohol for five minutes at each step. Upon reaching full concentration, the cells were bathed twice and then placed into the critical-point drier.

The critical-point dried cells were placed into a holder. The recording resist, which was 480 nm thick PMMA on a 120 nm thick Si_3N_4 windowed TEM substrate, was placed on top of the sample. The soft x-ray exposures were 24 hours long. The radiation emission line was V_{L_α} which has an energy of 511 eV. The power supply was operated at 37 mA and 3 kV, which implies a continuum of higher energy soft x-rays contributed to the total radiation emitted.

2. RESULTS

After the 24 hour exposure to V_{L_α} x-rays, the resists were developed in a solution of MIBK:IPA 1:1. The development time was approximately 30 seconds. Development of the resist was monitored by DIC and Nomarski optics. During development, some of the resist windows broke or fell apart; however, the frame of the resist was kept for SEM readout. The resists were shadowed with a coat of ~16 nm thick Au-Pd at a 7° angle using

Figure 46. Light micrograph of the x-ray resist image of 9L glialsarcoma cells (Magnification 1000X)

The scale on this micrograph is 1 cm: 6.2 μm (micrograph: actual).

XBB 895-4141

Fig. 46

Figure 47. Light micrograph of the x-ray resist image of 9L glialsarcoma cells (Magnification 1000X)

The scale on this micrograph is 1 cm: 6.2 μm (micrograph: actual).

XBB 895-4139

Fig. 47

Figure 48.. SEM of the x-ray resist image of a 9L glialsarcoma cell (Magnification 4030X)

The scale is given on the micrograph. The viewing angle is 75° from the horizontal.

XBB 895-4142

Fig. 48

Figure 49. SEM of the x-ray resist image of two 9L glialsarcoma cells (Magnification 3030X)

The scale is given on this micrograph. The viewing angle is 75^{o} from the horizontal.

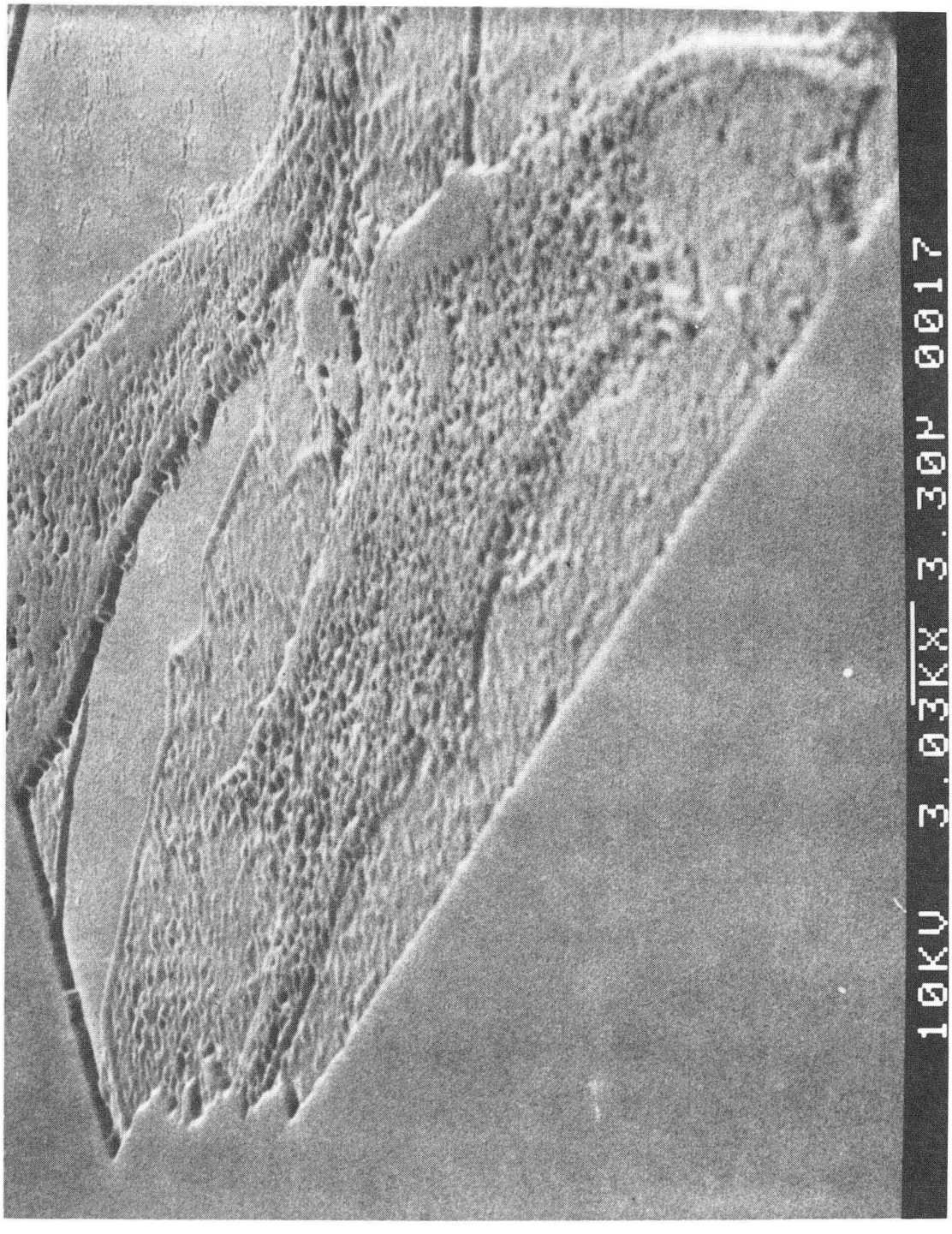

XBB 895-4140

Fig. 49

the Pella low-angle shadowing device. Viewing of the resist frame by SEM (ISI Model DS130) was done at a 75° angle. The TEM images were made on a Zeiss EM 109 using an operating voltage of 80 kV.

Figures 46 and 47 are light micrographs of the x-ray resist image of 9L glialsarcoma cells at a magnification of 1000X using DIC with Nomarski optics. The images of the cells are on the Si_3N_4 window of the TEM resist. Figure 46 shows three cells attached and spread out. The nucleus and nucleoli are defined in these cells. Figure 47 illustrates a number of cells that are attached and spread out. The nucleus and nucleoli are relatively prominent and the cell membrane is delineated. The attachment sites at the ends of the protrusions of the cell margins are readily seen. These two micrographs are comparable and may be of superior quality to the light micrographs of the x-ray images of human fibroblast, N140S, taken by **Shinohara** (1988). The preparation of the human fibroblast, N140S, involves fixation by glutaraldehyde and dehydration.

Figures 48 and 49 are SEMs of the x-ray resist image at a magnification of 4030X and 3030X respectively with a viewing angle of ~75°. These images appear on the resist frame due to overlap of the EM grid, that had covered the Si_3N_4 window also. Figure 48 illustrates some of the cytoskeletal architecture. The nucleus can be discerned within the cell, however this is not easily done. Continued development may enhance the image. Figure 49 shows the cytoskeletal architecture very well in both cells pictured and the nucleus and nucleoli are easily observable in the complete cell seen in this micrograph. The attached margin of the complete cell is also delineated.

Figures 50-60 are TEMs of the x-ray resist image with magnifications of 3000X or 7400X. Magnification is at 3000X unless stated otherwise. Figure 50 shows the nucleus, two nucleoli with a connecting bridge and a faint image of the nuclear membrane. The cytoskeletal architecture, probably a network of microtubules, is seen. A picture of the large nucleolus and small nucleolus with connecting bridge at higher magnification, 7400X, is seen in Figures 51 and 52 respectively. Figure 53 illustrates a portion of the

Figure 50. TEM of the x-ray resist image of the nucleus of a 9L glialsarcoma cell (Magnification 3000X)

The scale on this micrograph is 1 cm: 1.3 μm (micrograph: actual)

XBB 895-4143

Fig. 50

Figure 51. A higher magnification TEM of Figure 50 showing the larger nucleolus (Magnification 7400X)

The scale on this micrograph is 1 cm: 0.6 μm (micrograph: actual)

XBB 895-4144

Fig. 51

Figure 52. A higher magnification TEM of Figure 50 showing the smaller nucleolus and connecting bridge (Magnification 7400X)

The scale on this micrograph is 1 cm: 0.6 μm (micrograph: actual)

XBB 895-4145

Fig. 52

Figure 53. TEM of the x-ray resist image of the filiform protrusion from the nucleus toward the margin of a 9L glialsarcoma cell (Magnification 7400X)

The scale on this micrograph is 1 cm: 0.6 μm (micrograph: actual)

XBB 895-4146

Fig. 53

Figure 54. TEM of the x-ray resist image of the attachment sites at the ends of the filiform protrusion of the margin of a 9L glialsarcoma cell (Magnification 3000X) The scale on this micrograph is 1 cm: 1.4 μm (micrograph: actual)

XBB 895-4134

Fig. 54

Figure 55. TEM of the x-ray resist image of the nucleus of another 9L glialsarcoma cell (Magnification 3000X)

The scale on this micrograph is 1 cm: 1.5 μm (micrograph: actual)

XBB 895-4135

Fig. 55

Figure 56. A higher magnification TEM of Figure 55 (Magnification 7400X)

The scale on this micrograph is 1 cm: 0.6 μm (micrograph: actual)

XBB 895-4147

Fig. 56

Figure 57. TEM of the x-ray resist image of the nucleus of another 9L glialsarcoma cell (Magnification 3000X)

The scale on this micrograph is 1 cm: 1.5 μm (micrograph: actual)

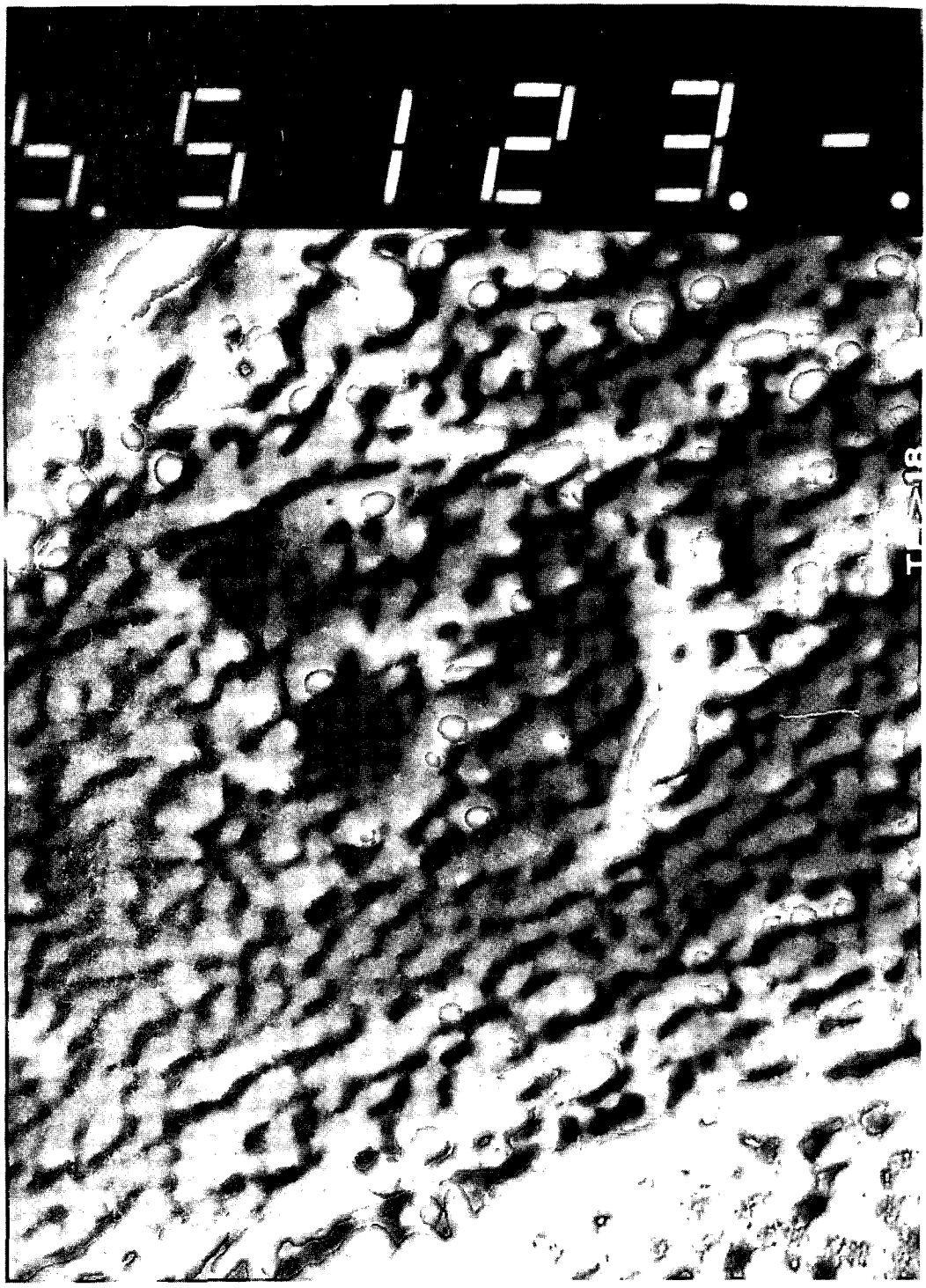

XBB 895-4136

Fig. 57

Figure 58. TEM of the x-ray resist image of the attachment sites at the ends of the filiform protrusions of the cell margin of another 9L glialsarcoma cell (Magnification 3000X)

The scale on this micrograph is 1 cm: 1.5 μm (micrograph: actual)

XBB 895-4148

Fig. 58

Figure 59. TEM of the x-ray resist image of the attachment sites at the ends of the filiform protrusions of the cell margin of a different 9L glialsarcoma cell (Magnification 3000X)

The scale on this micrograph is 1 cm: 1.5 μm (micrograph: actual)

XBB 895-4149

Fig. 59

Figure 60. TEM of the x-ray resist image of the filiform protrusion of a 9L glialsarcoma cell covering torn formvar (Magnification 3000X)
The scale on this micrograph is 1 cm: 1.5 μm (micrograph: actual)

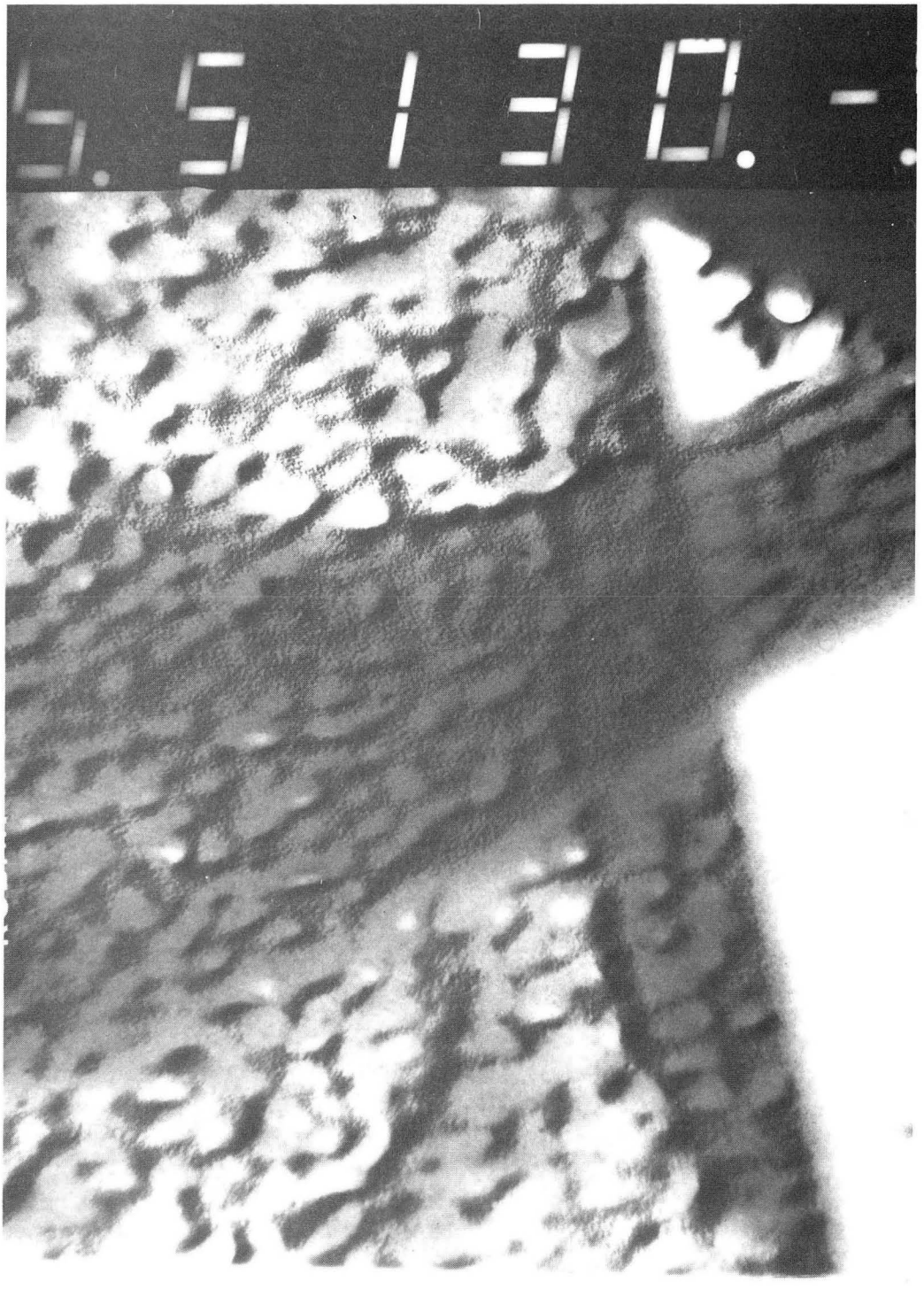

XBB 895-4150

Fig. 60

filiform protrusion away from the nucleus towards the margin at a magnification 7400X. Cytoskeletal architecture is obvious. The attached margin of the filiform protrusion is demonstrated in Figure 54. Filiform protrusions, which contain microfilaments, are noticeable as is the cytoskeletal architecture, a network of what are possibly microtubules and intermediate filaments. There is a possibility that a network of endoplasmic reticulum within the filiform protrusion is seen in this micrograph. Figure 55 shows another cell with the nucleus having a clearly defined nuclear membrane and possibly four nucleoli. The cell membrane is noticeable and probably enhanced by Fresnel diffraction fringes. Figure 56 is a higher magnification, 7400X, of one of the nucleoli seen in Figure 55. A different cell with a nucleus clearly defined by the nuclear membrane is shown in Figure 57. Two nucleoli and a cytoskeletal network are visible. The attachment sites at the ends of the filiform protrusions of the cell margin are seen in Figures 58 and 59. These micrographs are comparable to the 3T3 mouse fibroblast x-ray images viewed by TEM and taken by **Cheng** (1985, 1986b). Preparation of the 3T3 fibroblasts was similar to that of the human fibroblast, N140S, done by **(Shinohara 1988)**. Lastly, Figure 60 demonstrates the fidelity of the soft x-ray contact microscopy technique by being able to discriminate between two overlapping bodies. The protrusion of the cell margin overlaps a torn piece of formvar.

3. COMPARISON OF SOFT X-RAY CONTACT MICROGRAPHS WITH LIGHT MICROGRAPHS, TEMs AND SEMs

The light micrographs of the x-ray images of the 9L glialsarcoma cells are comparable or may be of higher quality than the light micrographs of the x-ray images of human fibroblast, N140S, taken by **Shinohara** (1988). Shinohara and workers were able to show the ends of the filiform protrusions of the cell margins and the nucleus of these cells very distinctly. The human fibroblast, N140S, is comparable in size to the 9L glialsarcoma cell. The soft x-ray contact micrographs, viewed by TEM, of the 9L glialsarcoma cells compare favorably with the images of 3T3 mouse fibroblasts generated

by **Cheng** (1985, 1986b). However, the size of the 3T3 mouse fibroblast (length > 60 μm and width ~35 μm) and its nucleus (diameter ~20 μm) are much larger than that of the 9L glialsarcoma cell. The 9L glialsarcoma cell is a fibroblast-like cell because the glial cell is the connective tissue cell or "glue" cell of the brain and sarcoma implies a cancer arising from mesenchymal tissue (**Alberts 1983, Robbins 1984**). Fibroblasts have been studied in great detail and current TEMs demonstrate a highly organized cytoskeletal architecture (**Fulton 1984**). The SEMs have also been successful in showing the topographical features and attachment sites at the ends of the filiform protrusions of the cell margins of fibroblasts (**Alberts 1983**). Fixation processes are used to prepare the fibroblasts for viewing with EM. The imaging of living fibroblasts would provide an excellent correlation between the EMs and the soft x-ray contact micrographs.

D. CHO-SC1 CELLS

1. MATERIALS AND METHODS

The CHO-SC1 cells were cultured and then exposed to 2 μg/ml of colchicine for 4 hours. Colchicine is a microtubule inhibitor (**Alberts 1983, Fulton 1984**). This treatment increased the number of mitotic cells to about 25% of the cell population. After trypsinization, the cells were washed once in phosphate buffered saline (PBS). A small drop of cell suspension was placed onto the Si_3N_4 window, which was glued onto the WCC sample plate. The cells were allowed to settle and then the PBS was wicked away until interference fringes were seen on the frame. At this time, a 900 nm thick PMMA SEM resist was placed on top of the cells and the resulting sandwich quickly mounted into the WCC. Samples were exposed to an intense, nearly instantaneous (nsec) x-ray pulse produced by a laser-induced plasma source (JANUS, LLNL). The target material used to generate the x-rays was a Ta foil, 25 μm thick. The dose given to the sample was ~6.5 kgray.

Figure 61.. Light micrograph of the x-ray resist image of living CHO-SC1 cells (Magnification 1000X)

The scale of the micrograph is 1 cm: 6.1 μm (micrograph: actual).

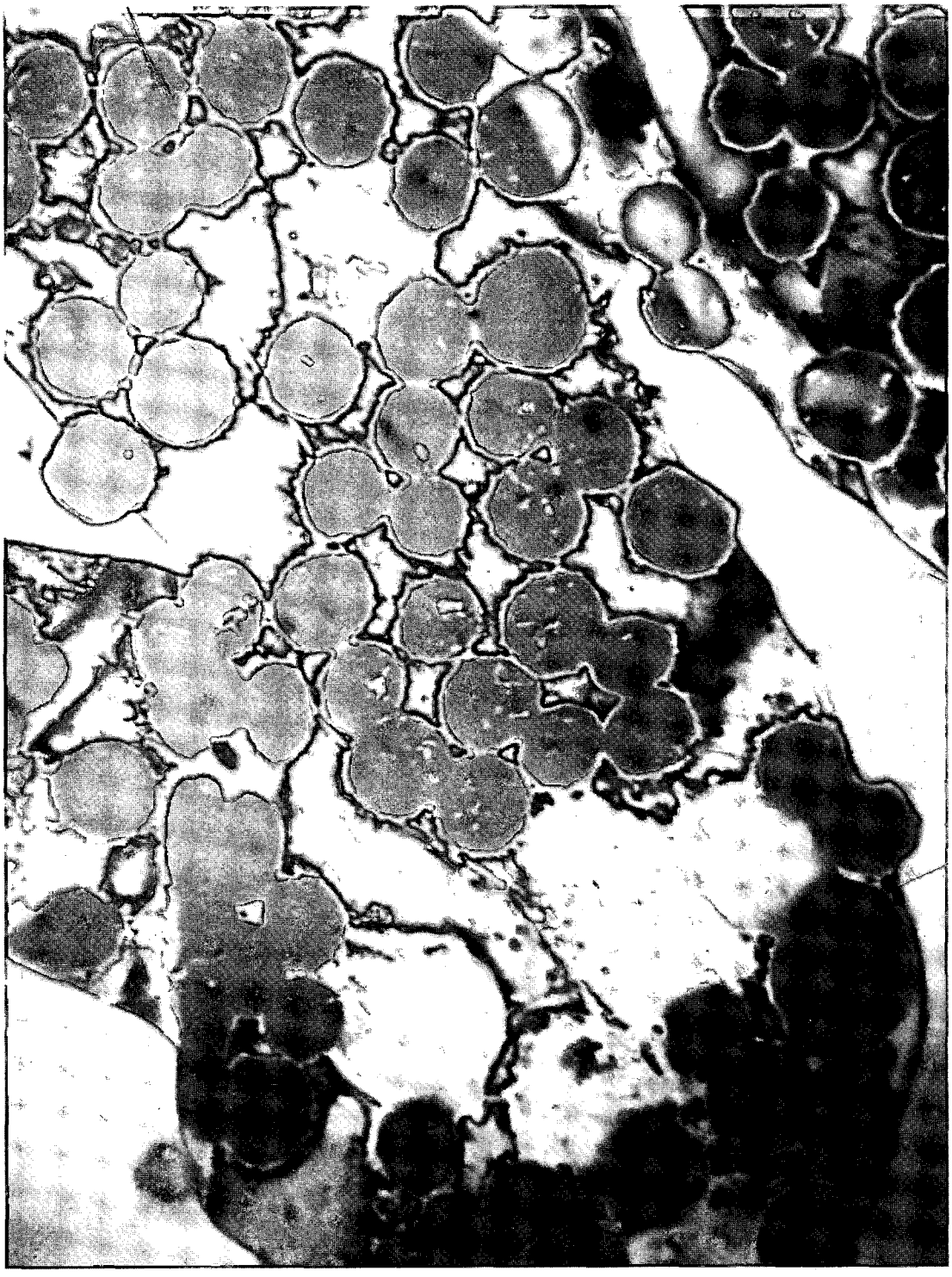

XBB 880-10625

Fig. 61

Figure 62. Light micrograph of the x-ray resist image of living CHO-SC1 cells (Magnification 1000X)

The scale of the micrograph is 1 cm: 6.1 μm (micrograph: actual).

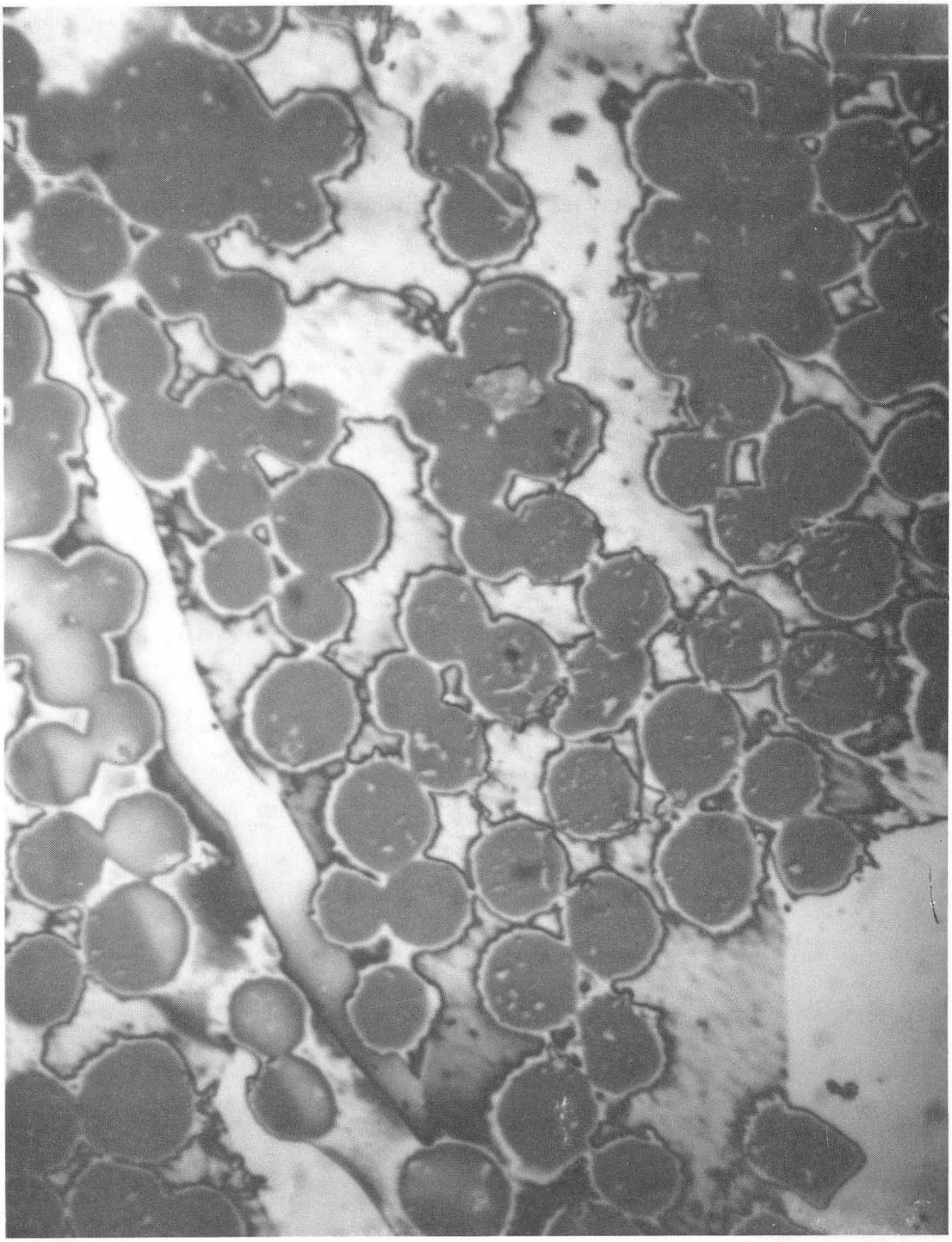

XBB 880-10626

Fig. 62

Figure 63.. SEM of the x-ray resist image of living CHO-SC1 cells (Magnification 7990X)

The scale is given on the micrograph. The viewing angle is 75^{o} from the horizontal.

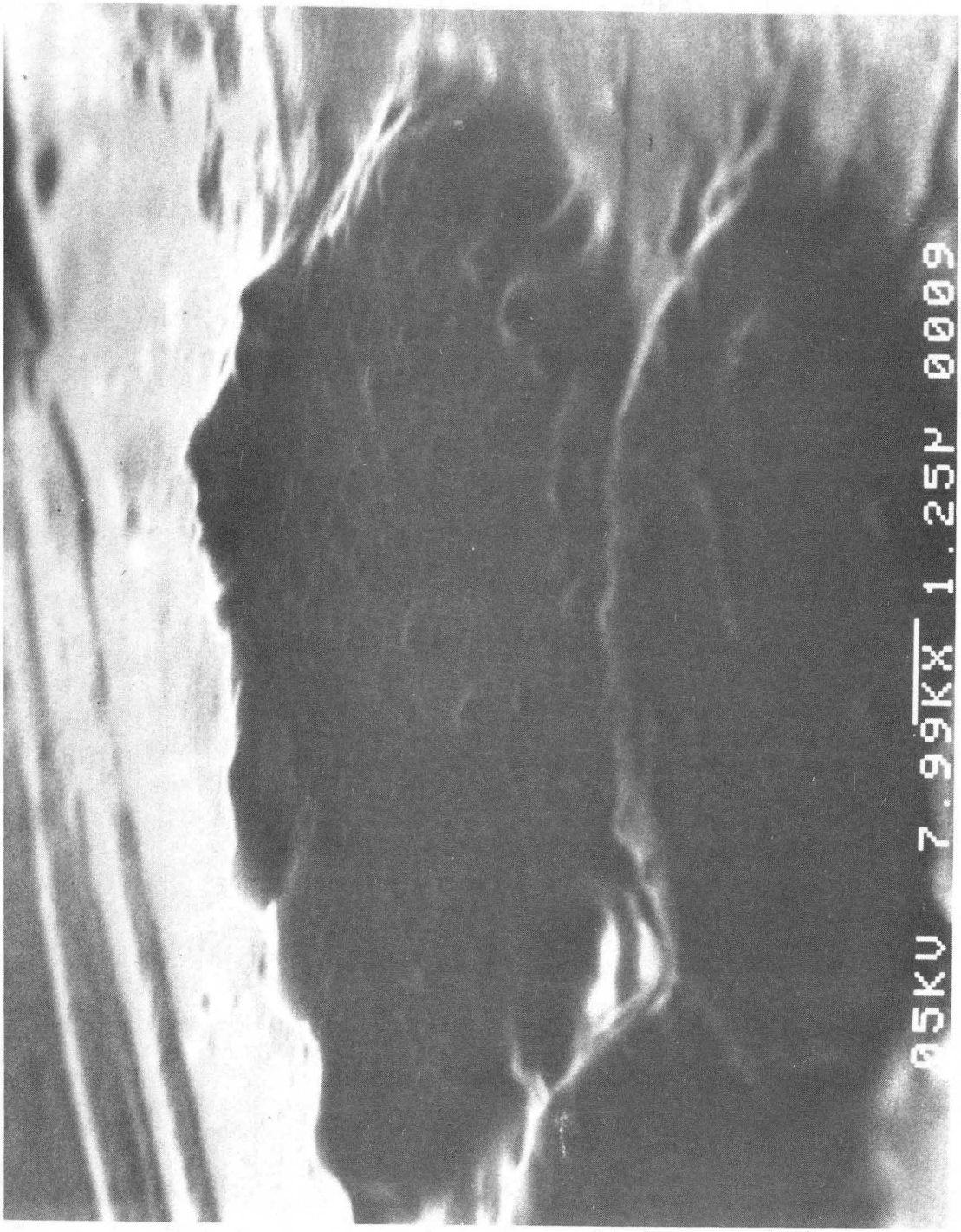

XBB 891-161

Fig. 63

Figure 64. SEM of the x-ray resist image of living CHO-SC1 cells (Magnification 6020X)

The scale is given on the micrograph. The viewing angle is 75^{o} from the horizontal.

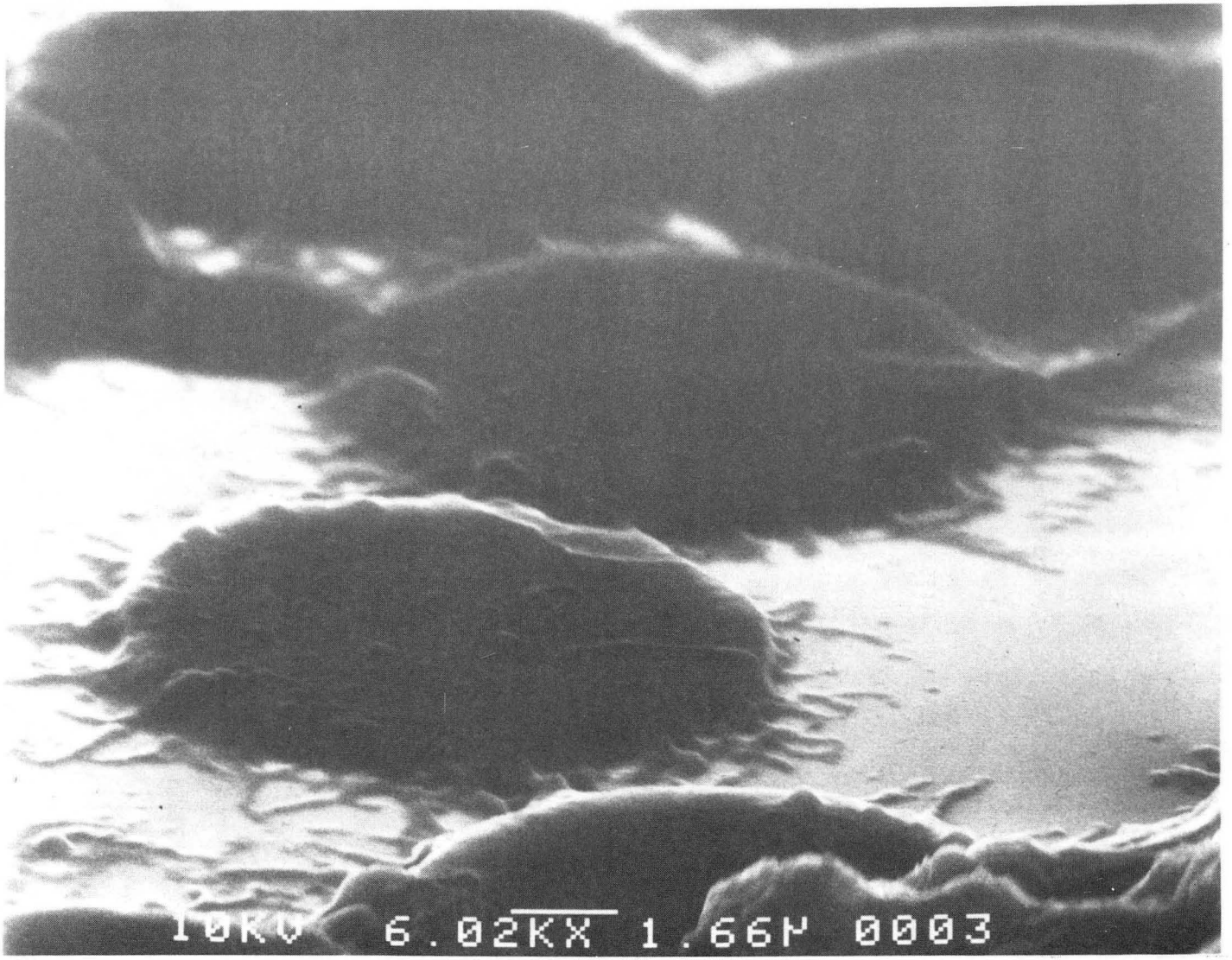

XBB 891-155

Fig. 64

Figure 65. SEM of the x-ray resist image of living CHO-SC1 cells (Magnification 6020X)

The scale is given on the micrograph. The viewing angle is 75^{o} from the horizontal.

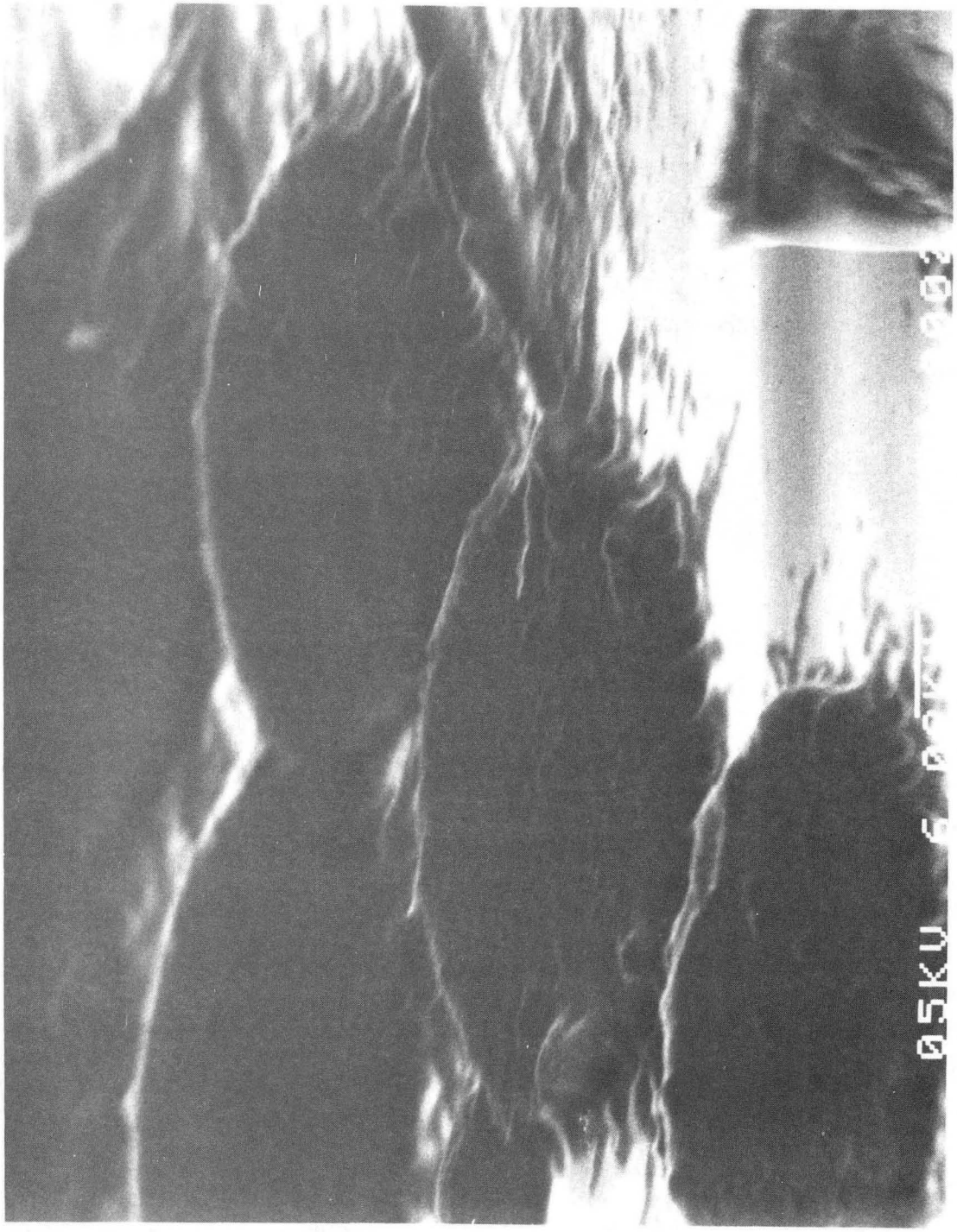

XBB 891-159

Fig. 65

Figure 66. SEM of the x-ray resist image of living CHO-SC1 cells (Magnification 5020X)

The scale is given on the micrograph. The viewing angle is 75° from the horizontal.

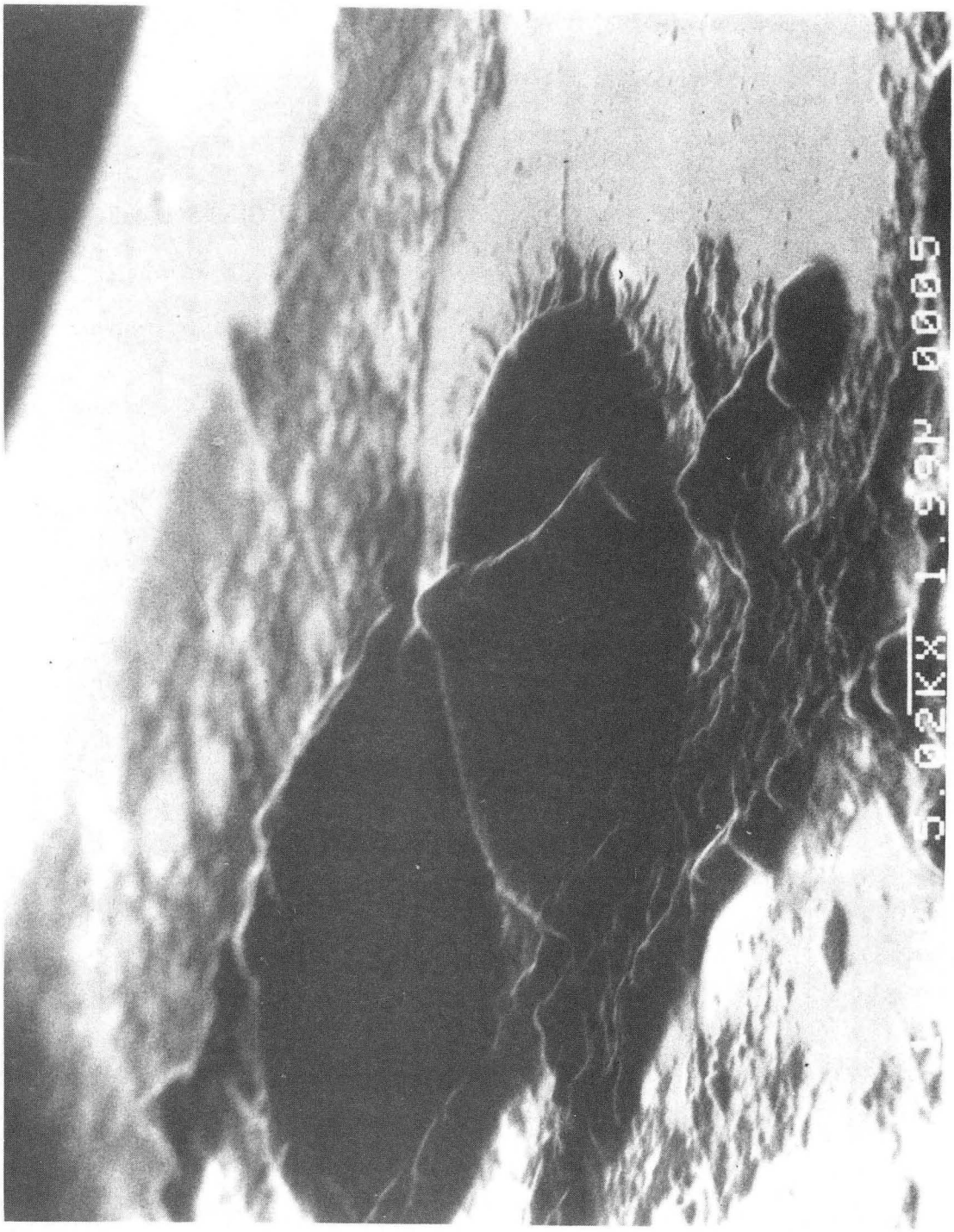

XBB 891-157

Fig. 66

Figure 67.. SEM of the x-ray resist image of living mitotic CHO-SC1 cells (Magnification 6020X)

The scale is given on the micrograph. The viewing angle is 75° from the horizontal.

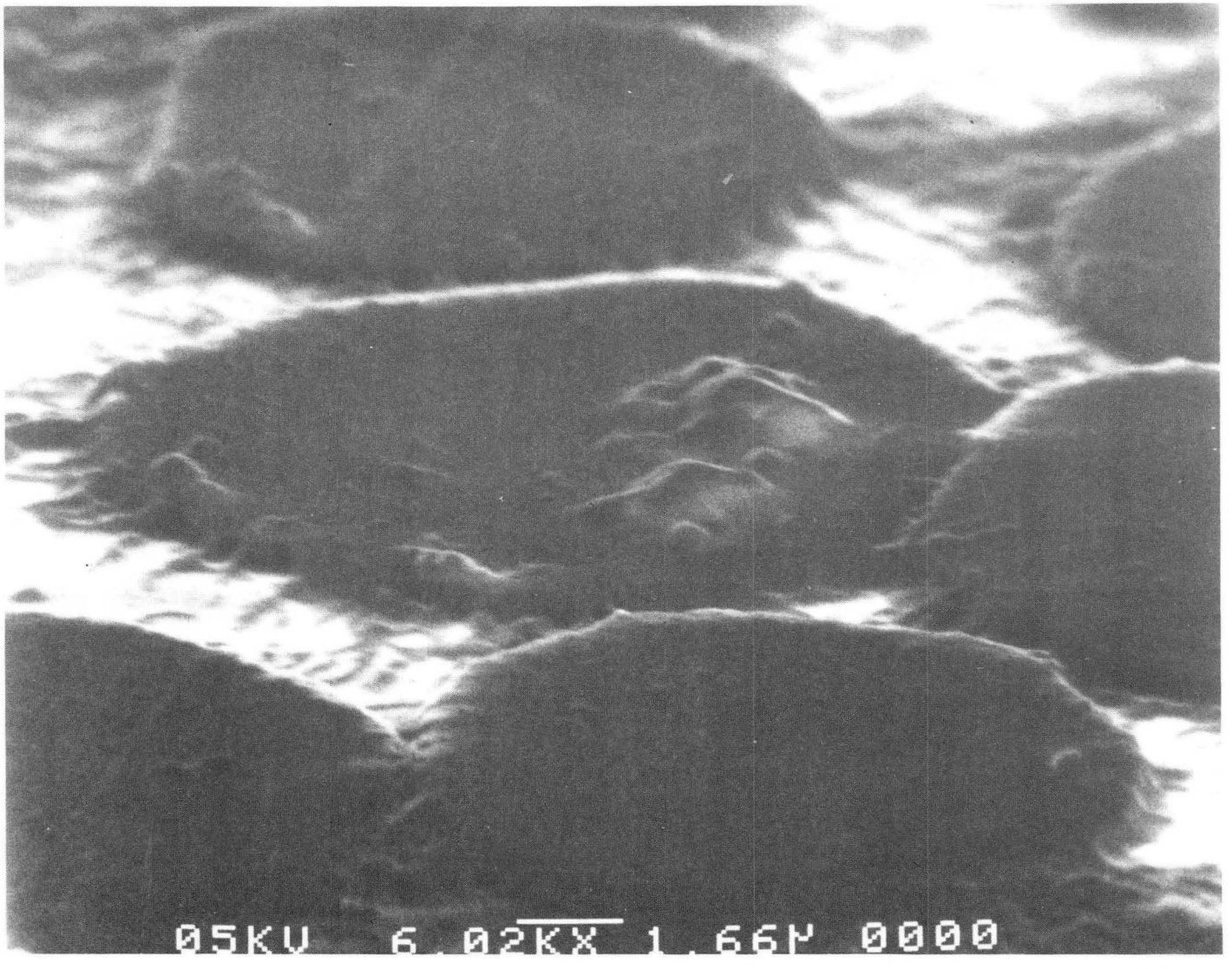

XBB 891-158

Fig. 67

Figure 68. SEMs of CHO-10B cells

Magnification of the top SEM is 2200X, while magnification of the bottom SEM is 9200X. The scale is given on the micrograph, where the bar segment is 5 μm. The SEMs were supplied and permission to use given by R. J. Sebring, Los Alamos National Laboratory.

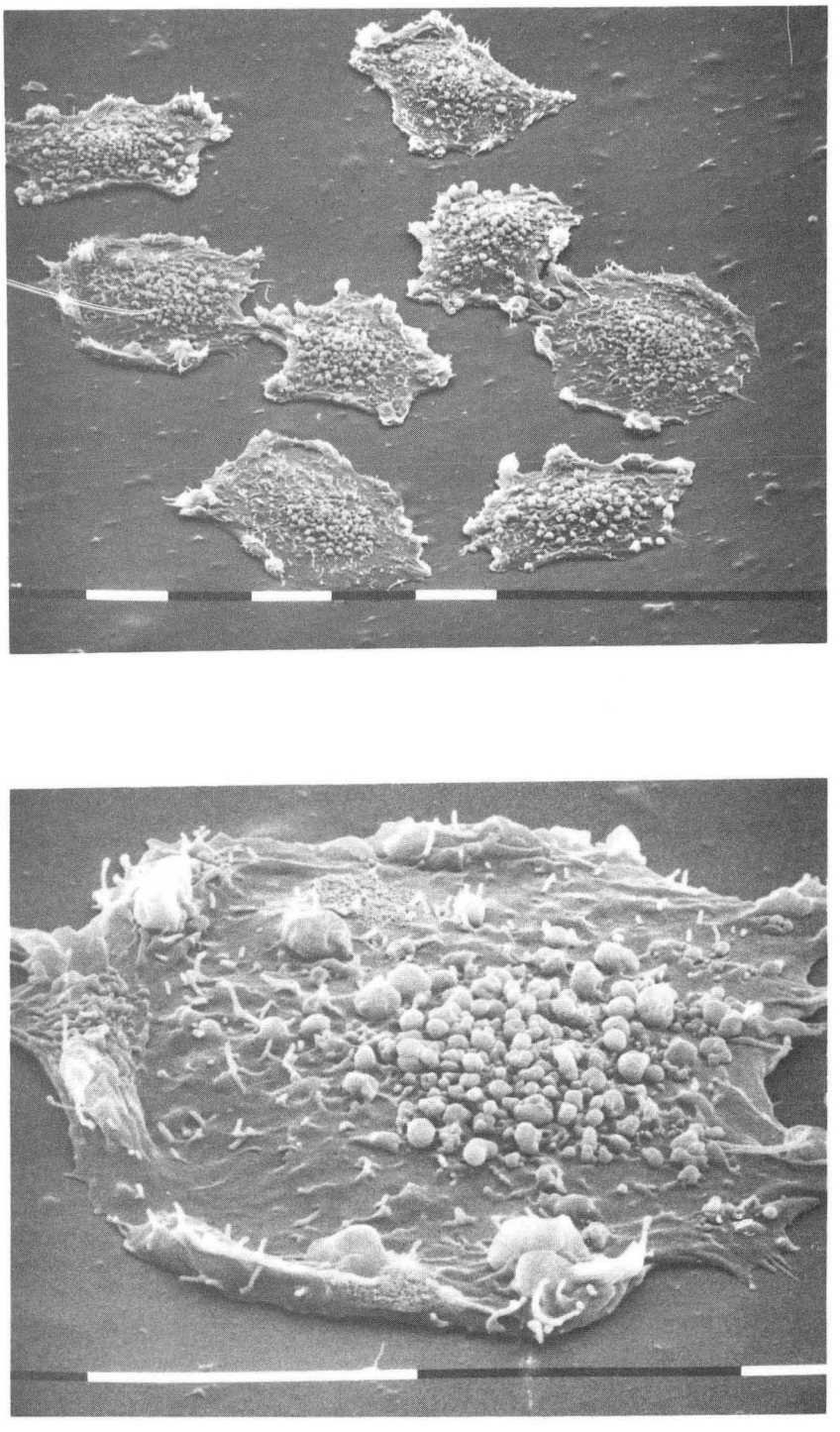

XBB 897-6056A

Fig. 68

2. RESULTS

After the exposure the resist was washed in an ultrasonic bath of isopropyl alcohol for 2 minutes. The next step was to develop the resist in a MIBK: IPA (1:1) solution for 105 seconds. Development of the resist was monitored by DIC and Nomarski optics. The resists were shadowed with a coat of ~13 nm thick Au-Pd at a 7.5° angle using the Pella low-angle shadowing device. Viewing of the resist by SEM (ISI Model DS130) was done at a 75° angle. An interesting feature seen in the soft x-ray contact micrographs of these cells are the many attachment fibers along the border. A certain amount of ruffling occurs along the border of the cells. The cells are ~8 μm in diameter. The attachment fibers are an interesting example of microfilament activity. The resolution of the attachment fibers is estimated to be 40 nm and their diameter is ~80-100 nm.

Figures 61 and 62 are light micrographs of the x-ray resist image of living CHO-SC1 cells. The magnification was at 1000X. Figure 63-67 are SEMs of the x-ray resist image of living CHO-SC1 cells. Cell ruffling is illustrated in Figure 63, magnification 7990X. Numerous organelles are seen inside the cytoplasm, however, their identities are not discernable. Attachment fibers are definitely seen on the cell borders and some cell ruffling is visible in Figure 64, magnification 6020X. Figure 65 is similar to Figure 64 except the cell ruffling is more prominent in the middle focussed cell. An unknown piece of debris laid on the cell and its surroundings in Figure 66, magnification 5020X. The next soft x-ray contact micrograph, Figure 67, probably depicts a mitotic cell, with the peaks possibly being chromosomes. Ruffling is noticeable on this cell and is involved in cell locomotion or cell adhesion. Again, attachment fibers are noticeable. Cell size also gives the implication that this cell is a mitotic cell. Further studies with a much higher population of mitotic cells may definitely determine their appearance using soft x-ray contact microscopy. None of the cells give an appearance of being physiologically dead at the time of exposure or being dehydrated because the Si_3N_4 vacuum window failed. Features of physiological death would include the loss of attachment fibers and a swelling of the cell to

maintain its osmolarity and pH balance and blebbing, which is a bubble-shaped or hemi-spherical protrusion from the cell.

3. COMPARISON OF SOFT X-RAY CONTACT MICROGRAPHS WITH LIGHT MICROGRAPHS, TEMs AND SEMs

The phase contrast light micrographs were unable to provide a good correlation with the soft x-ray contact micrographs. Figure 68 shows two SEMs of CHO-10B cells. CHO-10B cells are similar to CHO-SC1 cells in that they both come from the Chinese hamster ovary. The difference is the cell line from which they originated. The SEMs of the CHO-10B cells were supplied and permission to use given by R. J. Sebring, Los Alamos National Laboratory. The top picture has a magnification of 2200X and the bottom is magnified 9200X. The SEMs and soft x-ray contact micrographs correlate in the depiction of some of the attachment fibers and the ruffling. It is possible that the cell organelles depicted in the SEM could correlate with the soft x-ray contact micrographs.

VIII CONCLUSIONS

A. GENERAL DISCUSSION

1. CAN SOFT X-RAY CONTACT MICROSCOPY BE AN EFFECTIVE TECHNIQUE?

Soft x-ray contact microscopy is an effective imaging technique, that fills the "void" in resolution between light microscopy (~0.25 μm) and electron microscopy (0.2 nm) **(Cosslett 1957, 1960)** . Electron microscopy resolution may be increased (i. e. resolution may go below 0.2 nm) with higher energy (MeV) electrons. Applications to the fields of materials science and geology have been demonstrated **(Sayre 1988).** At this time, it is appropriate to do two-dimensional imaging in order to understand the mapping of cell densities. This is a preliminary step to three-dimensional imaging such as holography or microtomography. The maxim, "You've got to walk before you can run", is very true for soft x-ray contact microscopy. Section V demonstrates the resolution of this technique. Section VII illustrates the effectiveness of this technique in imaging fixed and living biological samples at a resolution of ~40 nm.

2. CAN SOFT X-RAY CONTACT MICROSCOPY BE A BIOLOGICALLY SIGNIFICANT TECHNIQUE?

SXCM can be a biologically significant technique to visualize subcellular structures, such as organelles, cytoskeletal architecture and macromolecules. One can look at these structures at a resolution of ~30-40 nm. Looking at subcellular structures pictured in the 9L glialsarcoma and living CHO-SC1 cells, one observes attachment microspikes and attachment fibers, respectively. Since the CHO-SC1 cells were treated with colchicine, the attachment fibers probably contain a number of microfilaments. Colchicine is a microtubule inhibitor **(Alberts 1983, Fulton 1984)**. Ruffling is noticeable in the SEMs of the x-ray resist image of the living CHO-SC1 cells. Therefore SXCM may contribute to the understanding of cell adhesion and cell locomotion.

Other subcellular components identified in the TEMs of the x-ray resist image of the 9L glialsarcoma cells are the nucleus, nucleoli, nuclear membrane and surface membrane. There is a possibility that a network of endoplasmic reticulum may be found in the filiform protrusion. The observation of chromosomes in mitosis is possibly evident in Figure 67. Heavy metal antibody specific labelling may enhance the image of chromosomes or microtubules in mitosis. The soft x-ray imaging of mitosis may be easier using Pt K2 cells, which spread out and remain thin during the cell cycle including mitosis.

Observation of molecular components of the cell requires better resolution. Macromolecular components, such as nucleic acids, particularly DNA, and globular or integral proteins, may be imaged by SXCM, however, one might not be able to identify them unless a heavy metal antibody specific label is attached. Differentiation of the components of the cytoskeletal network would also require heavy metal antibody specific labelling. If the resolution is 5 nm, identification of microfilaments (7 nm diameter), intermediate filaments (10 nm diameter) and microtubules (25 nm diameter) (**Leeson 1981, Alberts 1983**) could be made from the x-ray micrograph. At this time, the resolution is ~30-40 nm, which would allow the identification of chromosomes. The identification of DNA, which has a diameter of 2 nm and a contour length of 340 nm per kilobase (**Stryer 1981**), is very difficult even in its supertwisted state.

Physiological experiments utilizing SXCM may be done in either of two ways. The first method determines the elemental distribution in the cell using a subtraction procedure. The cell is irradiated at an x-ray energy above the absorption edge of the element of interest onto resist A and then again below the absorption edge onto resist B. The resists are developed, readout and compared. The elemental distribution is determined by subtracting the data of resist A from that of resist B. The determination of calcium in a cell is an example of the first method. There are two problems with this method. The first is the cell must be irradiated twice thus living cells cannot be used. The second is a registration or fidelity problem, where it would be necessary to maintain the same positioning,

development and readout of the resist. The other method is to instantaneously irradiate a large number of cells that have been stimulated or treated with a drug. The administration of the drug or stimulation would be done at an edge such that diffusion across the sample may occur. The intent is to create a range of the physiological process in the cells. The latter method is a statistical approach.

3. RADIOBIOLOGICAL CONCERNS

Soft x-rays have a more damaging effect, as measured by the relative biological effectiveness (RBE), on cells tnan hard x-rays **(Goodhead 1979 and 1987, Raju 1987)**. The absorption length of soft x-rays with energies in the "water window" is in the μm range in biological samples. Soft x-rays may have an absorption length as long as 10 μm within water. The thickness of mammalian cells may range from 2-50 μm though most cells are ~5-10 μm thick. Using the dimensional information, one can deduce that 1). most soft x-rays will be absorbed by the cell, 2). DNA strand breakage, which is the most significant radiation damage for cell killing, will be produced by the interaction of soft x-rays with the C and N atoms of DNA and 3). radiation damage caused by free radicals produced in water will be at a minimum. Radiation damage caused by the breakage of protein or enzyme chains is of minimal importance because there are many proteins or enzymes and the regeneration of these macromolecules will continue as long as the DNA is intact. The characteristics of soft x-rays permit them to be very useful probes to determine the molecular biology of a cell.

A major concern of SXCM is the high doses given to the biological sample in order to make an image. One may look to the crystallography literature or electron microscopy data to estimate the high dose effects of soft x-rays, however this is a rough and possibly poor correlation. The samples one would like to image by SXCM are living and not in a crystalline state. The effects of soft x-rays will differ from those of hard x-rays as already mentioned. Section II has shown that the absorption length of electrons (energy range 10-100 keV) within protein or water is very short (μ_l < 0.5 μm).

Figure 69.. Time sequence of radiobiological events (**Tobias 1980**)

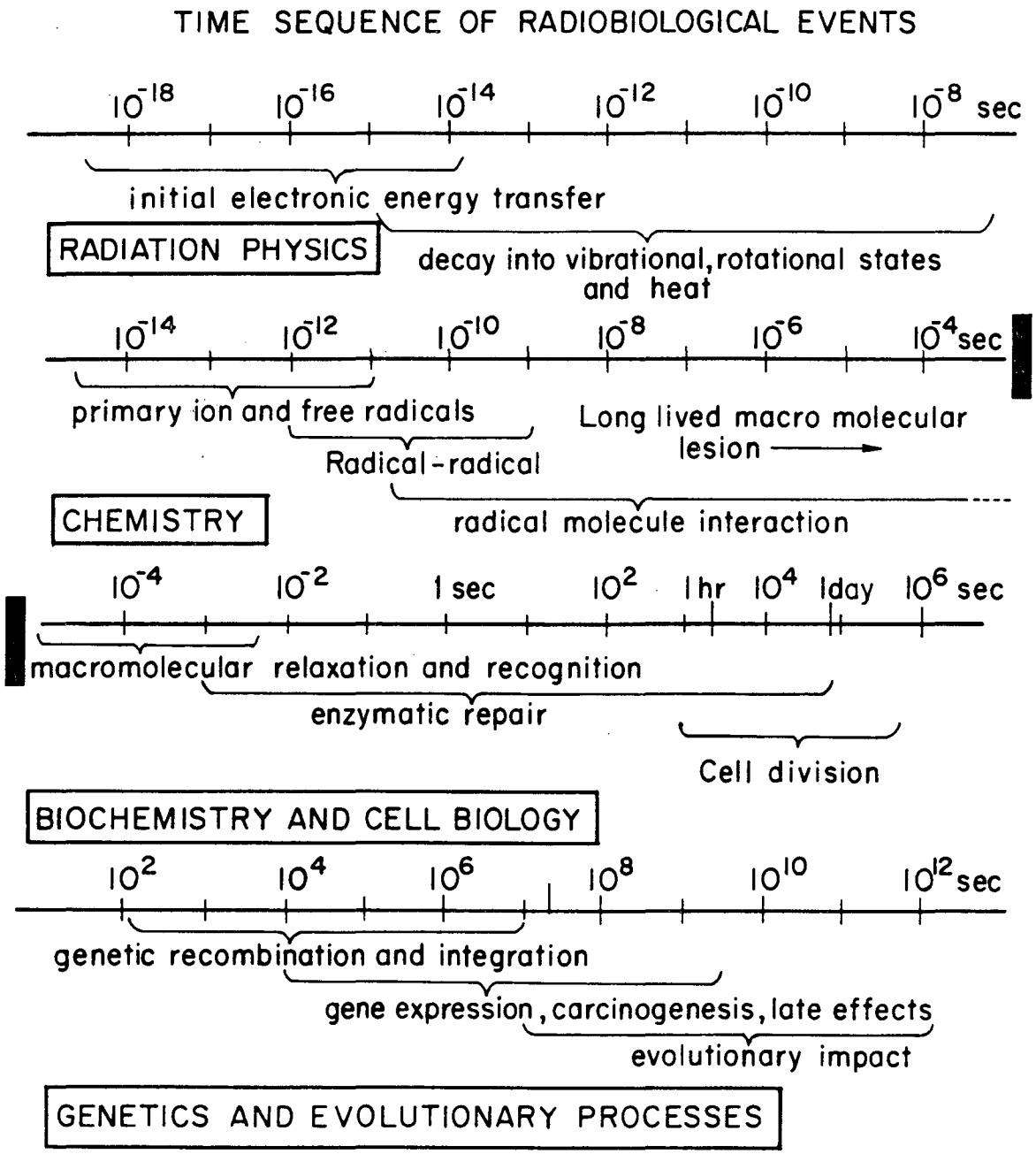

XBL 793-3312

Fig. 69

Another aspect to the radiobiological concerns of SXCM is the duration of the x-ray exposure. Section II has described the various x-ray sources and the exposure time necessary to make a contact image with each source type. Figure 69 is a time sequence of radiobiological events (**Tobias 1980**). The conventional laboratory source takes hours to make an exposure. The biological sample will be dead within a minute, however macromolecules may be rearranged, conformations changed, long-term lesions induced and surface membranes may breakdown. The cytoplasmic contents, i.e. organelles, are probably in motion or subject to Brownian motion. One may conclude that a SXCM image of a living cell is not possible using a conventional laboratory source. Synchrotron radiation sources may require minutes or seconds to make a SXCM image. Even in this short time period, conformational changes, long-lived macromolecular lesions and macromolecular rearrangement may occur. It is also probable that Brownian motion will affect the resolution of the SXCM image during an exposure using synchrotron radiation sources. Flash x-ray sources such the plasma gas puff z-pinch source and the laser-induced plasma source have exposure times of ~130 nsec and 1 nsec, respectively. The exposure time is significant in considering radiobiological events due to radiation chemistry and radiation physics, but insignificant when considering the events due to biochemistry and molecular and cell biology. One may conclude that conventional laboratory sources are effective for imaging fixed samples while synchrotrons may be able to image unaltered cell organelles. Flash sources are the best to image living cells without the consequence of physiological or anatomical change or radiobiological damage during exposure, however the cell is lost after exposure.

B. DISCUSSION OF FUTURE STEPS

1. APPARATUS IMPROVEMENT

One may improve the apparatus by making it bigger. A vacuum vessel 10-12 inches in diameter should replace the current 6 inch diameter tube. Increasing the number of ports and using 4 inch ports would allow easier access to SOXLIS. The electron optics

should be reworked to improve the focussing of the spot size. Also, a V-shaped hole in the target material of the anode may help focus the electrons and attain a smaller spot size (**Hawryluk 1989**). The addition of a carefully designed flight tube and properly monitored dosimetry system would make this apparatus useful to perform important soft x-ray radiobiological experiments.

2. TECHNIQUE IMPROVEMENT

Improving the technique requires the improvement of the developing and read-out of the resist. Current development methods are an 'art', which means the resist is developed until the features of interest are apparent. Development may continue because it is necessary to enhance these features for electron microscopy. A better method of monitoring development is to use an interferometer to gauge the thickness of resist that has been developed. To improve resist readout, one possibility is to use a scanning-tunneling microscope (STM) or an atomic force microscope (AFM). The disadvantage of an STM is the requirement to provide a conductive surface for the tip to scan. The usual conductive coating is AuPd and once applied, it is extremely hard to remove without injuring the resist. The reliability of the STM to provide a usable image is questionable at this time, however the AFM appears to produce reliable and useful images. The resist does not have to be coated to be imaged by the AFM thus further development may be done. These images have appeared to be reliable and useful (**Feder 1987**). Using these techniques one may be able to make a comparison between dose and resist depth. This comparison would assist in the interpretation of the peaks of a developed resist using attenuation factors found to be consistent in a cell. To improve TEM readout, one should use thin TEM resists where the thickness of the resist is 200 nm.

The construction of an x-ray optic to focus the "water window" soft x-rays from a laser-induced plasma source to a sample chamber would filter undesired x-rays and prevent breakage of the sample chamber Si_3N_4 window. Such an x-ray optic could be a reflecting

parabolic multilayered diffraction grating. The sample chamber may be placed behind or away from the laser target.

3. IMPROVING SAMPLE PREPARATION METHODS

The improvement of sample-preparation methods follows three paths. The first is to choose a cell line, where the cells are characteristically thin, especially during some of their physiological functions. PtK2 cells attach easily and are very thin, even when they are in mitosis. The second path is to culture cells on the Si_3N_4 window or onto the resist. Growing cells on the Si_3N_4 window was successful but growing these cells on the resist was unsuccessful since the resist and cells are both negatively charged. The third is to remove enough media so that salt crystals are not formed on the Si_3N_4 window and create a pattern on the resist but the cells are kept appropriately moist.

C. FUTURE PATH LENGTHS

This work is an intermediate step to obtaining a three-dimensional picture of a living cell by x-ray microscopy. Past results have been verified in this research. The success of the x-ray imaging of living CHO-SC1 cells has prepared a path for obtaining three-dimensional pictures of living cells by x-ray holography or tomography. This work is a preparatory step for observing physiological processes at a submicron or ~50 nm resolution. Improvements in resist technology, such as an understanding of secondary electron travel within a polymer, can lead to improved resolution at a lower dose. New types of high brightness sources are becoming available at a fast rate and will provide intense and extremely short pulses. One may hope that as the technology improves, soft x-ray contact microscopy will make "giant leaps" so that we can expand our knowledge of cell structure, locomotion and physiology.

REFERENCES

Agar, A. W., R. H. Alderson and D. Chescoe (1974) Principles and Practice of Electron Microscope Operation, (Practical Methods in Electron Microscopy, 2), Ed. A. M. Glauert, North-Holland, Amsterdam

Alberts, B., D. Bray, J. Lewis, M. Raff, K. Roberts and J. D. Watson (1983) Molecular Biology of the Cell, Garland, New York

Aoki, S. and S. Kikuta (1974) X-ray Holographic microscopy, *Japan J. Appl.Phys.*, 13, 1385

Ashcroft, N. W. and N. D. Mermin (1976) Solid State Physics, Saunders, Philadelphia

Asunma, S. K. (1960) X-ray sensitive recording materials for electron optical contrast, X-Ray Microscopy and Microanalysis, Eds. A. Engstrom, V. Cosslett, H. Pattee, Elsevier Publishing Company, Amsterdam, 66.

Attwood, D. and K-J. Kim (1988) Partial coherence and spectral brightness at x-ray wavelengths, X-ray Microscopy II, Eds. D. Sayre, M. Howells, J. Kirz and H. Rarback, Springer Series in Optical Sciences, 56, Springer-Verlag, Berlin, 16

Baldini, M. G., B. K. Kim, R. Feder, D. Sayre, V. Banton and J. Costa (1983) Possibilities for the study of blood platelets using soft x-ray microscopy, Science with Soft X-rays, Proceedings of SPIE-The International Society for Optical Engineering, 447, Eds. F. J. Himpsel and R. W. Klaffky, 164

Baldini, M. G., S. Morinaga, D. Minasian, R. Feder, D. Sayre, and V. Banton (1985) Defects of platelet function recognized by x-ray imaging and scanning electron microscopy, Proceedings of the 43rd Annual Meeting of the Electron Microscopy Society of America, Ed. G. W. Bailey, San Francisco, 610

Bellman, S. (1953) Microangiography, *Acta Radiol.*, Suppl. 102

Bigler, E., F. Polack and S. Lowenthal (1983) Quantitative mapping of atomic species by x-ray absorption spectroscopy and contact microradiography, *Nucl. Inst. Meth.*, 208, 387

Bjorklund, G. C. (1974) Vacuum Ultraviolet Holography, Ph. D. Thesis, Stanford University, (Microwave Laboratory Report No. 2339)

Blakely, E. A., T. L. Hayes, J. Schmidt and L. Lommel (1982) Heavy ion microscopy, Biology and Medicine Division Annual Report 1980-1981, Lawrence Berkeley Laboratory report LBL-13501, 65

Born, M. and E. Wolf (1980) Principles of optics, 6th ed., Pergamon Press, Oxford

Brenner, D. J., R. P. Bird, M. Zaider, P. Goldhagen, P. J. Kliauga and H. H. Rossi (1987) Inactivation of synchronized mammalian cells with low-energy x-rays-results and significance, *Radiation Research*, 110, 413

Cheng, P. C., H. B. Peng, R. Feder and J. W. McGowan (1982) The use of the transmission electron microscope as a viewing tool for high resolution soft X-ray contact microscopy, *Electron Microscopy (10th Int. Electron Microsc. Proc.)*, 1, 461

Cheng, P. C. (1985) Soft x-ray contact microscopy and absorption properties of biological materials, Ph.D. Thesis, University of Illinois at Chicago

Cheng, P. C., R. Feder, D. M. Shinozaki, K. H. Tan, R. W. Eason, A. Michette and R. J. Rosser (1986a) Soft x-ray contact microscopy, *Nuclear Instruments and Methods in Physics Research A*, 246, 668

Cheng, P. C., J. W. McGowan, K. H. Tan, R. Feder and D. M. Shinozaki (1986b) Ultra soft x-ray contact microscopy: A new tool for plant and animal cytology, Examining the Submicron World, Eds. R. Feder, J. W. McGowan and D. M. Shinozaki, NATO, Advanced Sciences Institute, Series B, Physics, 137, Plenum, New York, 277

Cheng, P. C. and G. J. Jan (1987) X-ray MIcroscopy-Instrumentation and Biological Applications, Springer-Verlag, Berlin

Chescoe, D. and P. J. Goodhew (1984) The operation of the transmission electron microscope, Microscopy Handbooks 02, Royal Microscopical Society, Oxford

Cosslett, V. E., A. Engstrom and H. H. Pattee (1957), X-Ray Microscopy and Microradiography, Academic Press, New York.

Cosslett, V. E. and W. C. Nixon (1960) X-ray Microscopy, Cambridge University, Cambridge

Cosslett, V. E. (1963) Methods of x-ray microscopy, X-Ray Microscopy and X-ray Microanalysis, Eds. H. H. Pattee, V. E. Cosslett and A. Engstrom, Academic Press, New York, 1.

Dauvillier, A. (1927) Sur un tube a rayons X de longeur d'onde effective egale a 8 unites Ångstrom, *C. R. Acad. Sci., Paris*, 185, 1460

Dauvillier, A. (1930) Realisation de la microradiographie integrale, *C. R. Acad. Sci., Paris*, 190, 1287

Deacon, D. A. G., L. R. Elias, J. M. J. Madey, G. J. Ramian, H. A. Schwettman and T. I. Smith (1977) First operation of a free-electron laser, *Phys Rev Lett*, 38, 892

Dietrich, J. (1963) Application de la microradiographie par contact a l'etude de la division cellulaire, Thesis, L'Universite de Strasbourg

Dyson, N. A. (1973) X-rays in atomic and nuclear physics, Longman Group, London

Eason, R. W., P. C. Cheng, A. G. Michette, R. J. Rosser, R. O'Neill, Y. Owadano, P. T. Rumsby, M. J. Shaw and I. C. E. Turcu (1986) Laser x-ray microscopy, *Optica Acta*, 33, 501

Engstrom, A. (1946) Quantitative micro and histochemical elementary analysis by roentgen absorption spectrography, *Acta Radiol.*, Suppl. 63

Engstrom, A., R. C. Greulich, B. L. Henke and B. Lundberg (1957) High resolution contact microradiography with ultrasoft polychromatic x-rays, X-Ray Microscopy and Microradiography, Eds. V. E. Coslett, A. Engstrom, and H. H. Pattee, Academic Press, New York, 218

Engstrom, A., V. Cosslett and H. Pattee (1960) X-Ray Microscopy and Microanalysis, Elsevier Publishing Company, Amsterdam

Engstrom, A. (1962) X-ray Microanalysis in Biology and Medicine, Elsevier, Princeton

Far West Technology, Inc., Private communication (December, 1986) Goleta, CA

Feder, R. (1970) X-ray projection printing of electrical circuits, IBM Technical Report, TR 22.1065

Feder, R., E. Spiller, J. Topalian, A. N. Broers, W. Gudat, B. J. Panessa, Z. A. Zadunaisky and J. Sedat (1977) High resolution soft x-ray microscopy, *Science*, 197, 259

Feder, R. and D. Sayre (1980) Recent developments in x-ray contact microscopy, Ultrasoft x-ray microscopy: Its application to biological and physical sciences, Ed. D. F. Parsons, Annals of New York Academy of Sciences, 342, 213

Feder, R., J. L. Costa, P. Chaudhari and D. Sayre (1981) Improved detail in Biological Soft X-ray Microscopy: Study of blood platelets, *Science*, 212, 1398

Feder, R., V. Banton, D. Sayre, J. Costa, M. Baldini and B. Kim (1985a) Direct imaging of live human platelets by flash x-ray microscopy, *Science*, 227, 63

Feder, R. and V. Mayne-Banton (1985b) X-ray contact imaging: The technique, Proceedings of the 43rd Annual Meeting of the Electron Microscopy Society of America, Ed. G. W. Bailey, San Francisco, 596

Feder, R. and V. Mayne-Banton (1986) X-ray contact microscopy, Examining the Submicron World, Eds. R. Feder, J. W. McGowan and D. M. Shinozaki, NATO Advanced Sciences Institute, Series B, Physics, 137, Plenum, New York, 277

Feder, R., J. W. McGowan and D. M. Shinozaki (1986a) Examining the Submicron World, NATO Advanced Sciences Institute, Series B, Physics, 137, Plenum, New York

Feder, R. Private communication (March, 1987) IBM T. J. Watson Research Center, Yorktown Heights, NY

Freund, H. P. and R. K. Parker (1989) Free-electron lasers, *Scientific American*, 260 (4), 84

Fulton, A. B. (1984) The Cytoskeleton, (Outline Studies in Biology), Chapman and Hall, London

Goby, M. P. (1913a) Une application nouvelle des rayons X: la microradiographie, *C. R. Acad. Sci., Paris*, 156, 686

Goby, M. P. (1913b) Micro-radiography, *Arch Roentg Ray, London*, 18, 247

Goby, M. P. (1913c) La microradiographie et ses applications a l'anatomie vegetale, *Bull. France Soc. Photogr. Cinemato.*, 4, 3rd series, 310

Goby, M. P. (1925) La microradiographie stereoscopique en relief et en pseudo-relief: la stereomicroradiographie, *C. R. Acad. Sci., Paris*, 180, 735

Goldstein, J. I., D. E. Newbury, P. Echlin, D. C. Joy, C. Fiori and E. Lifshin (1981) Scanning Electron Microscopy and X-ray Microanalysis, (A Text for Biologists, Materials Scientists, and Geologists), Plenum, New York

Goodhead, D. T., J. Thacker and R. Cox (1979) Effectiveness of 0.3 keV carbon ultrasoft x rays for the inactivation and mutation of cultured mammalian cells, *Int. J. Radiat. Biol.*, 36, 101

Goodhead, D. T. (1987) Relationship of microdosimetric techniques to applications in biological systems, The Dosimetry of Ionizing Radiation: Volume II, Eds. K. R. Kase, B. E. Bjarngard, and F. H. Attix, Academic Press, Orlando, 1

Gudat, W. (1982) Soft X-ray Contact Microradiography, Uses of Synchrotron Radiation in Biology, Ed. H. B. Stuhrmann, Academic Press, New York, 23

Guttmann, G. D., B. L. Henke and J. A. Kerner (1988) Using radiachromic films for soft x-ray dosimetry, X-ray Microscopy II, Eds. D. Sayre, M. Howells, J. Kirz and H. Rarback, Springer Series in Optical Sciences, 56, Springer-Verlag, Berlin, 151

Haelbich, R. P., J. P. Silverman and J. M. Warlaumont (1984) Synchrotron radiation x-ray lithography, *Nucl Inst Meth Phys Res*, 222, 291

Haller, I., R. Feder, M. Hatzakis and E. Spiller (1979) Copolymers of methyl methacrylate and methacrylic acid and their metal salts as radiation sensitive resists, *J Electrochem. Soc.*, 126(1), 154

Hansma, P. K., V. B. Elings, O. Marti and C. E. Bracker (1988) Scanning Tunneling Microscopy and Atomic Force Microscopy: Application to Biology and Technology, *Science*, 242, 209

Hawryluk, A., Private communication (April, 1989), Y Division, Lawrence Livermore National Laboratory, Livermore, CA

Hecht, E. (1987) Optics, 2nd ed., Addison-Wesley, Reading, Massachusetts

Henke, B. L. (1957a) Monochromatic sources of ulltrasoft x-radiation for quantitative microradiographic analysis, X-Ray Microscopy and Microradiography , Eds. V. E. Coslett, A. Engstrom, and H. H. Pattee, Academic Press, New York, 72

Henke, B. L., B. Lundberg and A. Engstrom (1957b) Conditions for optimum visual and photometric "contrast" in microradiograms, X-Ray Microscopy and Microradiography, Eds. V. E. Coslett, A. Engstrom, and H. H. Pattee, Academic Press, New York, 240

Henke, B. L. (1961) X-ray microscopy, Technical Report No. 4, Pomona College, Millikan Laboratory of Physics

Henke, B. L. (1962) Microanalysis with ultrasoft x-radiations, Advances in x-ray analysis, 5, Ed. Plenum , New York, 285

Henke, B. L. (1963) Production, detection, and application of ultrasoft x-rays, X-Ray Optics and X-Ray Microanalysis, Eds. H. H. Pattee, V. E. Coslett and A. Engstrom, Academic Press, New York, 157

Henke, B. L. and M. A. Tester (1975) Techniques of low energy x-ray spectroscopy (0.1 to 2 keV Region), Advances in x-ray analysis, 18, Ed. W. L. Pickles, C. S. Barrett, J. B. Newkirk and C. O. Ruud, Plenum, New York, 76

Henke, B. L. (1981) Low energy x-ray interactions: Photoionization, scattering, specular and Bragg reflection, Low Energy X-ray Diagnostics, American Institute of Physics (Conf. Proc. 75), New York, 146

Henke, B. L., P. Lee, T. J. Tanaka, R. L. Shimabukuro and B. K. Fujikawa (1982) Low energy x-ray interaction coefficients: Photoabsorption, scattering and reflection, *At Data Nucl Data Tables*, 27, 1

Hill, R. S., W. J. Myring, D. T. Clarke and C. J. Veltkamp (1987) Soft x-ray contact imaging of nucleolar chromatin using synchrotron radiation: a comparative scanning and transmission electron microscope study, *Journal of Microscopy*, 149, 127

Hobdell, M. H. and A. Boyde (1969) The correlation between microradiography and scanning electron microscopy of bone section surfaces, Fifth International Congress on X-Ray Optics and Microanalysis, Eds. G. Mollenstedt and K.H. Gaukler, Springer-Verlag, Berlin, 39.

Howells, M. R., J. Kirz, D. Sayre and G. Schmahl (1985) Soft-x-ray microscopes, *Physics Today*, August, 2

Howells, M. R., C. Jacobsen, J. Kirz, R. Feder, K. McQuaid and S. Rothman (1987) X-ray holography at improved resolution: A study of zymogen granules, *Science*, 238, 514

Humphreys, K. C. and A. D. Kantz (1977) Radiachromic: A radiation monitoring system, *Radiat Phys Chem*, 9, 737

Humphreys, K. C., W. O. Wilde and A. D. Kantz (1983) An opti-chromic dosimetry system for radiation processing of food, *Radiat Phys Chem*, 22, 291

Jackson, J. D. (1975) Classical electrodynamics, John Wiley and Sons, New York

Jenkins, F. A. and H. E. White (1976) Fundamentals of Optics, 4th ed., McGraw-Hill, New York

Kenney, J. M., C. Jacobsen, J. Kirz, H. Rarback, F. Cinotti, W. Thomlinson, R. Rosser and G. Schidlovsky (1985) Absorption microanalysis with a scanning soft X-ray microscope: mapping the distribution of calcium in bone, *J Microscopy*, 138, 321

Kim, K-J. (1986) Characteristics of synchrotron radiation, X-ray Data Booklet, Ed. D. Vaughan, Lawrence Berkeley Laboratory, Berkeley, PUB-490 Rev., 4-1

Kirz, J. and D. Sayre (1980) Soft X-ray microscopy of biological specimens, Synchrotron Radiation Research, Eds. H. Winick & S. Doniach, Plenum, New York, 277

Kirz, J. and H. Rarback (1985) Soft x-ray microscopes, *Rev. Sci. Instrum.*, 56, 1

Kraft, G., T. C. Yang, T. Richards, C. A. Tobias and T. L. Hayes (1981) Heavy-ion microscopy, Biology and Medicine Division Annual Report 1980-1981, Lawrence Berkeley Laboratory report LBL-11700, 56

Krinsky, S. (1988) Experience with synchrotron radiation sources, X-ray Microscopy II, Eds. D. Sayre, M. Howells, J. Kirz and H. Rarback, Springer Series in Optical Sciences, 56, Springer-Verlag, Berlin, 4

Kunkel, W. B. (1971) The many uses of plasma physics, Physik 1971, Teubner, Stuttgart, 37, also LBL report number LBL-344

Ladd, W. A., W. M. Hess and M. W. Ladd (1956) High-resolution microradiography, *Science*, 123, 370

Ladd, W. A. and M. W. Ladd (1957) High-resolution x-ray microscopy, X-Ray Microscopy and Microradiography, Eds. V. E. Cosslett, A. Engstrom, and H. H. Pattee, Academic Press, New York, 383.

Lamarque, P. (1936) Histologie-Historadiographie, *C. R. Acad. Sci., Paris*, 202, 684

Landau, L. D. and E. M. Lifshitz (1975) The Classical Theory of Fields, 4th ed., Course of Theoretical Physics, 2, Pergamon Press, Oxford

Landau, L. D. and E. M. Lifshitz (1975) Quantum Mechanics (Non-relativistic Theory), 3rd ed., Course of Theoretical Physics, 3, Pergamon Press, Oxford

Leeson, T. S. and C. R. Leeson (1981) Histology, 4th ed., W. B. Saunders, Philadelphia

Madey, J. M. J. (1971) Stimulated emission of bremsstrahlung in a periodic magnetic field, *J. Appl. Phys.*, 42, 1906

Manuelidis, L., J. Sedat and R. Feder (1980) Soft x-ray lithographic studies of interphase chromosomes, Ultrasoft x-ray microscopy: Its application to biological and physical sciences, Ed. D. F. Parsons, Annals of the New York Academy of Sciences, 342, 304

Matthews, D. L., P. L. Hagelstein, M. D. Rosen, M. J. Eckart, N. M. Ceglio, A. U. Hazi, H. Medecki, B. J. MacGowan, J. E. Trebes, B. L. Whitten, E. M. Campbell, C. W. Hatcher, A. M. Hawryluk, R. L. Kauffman, L. D. Pleasance, G. Rambach, J. H. Scofield, G. Stone and T. A. Weaver (1985) Demonstration of a soft x-ray amplifier, *Phy Rev Lett*, 54, 110

Matthews, D. L. and M. D. Rosen (1988) Soft x-ray lasers, *Scientific American*, 259 (6), 86

Michette, A. G., P. C. Cheng, R. W. Eason, R. Feder, F. O'Neill, Y. Owadano, R. J. Rosser, P. Rumsby and M. J. Shaw (1986) Soft x-ray contact microscopy using laser plasma sources, *J. Phys. D.:Appl. Phys.*, 19, 363

Motz, H. (1951) Applications of the radiation from fast electron beams, *J. Appl. Phy.*, 22, 527

Motz, H., W. Thon and R. N. Whitehurst (1953) Experiments on radiation by fast electron beams, *J. Appl. Phys.*, 24, 826

Nilsonne, U. L. (1959) Biophysical investigations of the mineral phase in healing fractures, *Acta Orthopaed.Scand.*, Suppl. 37

Panessa, B. J., M. M. Dewey, P. Brink, B. Gaylinn, R. A. McCorkle, G. Coleman and J. B. Warren (1981a) High resolution x-ray contact microscopy of hydrated muscle filaments, 39th Ann. Proc. Electron Microscopy Soc. Amer., Ed. G. W. Bailey, 512

Panessa, B. J., R. A. McCorkle, P. Hoffman, J. B. Warren and G. Coleman (1981b) Ultrastructure of hydrated proteoglycans using a pulsed plasma source, *Ultramicroscopy* , 6, 139

Panofsky, W. K. H. and M. Phillips (1962) Classical electricity and magnetism, Addison-Wesley, Reading, Massachusetts

Parsons, D. F. (1980) Ultrasoft X-ray Microscopy: Its Application to Biological and Physical Sciences, Annals of the New York Academy of Sciences, 342.

Pattee, H. H. (1960a) Electron optical enlargement of contact x-ray images, X-Ray Microscopy and Microanalysis, Eds. A. Engstrom, V. Cosslett, and H. Pattee, Elsevier Publishing Company, Amsterdam, 56.

Pattee, H. H. (1960b) High resolution radiosensitive materials for microradiography at long wavelengths, X-Ray Microscopy and Microanalysis, Eds. A. Engstrom, V. Cosslett, and H. Pattee, Elsevier Publishing Company, Amsterdam, 61.

Pattee, H. H., V. E. Cosslett and A. Engstrom (1963) X-Ray Microscopy and X-ray Microanalysis, Academic Press, New York, 1.

Pearlman, J. S. and J. C. Riordan (1981) X-ray lithography using a pulse plasma source, *J. Vac. Sci. Technol.*, 19, 1190

Pearlman, J. S. and J. C. Riordan (1985a) Bright discharge plasma sources for x-ray lithography, Microlithography, SPIE, 537,

Pearlman, J. S., J. C. Riordan and A. C. Kolb (1985b) A bright pulsed x-ray source for soft x-ray research and processing applications, 5th International Meeting on Radiation Processing

Phillips, M. H., J. M. Jaklevic, J. B. Schmidt, A. C. Birge, and C. A. Tobias (1984) Heavy-ion microscopy, Biology and Medicine Division Annual Report 1983-1984, Lawrence Berkeley Laboratory report LBL-11700, 103

Raju, M. R., S. G. Carpenter, J. J. Chmielewski, M. E. Schillaci, M. E. Wilder, J. P. Freyer, N. F. Johnson, P. L. Schor, R. J. Sebring, and D. T. Goodhead (1987) Radiobiology of ultrasoft X-rays, I. Cultured hamster cells (V79), *Radiation Research,* 110, 396.

Reimer, L. (1984) Transmission Electron Microscopy, Physics of Image Formation and Microanalysis, Springer Series in Optical Sciences, 36, Springer-Verlag, Berlin

Reimer, L. (1985) Scanning Electron Microscopy, Physics of Image Formation and Microanalysis, Springer Series in Optical Sciences, 45, Springer-Verlag, Berlin

Reitz, J. R., F. J. Milford and R. W. Christy (1979) Foundations of Electromagnetic Theory, 3rd ed., Addison-Wesley, Reading, MA

Richards, K. S. , A. D. Rush, D. T. Clarke and W. J. Myring (1988) Comparison of synchrotron and laser sources in x-ray contact microscopy of metal-contaminated biological tissue, *Nucl. Instrum. Meth. Phys. Res. A.*

Riordan, J. C., J. S. Pearlman, M. Gersten and J. E. Rauch (1981) Sub-kilovolt x-ray emission from imploding wire plasmas, Low Energy X-ray Diagnostics, American Institute of Physics (Conf. Proc. 75), New York, 35

Robbins, S. L., R. S. Cotran and V. Kumar (1984) Pathologic Basis of Disease, 3rd ed., W. B. Saunders, Philadelphia

Rontgen, W. C. (1896) On a new kind of rays, *Nature*, 53, 274

Rosen, M., P. Hagelstein, D. Matthews, E. Campbell, A. Hazi, B. Whitten, B. MacGowan, R. Turner, R. Lee, G. Charatis, Gar. E. Busch, C. Shepard and P. Rockett (1985) The exploding foil technique for achieving a soft x-ray laser, *Phys Rev Lett*, 54, 106

Rosser, R. J., K. G. Baldwin, R. Feder, D. Bassett, A. Coles and R. W. Eason (1985a) Soft x-ray contact microscopy with nanosecond exposure times, *Journal of Microscopy*, 138, 311

Rosser, R. J., R. Feder, A. Ng and P. Celliers (1985b) Single shot soft x-ray microscopy using plasmas generated by a laboratory sized Nd-glass laser, *Journal of Microscopy*, 140, RP1

Rothman, S. S., N. Iskander, K. McQuaid, H. Ade, D. T. Attwood, T. H. P. Chang, J. H. Grendell, D. P. Kern, J. Kirz, I. McNulty, H. Rarback, D. Shu and Y. Vladimirsky (1988) The biology of the cell and high resolution x-ray microscope, X-ray Microscopy II, Eds. D. Sayre, M. Howells, J. Kirz and H. Rarback, Springer Series in Optical Sciences, 56, Springer-Verlag, Berlin, 372

Rumsby, P. T. (1985) Laser produced plasmas as intense x-ray sources for microscopy at the Central Laser Facility, *Journal of Microscopy*, 138, 245

Saunders, R. L. DE C. H. (1969a) Biological Applications of Projection X-ray Microscopy, Fifth International Congress on X-Ray Optics and Microanalysis, Eds. G. Mollenstedt and K.H. Gaukler, Springer-Verlag, Berlin, 39.

Saunders, R. L. DE C. H., M. A. Bell and V. R. Carvalho (1969b) X-ray Histochemistry used for Simultaneous Demonstration of Neurones and Capillaries in the Human Brain, Fifth International Congress on X-Ray Optics and Microanalysis, Eds. G. Mollenstedt and K.H. Gaukler, Springer-Verlag, Berlin, 550.

Saunders, R. L. DE C. H., V. R. Carvalho and H. Cutmore (1972) A Study of the Visual Area of the Human Brain by X-ray Microscopy, Proceedings of the Sixth International Conference on X-Ray Optics and Microanalysis, Eds. G. Shinoda, K. Kohra and T. Ichinokawa, University of Tokyo Press, 895

Saxon, D. S. (1968) Elementary Quantum Mechanics, Holden-Day, San Francisco

Sayre, D., J. Kirz, R. Feder, D. M. Kim and E. Spiller (1977a) Potential operating region for ultrasoft x-ray microscopy of biological materials, *Science*, 196, 1339

Sayre, D., J. Kirz, R. Feder, D. M. Kim and E. Spiller (1977b) Transmission microscopy of unmodified biological materials: Comparative radiation dosages with electrons and ultrasoft x-ray photons, *Ultramicroscopy*, 2 (4), 337

Sayre, D., J. Kirz, R. Feder, D. M. Kim and E. Spiller (1978) Assessment of the potential of ultrasoft x-ray microscopy, Short Wavelength Microscopy, Annals of the New York Academy of Sciences, 306, 286

Sayre, D. and R. Feder (1979) Exposure and development of x-ray resist in microscopy, IBM Research Report RC 7498

Sayre, D., M. Howells, J. Kirz and H. Rarback (1988) X-ray Microscopy II, Springer Series in Optical Sciences, 56, Springer-Verlag, Berlin

Schmahl, G. and D. Rudolph (1984) X-ray Microscopy, Springer Series in Optical Sciences, 43, Springer-Verlag, Berlin

Shankar, R. (1980) Principles of Quantum Mechanics, Plenum, New York

Shinohara, K., S. Aoki, M. Yanagihara, A. Yagishita, Y. Iguchi and A. Tanaka (1986) A new approach to the observation of the resist in x-ray contact microscopy, *Photochemistry and Photobiology*, 44, 401

Shinohara, K., H. Nakano, M. Watanabe, Y. Kinjo, S. Kikuchi, Y. Kagoshima, K. Kobayashi and H. Maezawa (1988) X-ray contact microscopy of human chromosomes and human fibroblasts, X-ray Microscopy II, Eds. D. Sayre, M. Howells, J. Kirz and H. Rarback, Springer Series in Optical Sciences, 56, Springer-Verlag, Berlin, 429

Shinozaki, D. M., P. C. Cheng and R. Feder (1986) Soft x-ray induced surface roughness in PMMA, Proc. XIth Int. Cong. on Electron Microscopy, Kyoto, 1763

Shinozaki, D. M. (1988) High resolution image storage in polymers, X-ray Microscopy II, Eds. D. Sayre, M. Howells, J. Kirz and H. Rarback, Springer Series in Optical Sciences, 56, Springer-Verlag, Berlin,118

Spears, D. L. and H. I. Smith (1972) X-ray lithography-a new high resolution replication process, *Solid State Technology*, 15(7), 21

Spencer, M. (1982) Fundamentals of light microscopy, IUPAB Biophysics Series, 6, Cambridge University Press, Cambridge

Spiller, E., R. Feder, J. Topalian, E. Castellani, L. Romankiw and M. Heritage (1976a) X-ray lithography for bubble devices, *Solid State Technology*, 19, 62

Spiller, E., R. Feder, J. Topalian, D. E. Eastman, W. Gudat and D. Sayre (1976b) X-ray microscopy of biological objects with carbon K and with synchrotron radiation, *Science*, 191, 1172

Spiller, E. and R. Feder (1977) X-ray Lithography, X-ray Optics (Topics in Applied Physics, 22) Ed. H.-J. Queisser, Springer-Verlag, Berlin, 35

Spiller, E., R. Feder and D. Sayre (1979) X-ray Lithography and Microscopy, Synchrotron Radiation applied to Biophysical and Biochemical Research, Eds. A. Castellani and I. F. Quercia, Plenum, New York, 377

Stead, A. D., T. W. Ford, W. J. Myring and D. T. Clarke (1988) A comparison of soft x-ray contact microscopy with light and electron microscopy for the study of algal cell ultrastructure, *Journal of Microscopy*, 149, 207

Stroke, G. W. (1965) Attainment of high resolutions in image-forming X-ray microscopy with "lensless" Fourier-transform holograms and correlative source-effect compensation, X-Ray Optics and Microanalysis, Eds. R. Castaing, P. Deschamps, and J. Philibert, Hermann, Paris, 30.

Stryer, L. (1981) Biochemistry, Freeman, San Francisco

Suckewer, S., C. H. Skinner, H. Milchberg, C. Keane and D. Voorhees (1985) Amplification of stimulated soft x-ray emission in a confined plasma column, *Phys Rev Lett*, 55, 1753

Suckewer, S., C. H. Skinner, D. Kim, E. Valeo, D. Voorhees and A. Wouters (1986) Divergence measurements of soft x-ray laser beam, *Phys Rev Lett*, 57, 1004

Thompson, L. F. and M. J. Bowden (1983) Resist processing, Introduction to Microlithography, ACS Symposium Series 219, American Chemical Society, Washington, 162

Tobias, C. A., E. A. Blakely, F. Q. H. Ngo and T. C. H. Yang (1980), The repair-misrepair model of cell survival, Radiation Biology in Cancer Research, Raven Press, New York.

Trebes, J. E., S. B. Brown, E. M. Campbell, D. L. Matthews, D. G. Nilson, G. F. Stone and D. A. Whelan (1987) Demonstration of x-ray holography with an x-ray laser, *Science*, 238, 517

Vaughan, D. (1986) Editor, X-ray Data Booklet, Lawrence Berkeley Laboratory, Berkeley, PUB-490 Rev.

VG (1975) Operating Manual for EG2 Electron Bombardment Evaporation Source and Power Supply EHT4 110 Volts AC Mains, Vacuum Generators, Sussex, England

Wallgren, G. (1957) Biophysical analyses of the formation and structure of human fetal bone, *Acta Paediat .*, Suppl. 113

Willson, C. G. (1983) Organic resist materials - theory and chemistry, Introduction to Microlithography, ACS Symposium Series 219, American Chemical Society, Washington, 87

Yang, T. C., G. Welch, C. A. Tobias, H. Maccabee, T. Hayes, L. Craise, E. V. Benton and F. Abrams (1978) The feasibility of heavy charged-particle microscopy, Short Wavelength Microscopy, Annals of the New York Academy of Sciences, 306, 322

LAWRENCE BERKELEY LABORATORY
TECHNICAL INFORMATION DEPARTMENT
1 CYCLOTRON ROAD
BERKELEY, CALIFORNIA 94720